1984

Electron detachment in negative ion-molecule collisions

Mohammed Saiful Huq
College of William & Mary - Arts & Sciences

Huq, Mohammed Saiful

ELECTRON DETACHMENT IN NEGATIVE ION-MOLECULE COLLISIONS

The College of William and Mary in Virginia PH.D. 1984

ELECTRON DETACHMENT IN NEGATIVE ION-MOLECULE COLLISIONS

A Dissertation

Presented to

The Faculty of the Department of Physics

The College of William and Mary in Virginia

In Partial Fulfillment

Of the Requirements for the Degree of

Doctor of Philosophy

---

by

Mohammed Saiful Huq

April 1984

APPROVAL SHEET

This dissertation is submitted in partial fulfillment

of the requirements of the degree of

Doctor of Philosophy

Md. Saiful Huq.

Mohammed Saiful Huq

Approved, April 1984

Roy L. Champion

Roy L. Champion

Lynn D. Doverspike

Lynn D. Doverspike

John B. Delos

John B. Delos

Mark S. Conradi

Mark S. Conradi

Steve K. Knudson

Steve K. Knudson
Chemistry

ACKNOWLEDGMENTS

I would like to express my sincere appreciation to my advisors, Drs. Roy Champion and Lynn Doverspike, for their continued guidance, encouragement and friendship throughout the course of this research. Dr. Champion's "no data, no beer" mandates kept things humming in the lab throughout many a night. I would also like to thank Dr. John Delos for many stimulating discussions. To my friends and colleagues in the physics department, and especially my fellow volleyball enthusiasts, I extend thanks for the years of camaraderie and winning seasons as well as shared enthusiasm for physics. Sylvia Stout, Dianne Fannin and Paula Sprately have provided very helpful assistance and direction, attending to numerous details. Finally, I would like to thank Marian L. Vance profoundly for her encouragement, love and affection which was necessary for the fulfillment of this work.

ABSTRACT

Absolute total cross sections for electron detachment, reactive scattering, charge transfer and dissociative charge transfer have been measured for collisions of hydrogen and halogen negative ions with various molecular targets. The reactants investigated involve H^-, D^-, F^-, Cl^-, Br^-, and I^- ions as projectiles and H_2, D_2, HD, N_2, CO, O_2, CO_2, CH_4, and Cl_2 molecules as targets. The energy range of these experiments extended from about 1 eV to about 300 eV in the lab.

The threshold behavior of the detachment cross sections for the reactants $H^-(D^-)$ + H_2, D_2, and HD has been determined. The thresholds for detachment for both H^- and D^- ions are found to be larger than the electron affinity. Isotopic substitution reveals that the detachment cross sections scale with relative collision energy at low collision energies and with relative collision velocity at high collision energies. Upper and lower bounds on detachment-rate constants which are based upon the measurements are presented.

Studies of the reactants $H^-(D^-)$ and N_2, CO, O_2, CO_2, and CH_4 reveal that electron detachment is the dominant process for all the molecular targets except O_2 for which charge transfer dominates. Isotope effects are observed in all the cross sections. The general features of the charge-transfer cross section for the O_2 target are in agreement with the ideas of a simple two-state collision model. The cross sections for charge transfer (or dissociative charge transfer) are found to be small for all targets except O_2.

In the case of the collisions of F^- and Cl^- with H_2, D_2, and HD, reactive scattering is found to be the dominant inelastic channel for F^- projectile. Electron detachment of F^- is found to occur by two distinct mechanisms. A striking difference in the detachment and reactive cross sections is observed when Cl^- is substituted for F^- in that the electron detachment cross section is generally larger than that for reactive scattering. Isotope effects are observed in all the cross sections for both F^- and Cl^-.

The charge transfer and dissociative charge transfer cross sections are found to be the dominant channels for collisions of Cl^-, Br^-, and I^- with Cl_2. The electron detachment cross section for I^- + Cl_2 is found to be anomalously low. Some energy loss spectra are reported for I^- + Cl_2. They exhibit substantial inelastic scattering which is consistent with the calculated potentials of Cl_2.

DEDICATION

to my parents
Roashan Ara and Shariful Huq

CONTENTS

ELECTRON DETACHMENT IN NEGATIVE ION-MOLECULE COLLISIONS

Chapter I

INTRODUCTION

The history of the collisional detachment of negative ions by atomic and molecular targets dates back to the works of Dukel'skii[1] in Russia in 1951 and Hasted[2] in England in 1952. Much of the collisional electron detachment work done since then has been concerned with the collisions of atomic negative ions by atomic targets. The H^-+ He and H^-+ Ne reactants provide perhaps the simplest negative ion-atom systems, and a large amount of work, both experimental and theoretical, has been devoted to these systems.[3-9] Moreover, it is only for these reactants that both extensive theory and experiment exist. A description of electron detachment becomes more complicated when molecular targets are substituted for atomic targets because one has to deal with a number of molecular and negative-molecular ion potential surfaces and their interactions. With the possible exception[10] of H_3^-, there is currently very little detailed information about such surfaces. Despite these difficulties or perhaps because of them, there has been a shift in emphasis - at least on the part of experimentalists - to molecular targets, and much of the work on electron detachment by molecular targets is beginning to surface in the literature. This dissertation is devoted to the experimental investigations of various aspects of electron detachment resulting from collisions of atomic negative ions by various molecular targets.

Electron detachment is one of the most important processes that may result from collisions of atomic negative ions with atoms or molecules. The most common detachment mechanisms are :

Direct detachment in which the negative ion collides with a neutral atom or molecule to produce a free electron as in

$$A^- + BC \longrightarrow A + BC + e \qquad (1.1)$$

where no excited states of the reactants or products are involved. The above process is frequently the dominant inelastic channel for collision energies above the detachment threshold and is normally the principal mechanism for the destruction of negative ions.

In addition to direct detachment, several other distinct processes have been found to be important for electron detachment in collisions of negative ions with molecular targets. One such mechanism involves an initial

Charge transfer to a temporary negative ion state of the molecular target followed by a rapid decay of the negative molecular ion,

$$A^- + BC \longrightarrow (BC^-)^* + A \longrightarrow BC^* + A + e \qquad (1.2)$$

which is likely to leave the target molecule vibrationally excited. Evidence for this type of process has been found in the kinetic energy spectra of the detached electrons[11-13] as well as in the time-of-flight spectra for the fast neutral products of collisional detachment.[14-16]

Other detachment processes that involve excited states of either target or negative ion (or its neutral parent) include

Excitation to autodetaching levels,

$$A^- + BC \longrightarrow (A^-)^* + BC \longrightarrow A + BC + e \qquad (1.3)$$

and

Excitation of target or Negative ion parent,

$$A^- + BC \longrightarrow A + (BC)^* + e \qquad (1.4)$$

or

$$A^- + BC \longrightarrow A^* + BC + e \qquad (1.5)$$

Another mechanism of electron detachment by molecular targets is one in which

Reactive scattering (i.e., molecular rearrangement) accompanies detachment, as in

$$A^- + BC \longrightarrow AB + C + e \qquad (1.6)$$

Finally, at the lowest collision energies, i.e., from thermal energies to several electron volts, there is always the possibility of

Associative detachment for selected reactants as in

$$A^- + BC \longrightarrow ABC + e \qquad (1.7)$$

In general, the relative importance of (1.6) and (1.7) increases as the collision energy is lowered. Associative detachment is only important at low relative collision energies, $E \lesssim 1$ eV, and reactive scattering accompanied by detachment [i.e.,(1.6)] is important for $E \lesssim 10$ eV. For higher collision energies, i.e., $E \lesssim 1000$ eV, both direct detachment and detachment via charge transfer have been observed to be of similar magnitude for the few systems studied thus far.[15] For example, the time-of-flight studies of the collisional detachment of H^- by N_2[15] indicate that the total cross sections for direct detachment and detachment via charge transfer are approximately equal at $E \simeq 500$ eV.

Interest in gas phase negative ions and their collisional properties stems from the fact that the majority of the elements in the periodic table and an incredible variety of molecules and radicals form stable negative ions. The binding energy of an "additional" electron to the neutral atom or molecule is known as the electron affinity (EA) of the species, and for atoms many of these electron affinities have been determined in high precision experiments in which a laser is used to photodetach the negative ions. A complete review of the subject of atomic electron affinities has been presented by Hotop and Lineberger[17] and in the text by Smirnov.[18]

The definition of the electron affinity of a molecule is not so clear cut as for an atom owing to the vibrational and rotational degrees of freedom and, for polyatomic molecules, configurational degrees of freedom of the molecular negative ion and the neutral parent molecule. The electron affinity of a molecule is usually defined as the difference in energy between the neutral molecule plus an electron at rest at infinity and the molecular negative ion when both the neutral molecule and the negative molecular ion are in their ground electronic, vibrational and rotational states.[19] Recent reviews on the subject of molecular electron affinities have been given by Janousek and Brauman[20] and by Franklin and Harland.[21]

Binary collisions between negative ions and atoms or molecules form the basis for the understanding of many chemical reactions and physical processes that occur in nature. A few examples of these processes include reactions taking place in the upper atmosphere, in flames, in magnetohydrodynamic generators and in gas discharge plasmas.

In all of these environments, the principal method whereby negative ions are destroyed is thought to be collisional detachment.

Studies of hydrogen plasma discharges,[22,23] which are relevent to the development of ion sources for the production of intense $H^-(D^-)$ beams, have shown that the H^- equilibrium fractions in such discharges are higher than expected based upon current understanding of the processes believed to be involved in the production of H^-. Several suggestions[23] have been proposed to explain this observation. They involve dissociative attachment of electrons to vibrationally excited H_2,

$$e + H_2(v \geq 6) \longrightarrow H_2^-(^2\Sigma_u^+) \longrightarrow H(1s) + H^- \qquad (1.8)$$

and dissociative attachment to the long-lived electronically excited state of H_2,

$$e + H_2(^3\Pi_u) \longrightarrow H_2^-(^2\Pi_u) \longrightarrow H(2p) + H^- \qquad (1.9)$$

Recent work by Allan and Wong[24] and Wadehra and Bardsley[25] has shown that the cross section for process (1.8) increases dramatically if H_2 is vibrationally excited. However, a specific source for such a high concentration of $H_2(v \geq 6)$ has not been identified. If collisional detachment of H^- by H_2 proceeds via a charge transfer to a resonance of H_2^- (this may be unlikely, due to the rather large width of the $^2\Sigma_u^+$ resonance), then the decay of H_2^- resonance would probably leave the product hydrogen molecule in a highly excited vibrational state. It is therefore important to fully understand the collisional detachment mechanism for $H^- + H_2$ if one is to correctly model a hydrogen discharge.

Electron detachment in collisions of H^- with H_2 has been studied extensively.[9,26,27] This is partly because $H^- + H_2$ and its isotopic variants are perhaps the simplest triatomic negative-ion systems from a theoretical point of view. Furthermore, these systems are of considerable interest in the development of high intensity $H^-(D^-)$ ion beams which are used (after acceleration and subsequent neutralization) to "heat" magnetic-containment fusion devices.[23,28] Within negative-ion sources, the process of collisional detachment and its reverse—three-body-attachment—are of obvious importance. Also of significance are the mechanisms of collisional excitation by negative ions and electron transfer from negative ions. It is important to understand the inelastic processes that lead to the creation and destruction of negative ions because the intensity of $H^-(D^-)$ ions extracted from these ion sources depends upon the equillibrium conditions resulting from competition between the creation and destruction processes.

In this dissertation we report the results of measurements of absolute total cross sections for electron detachment for collisions of H^-, D^- and the halogen anions (F^-, Cl^-, Br^- and I^-) with such molecular targets as H_2, D_2, HD, N_2, CO, O_2, CO_2, CH_4, and Cl_2. The energy range of the experiments extends from below the energetic thresholds for detachment up to several hundred eV.

The near-threshold measurements of the collisional detachment cross section are important since they provide an essential tool which can be used in determining the salient features of the adiabatic potential surfaces. Additionally, detachment-rate constants, which are needed to model discharges, are strongly dependent upon the threshold behav-

ior of the detachment cross section. The collisional detachment of both H^- and D^- has been studied in order to determine the effects of isotopic substitution upon the total detachment cross section. Such "isotope effects" may provide valuable insights as to which mechanisms are responsible for detachment and these effects are often instrumental to a complete understanding of the collisional dynamics.

In addition to total cross section measurements for electron detachment we also report cross sections for the production of "slow" negative ions for collisions of the reactants listed above. In our experiments, the target molecule is essentially at rest prior to the collision and the word "slow" denotes processes in which the bulk of the energy and momentum are carried away in the laboratory frame by the unobserved reaction products (usually neutral), leaving a "slow" negative ion. Processes which give rise to these slow negative ions include charge transfer

$$H^- + O_2 \longrightarrow O_2^- + H, \tag{1.10}$$

dissociative charge transfer

$$H^- + CO_2 \longrightarrow O^- + CO + H, \tag{1.11}$$

and ion-molecule (or rearrangement) reactions such as

$$D^- + H_2 \longrightarrow H^- + HD. \tag{1.12}$$

In several cases it has been possible to see how such mechanisms compete with electron detachment.

A review of the recent activity in the field of collisional electron detachment of negative ions by molecular targets will be given in chapter II. Chapter III describes the experimental apparatus used for the measurements reported here. Two apparatuses will be discussed: one used to measure total cross sections for electron detachment and the other to obtain relative inelastic differential cross sections. Collisions between hydrogen (deuterium) negative ions and various molecules are discussed in chapters IV and V with chapter IV presenting the results of absolute cross sections for electron and ion production for H_2, D_2 and HD targets and chapter V presenting those for N_2, CO, O_2, CO_2 and CH_4 targets. Chapters VI-VII focus on collisions of halide ions with various molecular targets: cross sections for electron detachment and reactive scattering for collisions of F^- and Cl^- with isotopic hydrogen molecules are presented in chapter VI and the results for electron detachment and for reactive scattering between the Cl^-, Br^-, and I^- ions and chlorine gas, Cl_2 are presented in chapter VII. Some energy loss spectra for the reactants $I^- + Cl_2$ are also presented in this chapter.

It should be mentioned here that this dissertation is based upon several articles which have been published previously in various scientific journals. The following is a list of these articles, the journals in which they were first published, and the chapters of this dissertation in which they are presented.

i) "Electron detachment for collisions of H^- and D^- with hydrogen molecules" : M.S. Huq, L.D. Doverspike, and R.L. Champion, Phys. Rev. A27, 2831 (1983) [Chapter IV].

ii) 'Total cross sections for collisions of H^- and D^- with various molecules" : M.S. Huq, L.D. Doverspike, and R.L. Champion, Phys. Rev. A27, 785 (1983) [Chapter V].

iii) 'Reactive scattering and electron detachment in collisions of halogen negative ions with isotopic hydrogen molecules" : M.S. Huq, D.S. Fraedrich, L.D. Doverspike, R.L. Champion, and V.A. Esaulov, J. Chem. Phys. 76, 4952 (1982) [Chapter VI].

iv) 'Measurements of absolute total cross sections for charge transfer and electron detachment of halide ions on chlorine" : M.S. Huq, D. Scott, N.R. White, R.L. Champion, and L.D. Doverspike, J. Chem. Phys. (in press) April 15 (1984) [Chapter VII].

We have taken figures and materials liberally from the above references and cited these in the appropriate chapters of this dissertation.

Chapter II

ELECTRON DETACHMENT : A BRIEF REVIEW

2.1 INTRODUCTION

Considerable attention has been recently focused on the collisional detachment of atomic negative ions by atoms. Most of these works involve a theoretical description or experimental observation of total detachment cross sections, elastic and inelastic differential cross sections for the production of neutral atoms that result from detachment, and energy loss spectroscopy for nondetaching collisions. While electron detachment involving atomic reactants are generally well understood, the same is not true for molecular reactants. This is because the collisional dynamics becomes more complicated when molecular targets are involved. Because of this complexity and lack of adequate potential surface calculations, no extensive theory has been developed to explain the dynamics of negative ion-molecule collisions. Thus a large amount of experimental work has been done in this field with the hope that the information available from experiments will serve as a guide to the development of a comprehensive theory.

To introduce the subject of collisional electron detachment, we will first briefly discuss the collisional dynamics for a few selected atomic reactants. We will use these ideas to explain qualitatively some of the results presented in this study. A brief review of collisional detachment by molecular targets will then be given.

2.2 ATOMIC REACTANTS

Of all the negative-ion systems, those which involve collisions of H^- and D^- with the rare gases have been studied most extensively.[4,29] Due to the relative simplicity of the H^- + He and H^- + Ne systems, they have also been the subject of several theoretical studies.[5-8]

At low relative collision energies, the orbital velocity of the loosely bound electron on the negative ion is much larger than the collision velocity and a quasi-molecular description of the collision is expected to be adequate. The de Broglie wavelength associated with the nuclear motion is considerably smaller than the molecular size, and the motion of the nuclei can be described within the framework of classical mechanics. On the other hand, at high collision energies where the projectile velocity is larger than the orbital velocity of the detaching electron, the adiabatic picture of collision becomes inappropriate. Detachment in this high energy region is described with a sudden impulse approximation in which the collision is described as the elastic scattering of a free electron (which has a velocity equal to the velocity of the negative ion) with the target gas.[30]

Several theoretical descriptions for the dynamics of low energy collisional detachment have recently emerged. These include: i) a local complex potential model employed by Lam et al.,[4] ii) a zero-radius potential (ZRP) model by Gauyacq[5,6] and iii) a semiclassical close coupling calculation by Taylor and Delos[7] and Wang and Delos.[8] In all these formulations, it is believed that detachment occurs by way of an interaction between a discrete state and a continuum.

2.2.1 Local Complex Potential

The curve crossing mechanism involves the crossing of the bound negative ion-atom state with the continuum of states representing neutral atoms and a free electron of arbitrary energy (see Fig.1). In the local complex potential description, the $A^- + B$ state is considered to be quasibound for $R < R_x$, where R_x is the crossing radius of $A^- + B$ potential curve with that of $A + B + e$. In this region the state has a finite lifetime and is described by a complex potential

$$V(R) = V_1(R) - (i/2)\Gamma'(R) \tag{2.1}$$

The width $\Gamma'(R)$ is inversely proportional to the lifetime. The survival probability for the decaying system calculated for this model is given by

$$P_s = \exp\left[-2\int_{R_o}^{\infty} dR\ \Gamma'(R)/v(R)\right] \tag{2.2}$$

where $v(R)$ is the relative nuclear velocity. Equation (2.2) predicts an isotope effect: the detachment cross section for D^- is greater than that of H^- at the same relative collision energy. This is due to the fact that for the same relative collision energy the two isotopes follow the same trajectories but with different velocities and hence the time spent by D^- in the continuum is greater than for H^-, resulting in a larger detachment cross section. At low relative collision energies the predictions of this model are found to be in good agreement with the experimental observations for $H^-(D^-)$ + He reactants.[4,29,31] However, at high collision energies, the model fails to reproduce the experimental results.

Although the local complex potential model had some success in explaining the results for $H^-(D^-)$ + He, it failed completely to explain the total detachment cross sections observed for $H^-(D^-)$ + Ne.[31,32] Application of the complex potential model to the $H^-(D^-)$ + Ne reactants was found to be inappropriate because the internuclear potentials for NeH and NeH^- are found not to cross each other.[33] This is in contrast to the situation for the HeH and HeH^- potentials, which do cross. Thus a different approach is needed to explain the basic features of detachment observed for $H^-(D^-)$ + Ne reactants.

2.2.2 Zero Radius Potential (ZRP) Approximation

In this model detachment can occur for R near R_x where the binding energy $\varepsilon(R)$ of the outer electron in the $(AB)^-$ quasi-molecule can become very small [$\varepsilon(R)$ is the difference between the neutral and ionic potentials for $R > R_x$]. The wavelength of the electron then becomes much larger than the size of the AB molecular core. Hence the probability that the electron stays outside this core becomes large. The detachment problem is then addressed by dividing the whole space into two regions: an outer region where the electron is treated as a free particle and a molecular core where the electron feels an effective potential. In the ZRP approximation the radius of this core is taken to be zero and the effective potential is replaced by a δ-function potential. One then calculates the free particle Schrödinger equation for the electron wave function (assumed to be an s-state)

$$\left[\nabla^2 - 2\varepsilon(R) \right] \psi = 0 \qquad (2.3)$$

which gives $\Psi \approx \exp(-kr)/r$, where $k=[2\varepsilon(R)]^{\frac{1}{2}}$. The boundary condition is defined by specifying the logarithmic derivative of the wave function at the origin, i.e.,

$$\frac{1}{r\Psi}\frac{\partial(r\Psi)}{\partial r}\Big|_{r=0} = f[R(t)] \qquad (2.4)$$

where the time dependence of the boundary condition is due to the motion of the nuclei. For $f[R(t)] < 0$, there exists a bound state whereas for $f[R(t)] > 0$, no bound states exist. The survival probability of the negative ion is then calculated by projecting Ψ (r,t —> large) onto the bound eigenfunction.

Results of such a calculation for the D^- + He system[6] show that the detachment probability $P_d(b)$ is quite large for values of $R > R_x$. Furthermore, for large impact parameters, when the system does not enter the continuum, $P_d(b)$ is found to increase with increasing collision energy. This is due to the rising importance of dynamical transitions for $R > R_x$. Detachment in this mechanism thus occurs by a coupling of the nuclear motion of the colliding partners to the electronic motion. The isotope effect observed for $H^-(D^-)$ + Ne is nicely reproduced in this model.[6]

2.2.3 Semiclassical Close Coupling Calculation

A different approach to the theory of these processes has been developed by Taylor and Delos.[7] They expand the electronic wave function as

$$\Psi = C_0(t)\phi_0 + \int C_E(t)\phi_E\rho(E)dE \qquad (2.5)$$

where ϕ_0 is the state in which the electron is bound to the molecule, ϕ_E is a state in which the electron is free with kinetic energy E, and $\rho(E)$ is the density of states in this continuum. Thus $C_0(t)$ is the probability amplitude for finding the electron bound; $|C_0(-\infty)|^2 = 1$ and $1 - |C_0(\infty)|^2$ is the probability of electron detachment.

Taylor and Delos assume that the states ϕ_0, ϕ_E can be constructed in such a way that non-adiabatic couplings among them are negligible, and detachment occurs because of electrostatic couplings (i.e., matrix elements V_{0E} of the electronic Hamiltonian). Furthermore, they assume that transitions only occur between the bound state and the continuum (and vice versa), and that direct continuum-continuum transitions are insignificant.

From these assumptions, they derive coupled equations that are satisfied by the coefficients $C_0(t)$, $C_E(t)$:

$$i\hbar \frac{d}{dt} C_0(t) = V_{ion}(t)C_0(t) + \int V_{0E}(t)C_E(t)\rho(E)dE$$

$$i\hbar \frac{d}{dt} C_E(t) = \left[V_{neutral}(t) + E \right] C_E(t) + V_{E0}C_0(t) \qquad (2.6)$$

The problem then reduces to solving this non-denumerably infinite set of coupled equations.

Neglecting the time dependence of $V_{E0}(t)$, and approximating $V_{ion}(t) - V_{neutral}(t)$ by a quadratic function of time (which for the H^- + He system is fitted to the calculation of Olson and Liu[33]) they show that these equations can be solved, and proceed to derive a rather complicated formula for the survival probability. Results of these calculations for the total detachment cross section for $H^-(D^-)$ + He are found to be in good agreement with the experimental observations.[7]

Wang and Delos[8] have also calculated the detachment cross sections for $H^-(D^-)$ + Ne for $E \lesssim 200$ eV. The starting point of their calculation was Eq.(2.6), utilizing potential curves V_{ion} and $V_{neutral}$ close to those calculated by Gauyacq, and an assumed form for $V_{E0}(R)$:

$$V_{E0}(R) \approx A\sqrt{E}\exp(-0.66R) \tag{2.7}$$

Equations (2.6) were then solved by a first order approximation: taking

$$C_0(t) = \exp\left[-i/\hbar \int_0^t V_{ion}(t')dt'\right] \tag{2.8}$$

the equations for $C_E(t)$ are easily integrated, and the total probability of detachment is

$$P_d = \int_0^\infty |C_E(\infty)|^2 \rho(E)dE \tag{2.9}$$

Cross sections were calculated using these formulas, and the calculations were found to be in good agreement with experiments.[8]

The above discussions thus suggest that the low energy electron detachment for $H^-(D^-)$ + He, Ne reactants proceed by two distinct mechanisms: i) curve crossing of a discrete state into a continuum, ii) a dynamical transition in which the nuclear motion is used to promote the active electron into the continuum. The former mechanism is characterized by sharp, well defined thresholds, an isotope effect where the slower isotope (for a given relative collision energy) gives a larger detachment cross section and a detachment cross section which is fairly

large. The later mechanism is characterized by somewhat smaller cross sections and an isotope effect which is reverse of that stated above. These same ideas will be carried over to the discussion of electron detachment by molecular targets where one must substitute the ideas of potential surfaces for internuclear potential curves.

2.3 MOLECULAR REACTANTS

In recent years a great deal of effort has been made to understand the collision processes that involve negative ions and molecules as reactants. A large number of experiments have been performed to measure i) total cross sections for electron and "slow" ion production, ii) energy distributions of product ions as a function of scattering angle and iii) energy and angular spectra of detached electrons. These measurements provide information essential to our understanding of the dynamics of ion-molecule collisions.

Several techniques have been used to measure total detachment cross sections. In one approach a combined electrostatic and magnetostatic field is used to trap the detached electrons.[2,34-38] Slow ions which are the products of collisions can be separated from the electrons by a suitable choice of the magnetic field configuration. The kinetic energy of these product ions is small when compared with that of the reactant negative ion and thus can be trapped electrostatically.[39,40] A different approach is to observe the attenuation of the beam current as the target gas pressure[9,41] or the collision path length[42] is varied. In all these measurements it is generally not possible to separate direct detachment from detachment with ionization. At low collision energies detachment with ionization is usually negligible, however.

Differential cross sections have been measured by using i) a position sensitive channelplate detector[43] ii) time of flight (TOF) method[16,44] and iii) energy loss spectroscopy.[4] In order to investigate the role of excited states in collisional detachment, it is necessary to measure double differential cross sections and the TOF method is well suited for this purpose.

Earlier work on electron detachment from negative ions by molecular targets was limited mostly to the keV energy range. Those results published prior to 1974 have been reviewed by Risley and Geballe[9] and are summarized in table 1.

There have been several studies of electron detachment by molecular targets in the threshold region.[29,35,45] Total cross sections for electron production have been measured in these experiments and thresholds for detachment have been determined. Other studies involve the measurements of total charge transfer cross sections[46] and energy dependence of the total charge transfer cross sections in the threshold region.[47,48]

Recently an extensive amount of work has been done on the measurements of electron energy spectra arising from the collisions of atomic negative ions with various molecules.[11-13,49] These experiments give clear indication that the negative ion resonance states of various molecules play an important role in the dynamics of detachment in negative ion-molecule collisions. Further evidence on the involvment of the negative ion resonance states in electron production came from the TOF studies[14-16,50] of the fast neutrals which are the products of collisional detachment.

TABLE 1

Review of total electron detachment cross section from negative ions by molecules

Energy	Projectile	Target	References
2-100 eV	$H^-(D^-)$	N_2	Champion et al.[31]
3-100 eV	$O^-,(O_2^-)$	O_2	Roche and Goodyear[36]
7-400 eV	H^-	H_2	Muschlitz et al.[26]
8-350 eV	H^-,O^-,OH^-,O_2^-	O_2	Bailey and Mahadevan[38]
10-2500 eV	H^-,O^-	H_2,N_2,O_2	Hasted and Smith[27]
10-2500 eV	Cl^-	Cl_2	Hasted and Smith[27]
300-3000 eV	O^-,Cl^-,Br^-,I^-	O_2,CO_2	Dimov and Roslyakov[88]
0.2-10 keV	H^-	O_2	Risley and Geballe[9],Risley[58]

Chapter III

EXPERIMENTAL APPARATUS AND METHOD

3.1 INTRODUCTION

In this thesis we report the results of measurements of absolute total and relative differential cross sections for various processes that may result from collisions of atomic negative ions with molecules. Absolute cross sections are measured on one apparatus and the relative differential cross sections on another. The experiments are performed using a beam technique in which the negative ions are produced in an arc-discharge-type ion source, extracted, focused, mass analysed and then focused into a collision region where the target gas is present as a static gas at room temperature. The products of these collisions can be studied by various detection techniques, which will be discussed later. Variations in experimental techniques, peculiar to a particular measurement, will be explained in the appropriate chapter. In this chapter we give a description of each apparatus followed by a discussion of methods used in data analysis.

3.2 TOTAL CROSS SECTION APPARATUS

3.2.1 Ion Source

The ion source used in these experiments is an arc discharge type and consists of a stainless steel cylindrical unit that is closed at both ends. A V-shaped tungsten filament, held by two stainless steel posts, is mounted at one end of the source chamber. The "anode" is a stainless steel disk with an aperture of approximately 0.05 inches diameter in it along the cylinder axis. The tip of the filament is kept at a distance of approximately 0.056 inches from the anode plate. It has been found that a large current of negative ions could be extracted from the source if the filament tip is kept at that distance from the anode hole. Cooling for the source chamber is provided by water flow through a 1/4 inch copper tubing that is hard soldered around the chamber.

The filament is electrically insulated from the anode and is biased approximately -100 volts relative to the anode. To strike an arc, the 0.010 inches Tungsten filament is heated by about 8-11DC amps of current. Source gas is then admitted by a precision leak valve into the chamber through an inlet at the top of the chamber. Electrons, emitted from the filament, undergo collisions with the source gas and sustain an arc discharge. Negative ions are formed in this discharge presumably by dissociative attachment

$$\begin{aligned} e + H_2 &\longrightarrow H^- + H \\ &\longrightarrow H^- + H^*, \end{aligned} \qquad (3.1)$$

polar dissociation

$$e + H_2 \longrightarrow H^- + H^+ + e, \qquad (3.2)$$

or radiative capture

$$e + H \longrightarrow H^- + h\gamma . \qquad (3.3)$$

The negative ions thus produced will be accelerated towards the anode plate and extracted through the anode hole. The advantage of direct extraction of negative ions from a plasma lies in the compactness, smaller emittence and smaller energy spread of the ion beam. A typical energy spread of the primary ion beam within the collision chamber is 0.5eV full width at half maximum (FWHM) for a collision energy of about 30eV.

An energy analysis of the ion beam within the collision chamber indicates that all of the negative ions are formed essentially at the anode. Since all of the negative ions are formed at the anode potential and are accelerated to the collision chamber which is maintained at the ground potential, the final energy of the ion beam, expressed in eV, corresponds approximately to anode to ground voltage.

The ion source used a mixture of Argon with various gases for the production of the desired negative ion beam. For example, for an $H^-(D^-)$ ion beam, a source gas mixture of about 50% Argon and 50% $H_2(D_2)$ is used in a discharge of about 100 milliamps. For F^-, Cl^-, Br^- and I^- ion beams, mixtures of CF_4, CCl_4, CH_3Br, and CH_3I with Argon are used.

The intensity of the ion beam produced varied for different ions. For example, for $H^-(D^-)$, the beam currents ranged from 3-4 nanoamperes at high energy, to a few tenths of a nanoampere at low beam energies. On the other hand, for Cl^-, beam intensity as high as 40 nanoamperes were obtained at the highest collision energies.

3.2.2 Focusing Elements and Mass Spectrometer

After emerging from the source through the anode aperture, the ion beam passes through a series of focusing elements that focus the beam into a Wien velocity filter which serves as a mass spectrometer. A small permanent magnet is placed near the first focusing electrode to deflect undesired electrons from the beam.

The Wien filter utilizes crossed electric and magnetic fields to disperse unwanted charged particles from the beam. When a beam of charged particles enters the filter with a velocity v it will be deflected by the electric field in one direction and by the magnetic field in the opposite direction (see Fig.2). The charged particles will pass undeflected through the filter with a velocity v_o if the two opposing forces are equal, i.e.,

$$qv_oB = qE \tag{3.4}$$

Particles with velocities other than v_o will miss the aperture in the collision chamber, to be collected on the baffle.

The velocities of the charged particles can be obtained by accelerating them through a constant electric potential. In the present apparatus the negative ions are accelerated through a potential (V_k) between the anode and the Wien filter. If V_p is the potential difference between the two plates and d is the plate separation then from equation (3.4)

$$v = \frac{E}{B} = \frac{V_p}{dB} \tag{3.5}$$

since

$$v = \left[\frac{2qV_k}{m}\right]^{\frac{1}{2}} \tag{3.6}$$

we have

$$\frac{2qV_k}{m} = \frac{V_p^2}{d^2B^2} \tag{3.7}$$

or

$$m = 2qV_k\left[\frac{dB}{V_p}\right]^2 \tag{3.8}$$

Thus by adjusting V_k, B and V_p, the mass m of a particular ion can be selected.

3.2.3 Scattering Region

After passing through the Wien filter, the mass-selected primary ion beam enters the collision region which is shown schematically in Fig.3. The main features of the collision region are a cylindrical collision chamber B, a copper disk A, three plane parallel (~ 95% transparent) tungsten grids I-III and a Faraday collector C. A thin guard ring projects into the collision region slightly beyond the surface of elemant A. This prevents the primary ions (which may collide with the inner wall of the aperture) from reaching element A. The scattering path length is defined as the distance (4.643 cm) between the end of this guard ring and grid II. Grid I, element B and element A are kept at ground potential so that all reactions take place in a force free region. Grid II and III are shorted electrically and biased negatively to form the trap for electrons and slow ions. The primary beam current is measured at the Faraday cup C and is biased positively with respect to grid III to suppress secondarily emitted electrons.

The laboratory energy of the primary ion beam is determined by retardation analysis within the collision chamber. The analysis involves determining the primary ion beam intensity (I) as a function of the retarding potential (V) applied to the grids. The derivative of I(V) is observed to have an approximately gaussian shape and the centroid is taken as the beam energy. The full width at half maximum (FWHM) of this gaussian for both H^- and D^- ions is found to vary from 0.2 eV at the lowest collision energies to a maximum FWHM of about 1 eV at 50 eV.

3.2.3.1 Electron Trap

The collision chamber is wrapped with 33 turns of No. 18 magnet wire to provide an axial magnetic field within the chamber. Detached electrons and any slow product negative ions that may result from collisions are separated and trapped within the collision chamber. The trapping of the detached electrons is provided in the following manner: An axial magnetic field is maintained within the collision chamber with a magnitude (5-10G) so that the cyclotron radii of the detached electrons is less than the radius of element A (see Fig.3). Detached electrons with upstream longitudinal momenta go directly to element A. A weak electric field between grids I and II reflects the remaining electrons with opposite longitudinal momenta to plate A. In order to ensure that all electrons are reflected to element A, it is sufficient that the electrostatic potential between grids I and II be about 8% of the laboratory kinetic energy of the primary ion beam with a maximum of 5V. To assure that a negligible fraction of the detached electrons is collected

on the guard ring, the guard ring is maintained at a slightly negative bias of about 0.2V. Such a bias voltage saturates the electron current to element A.

Collisions of the primary ion beam with grids I and II will produce some electrons and slow ions even when there is no target gas in the scattering chamber(i.e., the pressure is $\sim 10^{-7}$ torr). The electron trap will trap these "gas-out" electrons to plate A and slow ions to both plate A and cup B. However the effect of these "gas-out" electrons and ions is small and can be subtracted from the appropriate "gas-in" signal to obtain an accurate indication of the intensity of the detached electrons and slow ions produced by gas phase conditions.

3.2.3.2 Ion Trap

The slow negative ions that may result from charge transfer, ion-molecule reaction, or dissociative charge transfer, although not affected appreciably by the axial magnetic field, will be electrostatically trapped and collected primarily on element B. If there are some energetic forward scattered products then an increase in the trapping voltage will increase the signal observed on element B. For some systems reported here, the signal observed on B was found to increase with increasing trapping potential. For such systems, it was necessary to perform experiments with higher values of trapping potential. This will be discussed in detail in the appropriate section. An additional contribution to the signal observed on B may arise from large angle ($\theta \geq 40^0$) elastic or inelastic scattering of the primary negative ions. The present apparatus does not have any provision for mass analyzing the

product ions and hence cannot distinguish between the slow product ions and elastically or inelastically scattered primary ions which are scattered through angles greater than 40^{o}. Thus the signal on element B cannot be unambiguously identified.

For higher collision energies, the partial cross sections due to large angle scattering of the primary negative ions should be small and this has been found to be the case for rare gas targets. For example, in the case of collisions of H^- and D^- with Ne, the cross sections due to large angle scattering drops smoothly from a value of about $2.5A^2$ at E = 3.5 eV to about 0.14 A^2 at E = 150 eV.

3.2.3.3 Mixed Signals on A

For some systems reported in this study there are several ways in which not only electrons, but negatively charged ions as well, reach element A. This causes some ambiguity about the nature of the signal observed on element A. For some light-on-heavy systems reported here, laboratory backscattering of elastically or inelastically scattered primary ions is possible. Such events are most probable only at very low collision energies and can "contaminate" the measurements of electron detachment cross sections for energies under a few eV. A detailed discussion about the magnitude of this effect has been given by Smith et al.[37] A second and not necessarily insignificant contribution to the ion signal observed on element A will be due to slow ions which arise from charge transfer, ion-molecule reaction or dissociative charge transfer. The fraction f of the product ions collected on element A depends upon the initial angular distribution of the product ions and the magnitude

of the trapping voltage applied between grids I and II. For some systems the product negative ion current collected on element A increases slightly with increasing trapping voltage, since there are some forward scattered product ions with kinetic energies in excess of a few electron volts which are specularly reflected to A by the electric fields between grids I and II.

The dependence of f upon the grid voltage can be explained by noting that product ions travelling forward in the laboratory frame are reflected by the grid II potential hill. If the reflection is specular, some may reach plate A, but if it is diffuse, most of them reach cup B. The reflection will be specular if it occurs in the smooth field between the grids. But if it occurs close to the grids the equipotentials will follow the grid weave, and large angle scattering of the ions becomes possible. Thus a high reflecting potential can scatter the slow forward ions to cup B.

3.2.3.4 Notations

For all the discussions which follow we will use the following notations:

$\sigma_A(E)$: Total cross section calculated by using the signal observed on element A.

$\sigma_B(E)$: Total cross section calculated by using the signal observed on element B.

$\sigma_e(E)$: Total cross section for electron detachment.

$\sigma_I(E)$: Total cross section for slow ion production.

The results of $\sigma_e(E)$ and $\sigma_I(E)$ for various reactants have been found to be markedly different in this study. For the sake of clarity we will break up the ensuing discussion of negative ion-molecule systems into groups for which direct detachment appears to be the dominant mechanism for electron production and one for which reactive (rearrangement) scattering accompanies direct detachment. We will present these results separately in different chapters.

3.2.4 Pressure Measurements

The target gas is maintained at room temperature and the target gas pressure in the collision region is usually in the range of 10^{-4} torr during the experiments. The background pressure prior to admitting the scattering gas into the collision chamber is typically 10^{-7} torr. The absolute pressure within the collision chamber is determined with an MKS Baratron capacitance manometer, which appears to have an accuracy of approximately 5%.[51] The Baratron head was maintained at a temperature of 322K whereas the scattering chamber was at room temperature. The effects of thermal transpiration are taken into account while determining the density of scattering centers

$$N = \frac{P_{MKS}}{k_B(T_{MKS} \times T_{coll})^{\frac{1}{2}}} = \frac{(9{\cdot}658 \times 10^{15})}{(300 \times 322)^{\frac{1}{2}}} P \text{ cm}^{-3} \qquad (3.9)$$

where k_B is the Boltzmann's constant and the subscripts MKS and coll denote MKS Baratron manometer and collision region. P in the above equation is expressed in mtorr and the denominator is the geometric average of the scattering cell temperature and that of the capacitance manometer head.

3.3 DIFFERENTIAL CROSS SECTION APPARATUS

The relative differential cross section apparatus, shown schematically in Fig.4, consists of three main sections. These are a primary ion gun which produces a mass selected ion beam, a collision region which contains the target gas, and a product ion analyzer and detection system.

3.3.1 Primary Ion Gun

The ion source is the same as that used in the total cross section apparatus. After extraction from the source the primary ions are accelerated and focused by a series of focusing elements into a magnetic mass analyzer. The mass analyzer is a 90^{o} double focussing sctor magnet, with a theoretical resolving power of about 1 in 100. The magnetic field for the analyzer is provided by an electromagnet with shaped pole pieces of the same approximate radius. The resolution is such that the spectrometer can very easily resolve the isotopes of chlorine (^{35}Cl, ^{37}Cl).

After emerging from the mass analyzer the primary ions enter the main vacuum chamber and are retarded to the desired collision energy by another series of focusing elements. The ions then enter the collision region.

3.3.2 Collision Region

The collision region consists of two stainless steel nested cylinders of which the inner one is stationary and has an inner diameter of 0.85 inches. A slit (0.125 x 0.035 inches) on this cylinder serve to

define the entering primary ion beam. The scattered products exit by a 0.125 inches high slot cut from 0^{o} to 90^{o} relative to the primary ion beam. The outer cylinder has a slot-slit geometry and can be rotated about the inner cylinder. The rotation allows the scattered products to be detected at various laboratory angles without obstructing the incoming primary beam, since the primary beam enters through the slot in the outer cylinder. Apart from the slits, the colision chamber is essentially "gas tight". Two parallel deflection plates, insulated from the main body of the collision chamber, facilitate the measurement of primary ion beam entering the collision chamber. This is done by deflecting the primary beam with a transverse electric field to one of the plates and reading the current to the same plate with a general radio electrometer. Current inside the collision chamber is typically in the range of $10^{-11} - 10^{-10}$ A.

3.3.3 Detection System

The collision region is followed by a one inch long grounded drift tube. The end of this tube which is farthest from the collision chamber is covered with a 95% transparent tungsten grid. This arrangement eliminates electric fringing fields from the collision region.

Scattered ions, emerging from the collision chamber, can be accelerated or retarded before they enter the electrostatic energy selector. The selector consists of $127^{o}17'$ coaxial cylindrical sections with radii 3 cm and 4 cm. The entrance slit is electrically insulated from the selector and is used to accelarate or retard the scattered ions before their energies are measured. In this way, the resolving power

and transmission of the 127° analyzer is held constant as the accelerating potential is scanned to perform the analysis. Consistent relative data are obtained in this manner, although no attempt is made to obtain absolute differential cross sections.

Mass analysis of the transmitted ions is then done by means of a quadrupole field radio-frequency mass filter (RFMF). This type of mass filter has been described previously in detail.[52-54]

Ions transmitted through the RFMS are detected with a channeltron multiplier whose design and operating characteristics have been well documented.[55] The output of the multiplier can be monitored as DC current on an electrometer, or in a pulse counting mode. The DC mode was always used to monitor the primary beam. The product ion currents were always measured by counting the output pulses. In this mode, the output is capacitively coupled to a charge sensitive preamplifier, followed by a linear amplifier which also shapes the pulse, and this signal is fed to a single channel pulse height analyzer.

The whole experimental setup is interfaced with a Commodore 2001 series personal computer. During the experiments the computer acquires the data, stores it in the memory and plots it.

As the product energy approaches zero, the sensitivity of the secondary ion analysis system will also fall, possibly at a faster rate. As a result, product ions with more than 10 eV energy are easily detected, but for the product ions below a few eV detection becomes difficult.

The entire detection system is mounted on a rotatable platform which pivots about the center axis of the collision chamber. The exit slit which defines the scattering angle is mechanically coupled to this

platform such that the exit slit of the collision chamber and the entrance slit of the velocity selector are in parallel planes, each having a normal plane which bisects the centers of both apertures simultaneously.

The scattering angle θ is accurately determined by a potentiometer circuit located inside the vacuum system. A wiper connected to the rotatable platform slides along a precision resistor wire which carries a constant current and is supported on a circular metal form. The wire is insulated from the metal by a Teflon strip. By measuring the voltage drop between the wiper and one end of the wire the scattering angle can be determined accurately to within one-tenth of a degree.

3.3.4 Vacuum System

The vacuum system consists of a main chamber and an ion gun chamber, which are connected by the momentum analyzer tube as shown in Fig.4. The ion gun chamber contains the ion source and the focusing elements and is pumped by two 2-inch, 30 liters/sec mercury diffusion pumps which are liquid nitrogen trapped and water cooled and backed by a mechanical fore pump. The main vacuum chamber contains the collision region and the detection system and is housed in an aluminium cylinder with an inner diameter of 28 inches and a height of 24 inches. This chamber is evacuated by a 6 inch 260 liters/sec diffusion pump and is backed by a mechanical fore pump. The pressure in each chamber is monitored by an ionization gauge. It normally takes 3–4 hours for the whole system to pump down to a working pressure of 10^{-6} torr.

3.4 DATA ACQUISITION AND REDUCTION

3.4.1 Total Cross Section

The total cross sections for slow ion and electron production are determined separately. The detached electrons and slow ions are collected on plate A and cup B as currents I_A and I_B respectively. The cross sections $\sigma_A(E)$ and $\sigma_B(E)$ are calculated by using the currents on plate A and cup B in the equation

$$I_{A,B} = I_o\left[1 - \exp(-NL\sigma_{A,B})\right] \tag{3.10}$$

where I_o is the primary ion current, L is the reaction path length, and N is the density of scattering centers. The above equation can be written in the form

$$\sigma_{A,B} = -\left[\frac{1}{NL}\right] \ln\left[1 - \frac{I_{A,B}}{I_o}\right] \tag{3.11}$$

Grids I-III have the effect of absorbing fractions of detached electrons, slow ions and the primary ion beam. Before being collected on A (or B), some of the detached electrons (or ions) must pass through grid I twice, causing some absorption of the detached electrons (or ions). This absorption has been determined to be 2 ± 2 %.

The attenuation of the primary ion beam by the grids was determined to be $(20 \pm 1$ %). This was done by retarding the primary ion beam with grid I and measuring the ion currents collected on A and B. This number was confirmed by measuring the current to each of the three grids independently when the primary beam was allowed to pass through

all the grids. The attenuation was found to be independent of the primary beam energy and corresponds roughly to the absorption predicted by the optical transparency of the grids (95% each).

Including the above corrections, the cross section is then determined by

$$\sigma_{A,B} = -\left[\frac{1}{NL}\right] \ln\left[1 - \frac{1.02I_{A,B}}{1.20I_C}\right] \qquad (3.12)$$

3.4.2 Differential Cross Section

To facilitate analysis of the differential data, a brief discussion of the collision kinematics will now be given. Consider a general binary collision of the type

$$A + B \longrightarrow C + D \qquad (3.13)$$

Here A is regarded as the projectile particle, B as the target molecule which is at rest in the laboratory frame, and C as the product particle which is observed at an angle θ with respect to the incident beam direction. Let M_1, M_2, M_3, and M_4 denote the masses and E_1, E_2, E_3, and E_4 the laboratory kinetic energies of the incident, target, detected and unobserved particles. Notice that the suffix 3 always refers to the observed product. The endothermicity is represented by Q. Thus an endothermic reaction has negative Q. Conservation of energy and linear momentum then gives for E_3 as

$$E_3 = \frac{M_1M_3E_1}{(M_1+M_2)^2}\left[\cos\theta \pm (1/\gamma^2 - \sin^2\theta)^{\frac{1}{2}}\right]^2 \tag{3.14}$$

where

$$\gamma = \left[\frac{M_2M_4}{M_1M_3}\left\{1 + Q\,\frac{(M_1+M_2)}{E_1M_2}\right\}\right]^{-\frac{1}{2}} \tag{3.15}$$

It is convenient to rewrite this in terms of θ

$$\theta = \text{arc cos}\left[\frac{1 + \beta^2 - 1/\gamma 2}{2\beta}\right] \tag{3.16}$$

where

$$\beta = \left[\frac{(M_1+M_2)^2}{M_1M_3}\,\frac{E_3}{E_1}\right]^{\frac{1}{2}} \tag{3.17}$$

and of Q

$$Q = E_3\left(1 + \frac{M_3}{M_4}\right) - E_1\left(1 - \frac{M_1}{M_4}\right) - \frac{2(E_1E_3M_1M_3)^{\frac{1}{2}}}{M_4}\cos\theta \tag{3.18}$$

Note that if $\gamma > 1$, then the observed product particles always travel in the forward direction in the lab within a cone of half-angle θ_{max} where

$$\theta_{max} = \text{arc sin}\,(1/\gamma) \tag{3.19}$$

For such a situation two center of mass scattering angles, χ_f and χ_b, exist for each laboratory angle θ. Scattering associated with

χ_f is referred to as "forward scattering" whereas that associated with χ_b is referred to as "back-scattering". If $\gamma < 1$, then all laboratory angles are accessible to the product particles and hence laboratory back-scattering of the product particles is possible.

The differential cross section apparatus can be used to measure doubly differential cross sections for a given product ion. For example, differential cross section in angle can be obtained by fixing the energy of the primary ion beam and observing the intensity of the scattered ions at various angles. Similarly, for a given scattering angle, the differential cross section in energy can be obtained by varying the energy of the primary ion beam and observing the intensity of the scattered ions at the given angle.

In connection with the present studies, this apparatus has been used to measure the inelastic energy loss spectra of the scattered projectile. Furthermore, this apparatus has also been used to identify the product ions which are the results of negative ion molecule collisions.

Chapter IV

TOTAL CROSS SECTIONS FOR COLLISIONS OF H^- AND D^- WITH HYDROGEN MOLECULES

4.1 INTRODUCTION

Absolute cross sections for electron detachment have been measured for collisions of H^- and D^- with H_2, D_2, and HD for energies E ranging from the energetic thresholds for collisional detachment up to several hundred electron volts. Special emphasis is given to the cross section measurements near the threshold region. Rate constants are calculated from the measured detachment cross sections for various systems. In addition to the electron detachment cross sections, we have also measured the cross sections for the production of slow negative ions that result from collisions of the above reactants. These low-energy product ions may arise from ion-molecule (or rearrangement) reactions such as

$$D^- + H_2 \longrightarrow H^- + HD, \tag{4.1}$$

or dissociative charge transfer

$$D^- + H_2 \longrightarrow H^- + H + D. \tag{4.2}$$

4.2 EXPERIMENTAL METHOD

For these systems the detachment and ion production cross sections are determined by using the expression (3.12). The trapping of electrons and ions is accomplished by using an electrostatic potential which is about 8% of the laboratory kinetic energy of the primary ion beam with a maximum of 5V.

The absolute calibration of the laboratory energy scale is subject to errors associated with surface and contact potentials. A detailed discussion of these problems has been given by Smith et al.,[37] where experiments were performed in the present apparatus to estimate the uncertainty in the energy scale of the primary beam. The results of those experiments suggested that the uncertainty in absolute calibration of the laboratory energy of the primary beam was less than 0.25 eV. Extreme caution was taken in measuring the energy of the primary beam in the present studies and all the detailed considerations which assure accurate determination of collision energy, as discussed by Smith et al., were also followed in the present experiments. The uncertainty in the laboratory energy scale of the primary ion beam in the present studies should be no more than 0.25 eV. Furthermore, in the present studies, a mixture of H_2 and D_2 was maintained in the ion source and H^- and D^- ion beams were available in all the experiments simply by tuning the Wien filter to pass the desired ion. All the measurements reported here were done in a continuous experimental run without turning the filament off or venting the system to atmosphere. This assures that any systematic error that might affect the measurements should be identical for both ion beams.

The ion production cross section $\sigma_I(E)$ is found to be much smaller than the detachment cross section $\sigma_e(E)$ over the entire energy range investigated. Thus, the measurements of the electron detachment cross sections, $\sigma_e(E)$, which are based on the signal observed at element A will represent a true measure of detachment for these systems.

For $E \geq 2$ eV, the measurements for the electron detachment cross sections are estimated to have an accuracy of $\pm 10\%$ and they are reproducible to within 5%. For $E \leq 2$ eV, the uncertainty in the measurements increases as the energy is decreased because the intensity of the primary beam at the lowest collision energies drops significantly. The smallest cross sections which can be measured with any statistical significance are 0.02 and 0.03 A^2 for the D^- and H^- projectiles, respectively.

4.3 RESULTS AND DISCUSSION

At low collision energies, there are several inelastic processes that may be important in collisions of negative ions with molecular targets. The reactions that are important for the present studies (in addition to target vibrational and rotational excitation) are

$$H^- + BC \longrightarrow e + H + BC, \tag{4.3}$$

$$\longrightarrow B^- + HC, \tag{4.4}$$

$$\longrightarrow B^- + H + C. \tag{4.5}$$

In the discussion to follow we will first examine the near threshold region for electron detachment for all the systems studied, followed by a discussion of $\sigma_e(E)$ and $\sigma_I(E)$ at higher energies. Finally, rate constants, calculated from the measured detachment cross sections for various systems, will be presented.

4.3.1 THRESHOLD BEHAVIOR

The experimental results for $\sigma_e(E)$ for collisions of H^- and D^- with H_2, D_2, and HD in the threshold region are given as functions of relative collision energy in Figs. 5 and 6. These low energy results are subject to the effects of apparatus broadening which is due primarily to the thermal motion of the target gas (at 300K). A manifestation of this broadening is an apparent onset for detachment which is lower than the true threshold for the process.

Thus, in order to obtain significant information about the true threshold, it is necessary to correct the experimental data for the

effects of broadening. This has been done for all the systems reported here by assuming that the actual cross section for the reactions studied has the form

$$\sigma = 0 \quad \text{for } E < E_T , \tag{4.6}$$

and

$$\sigma = Q(E - E_T) \quad \text{for } E \geq E_T. \tag{4.7}$$

The next step consists of convoluting this assumed cross section and then fitting the convoluted results to the experimental data by varying Q and E_T. The convolution problem has been discussed in detail by Chantry[56] and we have employed his results [Eq.(30) of Ref. 56] to determine the effects of broadening.

It should be mentioned here that the only other important source of apparatus broadening is due to the laboratory energy spread of the primary ion beam. For the $H^- + H_2$ system, this broadening effect can be described by a convolution function of characteristic width $W_b = 0.20(2/3) \simeq 0.13$ eV where 0.20 eV is the laboratory energy spread of the primary ion beam at the lowest collision energies. This source of broadening is uncorrelated with that arising from the thermal motion of the target gas. The broadening due to thermal motion alone can be approximated by a Gaussian function with FWHM given by[56]

$$W_a = (11.1\gamma k_B T E)^{\frac{1}{2}} \tag{4.8}$$

where γ is the ratio of the projectile mass to the total mass. For the $H^- + H_2$ system, with $k_B T = 0.025$ eV and E = 1.5 eV, Eq.(4.8) gives $W_a = 0.37$ eV. Thus, the effective width is

$$W = (W_a^2 + W_b^2)^{\frac{1}{2}} \approx W_a \qquad (4.9)$$

and it is reasonable to neglect the broadening due to the energy spread in the primary ion beam.

The results of fitting the convolutions of (4.7) are given as solid lines in Figs. 5 and 6. As can be seen from the figures, the convolutions can be brought into excellent agreement with the experimental observations. The parameters that have been used to fit the experimental data for various molecular targets (which are at a temperature of 300K) are listed in table 2.

TABLE 2

Threshold parameters for collisional detachment

Projectile	Target	True Threshold E_T(eV)	$Q(A^2/eV)$
H^-	H_2	1.45±0.10	1.12
H^-	D_2	1.45±0.10	1.12
H^-	HD	1.45±0.10	1.06
D^-	H_2	1.20±0.10	0.70
D^-	D_2	1.20±0.10	0.98
D^-	HD	1.30±0.10	0.98

An interesting aspect of these observations is that the thresholds for collisional detachment are considerably higher than the electron affinity of hydrogen atom, i.e., 0.75 eV. Similar observations have been re-

ported in studies of the collisional detachment of halogen anions by various molecular targets.[45,29] It should be stressed that the differences in the observed values of the thresholds for the H^- and D^- projectiles should not be affected by any systematic error in the determination of the laboratory energies of the primary ion beams.

It is of interest to know if detachment involves a charge transfer to the $^2\Sigma_u^+$ shape resonance of H_2^- which lies about 2 eV above the ground state of H_2. This point has been investigated for 420 $\leq E \leq$ 1000 eV by Tuan and Esaulov[15] in experiments which measure the energy loss spectra of neutral hydrogen atoms produced in collisions of H^- with D_2. Their spectra (for E ~ 420 eV) show a most probable energy loss well below the minimum endothermicity (~2.75 eV) for charge transfer to the resonance, indicating that the resonance is not involved in the detachment processes. Recent experiments by Esaulov et al.[13] on the kinetic energy spectrum of detached electrons in $H^- + H_2$ collisions over the energy range from 10 eV to 4 keV give further evidence that the $^2\Sigma_u^+$ state of H_2^- is not involved in electron production. The present results for $\sigma_e(E)$ do not show any structure at low collision energies. Thus, these low energy measurements cannot be used to infer that the resonance is involved for lower collision energies. Detachment in these systems probably occurs via direct detachment, governed by an appropriate coupling of the ground electronic state of the relevant molecular and negative ion potential surfaces, similar to that already discussed for atomic reactants.

Calculations for the lowest singlet potential-energy surface for H_3^- have been reported by Michels and Paulson.[10] The calculations

were carried out for both linear and triangular (C_{2v}) geometries and for internuclear separations such that the interaction potentials ranged up to about 1.6 eV for the linear geometry and 8.7 eV for the C_{2v} geometry. Moreover, it is reported[57] that the surface for H_3^- lies below the ground state of the corresponding H_3 molecular surface for both geometries. This observation implies that detachment does not occur by the crossing of one surface (H_3^-) into the continuum represented by H_3 (with geometry congruent to H_3^-) plus a free electron. If one assumes that the H_3^- and H_3 surfaces do not exhibit low-energy crossings for intermediate orientations (other than linear and C_{2v}) then detachment probably involves a mechanism in which the reactant states are connected to the product states by some "dynamic coupling". According to this scheme, the energy necessary to promote the electron to the continuum of product states (representing $H + H_2$ along with a free electron of arbitrary energy) is provided by the kinetic energy of the nuclei. As discussed earlier, such a dynamic coupling has been used to describe detachment involving atomic reactants as in the case of H^- + Ne.[6]

It was mentioned in the introduction that an important channel that may compete with electron detachment at low energies is the reactive (or rearrangement) channel. The potential-energy surface calculations for the H_3^- system by Michels and Paulson indicate that the minimum energy reaction path for the ion exchange reaction

$$H^- + D_2 \longrightarrow D^- + HD \qquad (4.10)$$

can occur for a linear configuration with a barrier height of 0.65 eV. On the other hand, the same calculations performed for the C_{2v} symmetry indicate that the minimum energy reaction path leads to dissociation

$$H^- + H_2 \longrightarrow H^- + H + H \qquad (4.11)$$

rather than ion exchange. Studies of the production of H^- and D^- ions from the four reactions

$$D^- + HD \rightleftharpoons D_2 + H^- \qquad (4.12)$$

and

$$D^- + H_2 \rightleftharpoons HD + H^- \qquad (4.13)$$

have been reported by Michels and Paulson.[10] The characteristic features of these cross sections are a common threshold value of ~ 1 eV, a rapid increase from threshold with a maximum between 2 and 3 eV and a sharp decrease thereafter. The most striking features of these cross sections are the large isotope effects which appear to be larger than any others found to date for such abstraction reactions. The cross sections for D^- production for both the processes (4.12) and (4.13) were observed to be smaller than those for H^- production over the entire energy range investigated. For reactions (4.12), the cross section to the right exceeds that to the left by 3:1 for E ~ 3 eV. Reactions (4.13) behave similarly, but with a ratio of 5:1. It is possible that these large isotope effects are related to the differences in thresholds observed in the detachment channels for H^- and D^- in the present studies.

In conclusion, it should be noted that at low collision energies, the de Broglie wavelength of the H^- or D^- ion is comparable to the range of the interaction for $H^- + H_2$, indicating that a detailed quantum treatment may be necessary to adequately describe the collision dynamics for the systems reported in this study.

4.4 CROSS SECTION AT HIGHER ENERGIES

4.4.1 $H^-(D^-) + D_2$

The measured electron detachment cross sections $\sigma_e(E)$ for collisions of H^- and D^- with D_2 are given in Fig.7 for $E \lesssim 200$ eV. $\sigma_e(E)$ shows two distinct features in two different regions of energy. At low collision energy ($2 < E < 10$ eV), $\sigma_e(E)$ scales with relative collision energy whereas at high collision energies ($E > 15$ eV), $\sigma_e(E)$ scales well with relative collision velocity. The velocity scaling of $\sigma_e(E)$ is demonstrated in Fig.8 where the cross sections are plotted as a function of relative collision velocity. These plots show clearly that at high collision energies the detachment cross sections for both isotopes are the same at identical relative collision velocities. Similar isotopic studies of the $H^-(D^-) + H_2$ and other systems by Risley[58] show that velocity scaling of these cross sections continues upto at least 10 keV.

Fig.9 gives the experimental results for the production of slow ions (H^- or D^-) which are products of rearrangement reactions and dissociative charge transfer. An additional contribution to this cross section possibly arises from large angle elastic or inelastic scattering of the primary ions. At high collision energies, the partial cross section due to large angle elastic scattering of H^- or D^- has been found to be small for $H^-(D^-)$ + Ne systems, being about 0.14 A^2 at E = 150 eV. On the other hand, at low energies ($E < 10$ eV), the partial cross section for large angle elastic and inelastic scattering for H^- becomes large, rendering an unambiguous interpretation of the low energy data for $\sigma_I(E)$ impossible. Nevertheless, it is interesting to compare the

present results for $\sigma_I(E)$ for the reaction $H^- + D_2 \longrightarrow D^- + HD$ with those reported by Michels and Paulson.[10] Their measurements indicated that the D^- cross section reached a maximum of about 0.65 A^2 at 3 eV and then decreased smoothly to a minimum in the neighborhood of 10 eV. The present results for $\sigma_I(E)$ indicate that $\sigma_I(3\ eV) \simeq 1.9\ A^2$ and then drops smoothly to a minimum of 0.06 A^2 at $E \simeq 9$ eV. This latter observation is consistent with that of Michels and Paulson while the discrepancy between the two measurements at $E \simeq 3$ eV may, in the present measurements, be due to contributions to $\sigma_I(E)$ which are due to large angle elastic or inelastic scattering of the primary ion beam. The H_3^- potential surface calculations of Michels and Paulson indicate that for the C_{2v} symmetry, the minimum energy reaction path leads to dissociation:

$$H^- + H_2 \longrightarrow H^- + H + H \qquad (4.14)$$

rather than ion exchange. The above process is endothermic by 4.6 eV and the signal observed in the present measurements for $E \geq 9$ eV is probably due to dissociative charge transfer.

4.4.2 $\underline{H^-(D^-)} + \underline{H_2}$

Measurements of $\sigma_e(E)$ for H^- and D^- on H_2 are given in Fig.10. Also given in the figure are some previous results reported by Hasted,[27] Risley and Geballe,[9] and Muschlitz et al.[26] It can be seen that the results of Hasted and Muschlitz et al. lie much lower than the present measurements in the energy range where they overlap, whereas the lowest energy measurements of Risley and Geballe lie about 25% higher than any reasonable extrapolation of the present highest energy measurements. A close inspection of the present measurements for $E > 10$ eV reveals that the velocity scaling of the detachment cross section that has been observed for D_2 and other molecular targets is also operative in the present case. The cross sections $\sigma_I(E)$ for the H_2 target are found to be qualitatively similar to those observed for D_2 over the entire energy range investigated.

4.4.3 $\underline{H^-(D^-)} + \underline{HD}$

The experimental results for $\sigma_e(E)$ are displayed in Fig.11 for the HD target. The cross sections display behavior similar to that observed for other molecular targets: At low collision energies ($2 < E < 10$ eV), $\sigma_e(E)$ scales remarkably well with relative collision energy and at high collision energies the cross sections scale roughly with relative collision velocity. $\sigma_I(E)$ for the HD target shows features that are qualitatively similar to those observed for D_2 presented in Fig.9.

4.5 RATE CONSTANTS

The detachment rate constant K(T) is related to $\sigma_e(E)$ by the expression

$$K(T) = (1.57\times10^{-10}) \frac{1}{\mu^{\frac{1}{2}}} \left[\frac{1}{k_B T}\right]^{3/2} \times \int_{EA}^{\infty} E\sigma_e(E)\exp(-E/k_B T)dE \qquad (4.15)$$

where k_B is the Boltzmann constant expressed in units of eV/K, μ is the reduced mass of the reactants expressed in atomic mass units, EA is the electron affinity, and $\sigma_e(E)$ is the total cross section for electron detachment expressed in units of A^2. With this choice of units of rate constant K(T) is expressed in $cm^3 sec^{-1}$.

The rate constant for a particular reaction is usually defined by assuming that all degrees of freedom of the reactants are in thermodynamic equilibrium and that the equipartition theorem approximately holds true. The translational and internal energies of the reactants are obviously not in equilibrium (in the present experiments) and the assumption of equipartition is not fulfilled. There is no general method available to map rate constants given by Eq.(4.15) into "correct" rate constants in which equipartitioning is satisfied. This problem, in conjunction with drift-tube measurements, has been discussed in some detail by Albritton et al.[59] Nevertheless, a rate constant as defined by (4.15), may be quite close to the true rate constant and could be useful in the modeling of discharges.

An upper limit to K(T) can be obtained from (4.15) by assuming that $\sigma_e(E)$ is the maximum possible value, consistent with the uncer-

tainties in the present measurements. Such an upper limit is obtained by using the experimental measurements of $\sigma_e(E)$ for $E > 1.4$ eV and assuming $\sigma_e(E)=0.03$ A^2 for $0.75 \leq E \leq 1.4$ eV, where 0.03 A^2 represents the previously discussed uncertainty and an upper limit to $\sigma_e(E)$ for $E < 1.4$ eV. A lower bound to K(T) can be determined by inserting the (deconvoluted) linear cross section, given by Eq.(4.7), into the expression for K(T).

The calculated upper and lower bounds of the detachment rates for collisions of H^- with H_2, D_2, and HD are given in Fig.12 as a function of inverse temperature. The rate constants for all the molecular targets increase by more than an order of magnitude as the temperature is increased from 3000 to 6600K. The H_2 target is found to give the largest detachment rate whereas the D_2 and HD targets give almost identical values for the upper bounds of K(T). As the temperature is increased above 5000K, the lower bound of K(T) for H_2 becomes almost indistinguishable from the upper bounds of K(T) for D_2 and HD. Finally, HD is found to give the smallest value of K(T) at all temperatures.

Results for K(T) for the D^- projectile are given in Fig.13. They have been determined in the same manner as that discussed for H^- + H_2, D_2, and HD cases. As can be seen from the figure, the results are qualitatively similar to those found for the H^- projectile.

In conclusion it should be pointed out that the true rate constants (for reactants which are in thermal equilibrium) could, in principle, be considerably different from the upper limits determined with the present measurements. This could be the case if the threshold for detachment is a sensitive function of the vibrational-rotational energy

of the target molecule. However, since the dominant mechanism for detachment in the threshold region is believed to be a direct process, such a sensitivity of the threshold on internal energy is believed unlikely.

4.6 SUMMARY

Absolute total cross sections for electron detachment and negative ions produced by rearrangement or dissociative charge transfer have been measured for collisions of H^- and D^- ions with the isotopic hydrogen molecules in the energy range extending from below detachment thresholds up to several hundred electron volts. The detachment cross sections show a general behavior: At low collision energies ($2 < E < 10$ eV), the detachment cross sections scale with relative collision energy, whereas at high collision energies the cross sections scale with relative collision velocity. It is suggested that detachment in these systems occur via direct detachment with an appropriate coupling between the ground electronic states of the relevant molecular and negative molecular ion potential surfaces.

The corrected detachment cross sections show thresholds for H^- and D^-, which are larger than the electron affinity of the hydrogen or deuterium atom. For H^-, the threshold for detachment is found to be about 0.25 ± 0.10 eV larger than that for D^-. The difference in the observed thresholds is probably related to large isotope effects in the rearrangement channel or diffraction efects that may be important at the lowest collision energies. A detailed quantum mechanical calculation may be necessary to give a reasonable description of the low energy collisional detachment of $H^- + H_2$ (and its isotopic variants) systems.

The results of the cross sections for ion production show similar behavior for all the systems studied. However, only the results above 8 eV are reliable since there is contamination by large-angle scattering at the lowest energies. The possible sources of these ions are rearrangement reactions or dissociative charge transfer.

Upper and lower bounds on detachment rate constants for collisions of H^- and D^- with the isotopic hydrogen molecules have been determined from the measured detachment cross sections. These rate constants are found to be qualitatively similar to each other over the entire temperature range investigated.

Chapter V

TOTAL CROSS SECTIONS FOR COLLISIONS OF H^- AND D^- WITH VARIOUS MOLECULES

5.1 INTRODUCTION

This chapter is concerned with the measurements of $\sigma_e(E)$ and $\sigma_I(E)$ for collisions of H^- and D^- with N_2, CO, O_2, CO_2, and CH_4. The relative collision energies investigated range from about 1 eV up to several hundred eV.

Processes which give rise to the slow negative ions include charge transfer

$$H^- + O_2 \longrightarrow O_2^- + H, \tag{5.1}$$

and dissociative charge transfer as in

$$H^- + CO_2 \longrightarrow O^- + CO + H. \tag{5.2}$$

In several cases it is possible to see how such mechanisms compete with electron detachment.

In what follows, we will present the experimental method and then discuss the results for each molecular target separately.

5.2 EXPERIMENTAL METHOD

The proceses that are important in the present studies are

$$H^- + BC \longrightarrow e + \text{products} , \tag{5.3}$$

$$\longrightarrow (BC)^- + H , \tag{5.4}$$

$$\longrightarrow B^- + HC , \tag{5.5}$$

$$\longrightarrow H^- + BC , \tag{5.6}$$

$$\longrightarrow H^- + (BC)^* , \tag{5.7}$$

$$\longrightarrow B^- + H + C . \tag{5.8}$$

The detachment (5.3) and slow ion (5.4-5.5, 5.8) production cross sections are determined in the usual manner from Eq.(3.12). The potentials used to trap the products are the same as that used for the H_2, D_2 and HD targets.

For the analysis of these data it is assumed that $d\sigma_I/d\Omega$ has an isotropic angular distribution. With this assumption, 20% of all product ions resulting from charge transfer or dissociative charge transfer will arrive at element A and 80% will be detected on element B. This figure (20%) results from averaging (along the collision path) the solid angle subtended by element A for both forward- and backward-moving product ions. Specular reflection by the trapping electric field is assumed for the ions which are initially moving in the forward (primary ion beam) direction. If $d\sigma_I/d\Omega$ is zero for laboratory scattering angles, $\theta \geq 90^o$ (no backscattered products) and isotropic in the forward hemisphere, then only 2.3% of the slow ions arrive at A.

Thus, $\sigma_e(E)$ may overestimate the true detachment cross section by as much as 20% of $\sigma_I(E)$. For all of the targets except O_2, this is inconsequential since $\sigma_e(E)/\sigma_I(E) \sim 5\text{-}10$. The measurements of $\sigma_e(E)$ are reproducible to within 5%. Systematic errors (e.g., pressure and path length measurements) when combined with the uncertain contamination from slow product ions limit the accuracy of the detachment cross section measurements to an uncertainty of ~15% except for the O_2 target where the uncertainty is 20%. Both H^- and D^- are in the ion beam and the measurements for each isotope are made by allowing the appropriate ion to pass through the Wien filter. The ratios of the cross sections, $\sigma_e(E,H^-)/\sigma_e(E,D^-)$, are accurate to 2%.

5.3 RESULTS AND DISCUSSION

5.3.1 $H^-(D^-) + N_2$

The experimental results for the total electron detachment cross sections $\sigma_e(E)$ for collisions of $H^-(D^-)$ with N_2 are given in Fig.14 as a function of relative collision energy. Detachment cross sections for these systems over the energy range 2-100 eV were reported previously.[31] The high energy measurements of these previous experiments did not appear to extrapolate smoothly to the measurements of Risley and Geballe.[9] It was suggested that this "connection" problem might be due to sudden increases in the cross sections in the energy range not covered by either experiment. Thus it was felt that total electron detachment cross sections for these systems should be remeasured with special emphasis on the energy region not covered by any experiments.

The present results for $\sigma_e(E)$ are about 10% below earlier measurements,[31] except in the near threshold region ($E \leq 6$ eV) where the present measurements lie about 20% lower. The 10% discrepency has been noted before[37] and was attributed to possible errors in determining the target gas pressure in the previous measurements. The larger error in the near threshold region is a consequence of using a primary ion beam in the present experiments which has a much narrower energy width than that used in previous experiments, since any broadening effect tends to increase the apparent cross section in the near threshold region. The measured low energy cross sections for $\sigma_e(E)$ should not be contaminated by any low energy product ions, since $\sigma_I(E) = 0$ for the $H^-(D^-) + N_2$ systems.

An important feature of the cross sections shown in Fig.14 is the observation of a dual isotope effect when σ_e is exhibited as a function of E: at the higher relative collision energies, the reactants with the higher relative collision velocity exhibit the larger detachment cross section whereas the trend is just the opposite at low relative collision energies. It is possible that this difference is due to the fact that there are different mechanisms which dominate the detachment in the high and low energy regions. The magnitude of the low energy isotope effect varies from about 5-10% over the energy range 10-40 eV and is consistent with a description of electron detachment that involves the crossing or merging of the discrete reactant state (which represents the interaction potential of the negative ion with N_2) with the continuum of product states (representing $H + N_2$ along with a free electron of arbitrary energy). According to this description, for a given E, both D^- and H^- will follow the same trajectories but with different velocities (the isotopic masses being different) and hence the time spent by D^- in the continuum is larger than that of H^-, resulting in a larger detachment cross section for D^-.

At higher relative collision energies (i.e., E > 50 eV), the isotope effect reverses its character, where the faster reactants give the larger detachment cross section. In addition, it is found that the detachment cross sections in this energy region (i.e., E > 50 eV), increase with relative collision energy and more importantly scale with relative collision velocity: for the same relative velocity the cross sections for the isotopic doublet are approximately the same. This can be seen very clearly from Fig.15 where the electron detachment cross

sections for both isotopes are plotted as a function of relative collision velocity. The experimental results for these systems illustrate that the detachment cross sections are not the same function of relative collision energy, nor are they the same functions of relative collision velocity over the energy range 1-200 eV. The present experiments thus connect two regions: at low collision energy, detachment cross sections for both isotopes are found to be the same at identical collision energies, whereas at high collision energy, detachment cross sections are found to scale with relative collision velocity. For collision energies greater than several hundred eV, this velocity scaling for $H^-(D^-) + N_2$ has been investigated previously[58] and has been found to be valid for energies up to at least 10 keV.

It was mentioned in the introduction that an important contribution to detachment may arise from a process which involves an initial charge transfer to a shape resonance of the molecular target, followed very quickly by decay of the molecular negative ion. This charge transfer process has been studied by Tuan and Esaulov[15] for $200 \leq E \leq 1000$ eV and is found to be quite important in the collisional detachment of H^- by N_2. The energy-loss spectra of the scattered H atoms show three distinct peaks which the authors attribute to direct detachment, detachment via charge transfer and detachment with electronic excitation of N_2. They estimate that 25% of the total electron detachment cross section at $E \simeq 500$ eV is due to detachment with excitation and the remainder is distributed equally between direct detachment and detachment via charge transfer to a shape resonance of N_2^-. These data unambiguously demonstrate the possible role of the shape resonance in the dynamics of detachment by molecular targets.

A theoretical study of the $H^- + N_2$ system has been reported by Tuan et al.[60] in which electron scattering data (i.e., $e + N_2$) are used to calculate the scattering amplitude (taken as a Breit-Wigner resonance amplitude) for the shape-resonance-assisted detachment channel. These calculations nicely reproduce the energy loss spectra of the neutral H-atoms observed in the TOF study in $H^- + N_2$ collisions. Furthermore, these calculations also correctly indicate the relative importance of the $^2\Pi_g$ state in detachment process, viz., ~40% of total detachment cross section at E ~ 1 keV. Such calculations have not been extended to low collision energies, i.e., $E \lesssim 1$ keV.

Risley has measured the kinetic energy spectra of electrons arising from the collisional detachment of H^- by N_2.[11] These measurements show regular oscillations in the kinetic energy spectrum of the detached electrons which is consistent with $N_2^- [^2\Pi_g(v')] \longrightarrow N_2 [^1\Sigma_g^+(v)]$ transitions. The experiments thus give clear indication that the $^2\Pi_g$ resonance state of N_2^- is involved in the detachment mechanism, at least for $E \gtrsim 1$ keV.

Recently, Montmagnon et al.[12] and Esaulov et al.[13] have performed experiments in which the detached electron energy spectra in $H^- + N_2$ collisions was measured for collision energies ranging from about 4 eV to 4 keV. These studies also show spectra which are similar to those observed by Risley and give further evidence that charge exchange to the $^2\Pi_g$ shape resonance of N_2^- is important in the dynamics of detachment for collision energies $E \gtrsim 50$ eV.

Finally, it is reasonable to suggest that the increase in $\sigma_e(E)$ in the present experiments, for $E \gtrsim 50$ eV is due to the onset of

detachment via charge transfer. Despite this increase in $\sigma_e(E)$, the present results still fall about 30% below a previous measurement[9] of electron detachment in $H^- + N_2$ collisions at 193 eV.

The cross sections obtained from the signal observed on element B, $\sigma_B(E)$, for collisions of H^- and D^- with N_2 are shown in Fig.16 as a function of relative collision energy. Also shown in the figure are measurements of $\sigma_B(E)$ for collisions of both H^- and D^- with Ne.

Since $\sigma_I(E)$ should be zero for these reactants, we can view $\sigma_B(E)$ as presented in Fig.16 as the partial (large-angle) elastic and inelastic scattering cross section. The results for Ne represent a partial cross section for only elastic scattering, whereas the minima observed at 9.5 eV for the N_2 target no doubt indicates the region where the partial inelastic and elastic cross sections are comparable.

For a given E and impact parameter b, the c.m. scattering angle (suitably averaged over molecular orientations) for H^- should be equal to that for D^- for potential scattering. However, the laboratory scattering angle for H^- will be slightly greater. This may be the reason that $\sigma_B(E,H^-)/\sigma_B(E,D^-) > 1$, but such effects cannot be separated from possible velocity-dependent collision mechanisms which may be operative.

5.3.2 $\underline{H^-(D^-)} + \underline{CO}$

Fig.17 shows the measured electron detachment cross sections $\sigma_e(E)$ for collisions of H^- and D^- with CO as a function of relative collision energy. A comparison of the detachment cross sections for the CO target with those for N_2 shows that $\sigma_e(E)$ for CO is similar in shape and magnitude to the results for N_2, especially in the high-energy range. Furthermore, for $E \geq 50$ eV, $\sigma_e(E)$ for CO scales approximately with relative collision velocity. At low collision energies (i.e., $E < 30$ eV), the detachment cross sections are found to scale with relative collision energy, with no discernible isotope effect. The scaling behavior suggests that electron detachment proceeds via two distinct mechanisms, one dominating at energies below ~ 30 eV and a different process showing up at higher energies.

The importance of charge exchange in H^- + CO collisions have been investigated by Tuan and Esaulov.[15] Their measurements on the energy-loss spectra of neutral H atoms produced in collisions of 420 eV H^- with CO indicate that the contribution of the $^2\Pi$ resonance of CO to electron production is comparable to that from direct detachment. The increase in $\sigma_e(E)$ with energy, for $E \geq 50$ eV, may then be due to detachment via charge transfer to a shape resonance of $CO^-(^2\Pi)$. For $E < 50$ eV, $\sigma_e(E)$ can be described by the crossing or merging of the negative-ion bound state with the continuum of states representing a neutral molecule and a free electron of arbitrary energy.

As in N_2, a small signal is observed for CO on element B. The cross sections $\sigma_B(E)$ for CO are shown in Fig.18 as a function of relative collision energy. These results are essentially identical to those

for N_2 with the same isotope effect. Based upon this similarity to N_2 (where $\sigma_I = 0$) it is reasonable to assume that σ_I is quite small for CO. Consequently there should be a negligible flux of product ions resulting from the reactions

$$H^- + CO \longrightarrow O^- + O + H \qquad (5.9)$$

$$\longrightarrow C^- + O + H \qquad (5.10)$$

and the results presented in Fig.17 for $\sigma_e(E)$ will not be contaminated by such ions.

The minima in $\sigma_B(E)$ for both isotopes occur at about 12 eV (compared to 9.5 eV for N_2). The increasing signal observed for $E < 12$ eV is due to large-angle elastic scattering of the primary ions. For $E \geq 12$ eV, the signal is probably due to large-angle inelastic scattering of the primary negative ions.

5.3.3 $\underline{H^-}(\underline{D^-}) + \underline{O_2}$

For these reactants, there are several different product channels that are important in the present studies. For the H^- projectile, they include

$$H^- + O_2 \longrightarrow H + O_2 + e \quad (0.75\ eV), \tag{5.11}$$

$$\longrightarrow HO_2 + e \quad (\lesssim -1\ eV), \tag{5.12}$$

$$\longrightarrow O_2^- + H \quad (0.31\ eV), \tag{5.13}$$

$$\longrightarrow OH^- + O \quad (-0.36\ eV), \tag{5.14}$$

$$\longrightarrow O^- + OH \quad (0.003\ eV), \tag{5.15}$$

$$\longrightarrow O^- + O + H \quad (4.403\ eV). \tag{5.16}$$

The energy defects for ground-state reactants and products are also given along with each channel. The measurements of the cross sections for electron detachment, $\sigma_e(E)$, for these systems are influenced somewhat by channels (5.13)-(5.16), i.e., the production of slow negative ions. Thus, the measurements of the cross sections for slow ion production, $\sigma_I(E)$, will be discussed first [by assuming $\sigma_I(E) \simeq \sigma_B(E)$], followed by a discussion of electron detachment.

The experimental results for $\sigma_I(E)$ for collisions of both H^- and D^- with O_2 are given in Fig.19 where the cross sections are presented as a function of relative collision energy. Also given in the figure is a curve representative of the results of Bailey and Mahadevan[38] for the production of slow ions in collisions of H^- with O_2. As is clear in the figure, the cross sections exhibit two distinct peaks for both iso-

topes in two different regions of energy. In order to identify the products contributing to $\sigma_I(E)$, experiments were done for the $D^- + O_2$ system on the apparatus used for differential cross section measurements. The energy for these experiments was varied from about 5 eV up to 150 eV. An extensive search for low-energy O_2^-, OD^-, and O^- was carried out, revealing that at least 98% of the slow product ions were O_2^-. Hence, the measurements presented in Fig.19 are for the production of O_2^-, as given by Eq.(5.13). The O_2^- thus produced will have vibrational quantum numbers $v' \lesssim 3$, since the energy of the O_2^- ($v' \lesssim 3$) molecular ions lies slightly below that of $O_2(v = 0)$. For $v' > 3$, $O_2^-(v')$ is unstable with respect to electron detachment.

A striking feature of the cross sections shown in Fig.19 is the strong isotope effect observed over the entire energy range. The most remarkable feature of $\sigma_I(E)$ is seen when the cross sections due to different isotopes are compared at identical collision velocities rather than identical relative energies. Such plots are shown in Fig.20 where the cross sections $\sigma_I(E)$ are displayed as a function of relative collision velocity. As can be seen from the figure, the cross sections for each isotope are the same at the same relative collision velocity.

In an attempt to understand the mechanism(s) responsible for such behavior, let us assume that the basic dynamics for the charge transfer can be described within the framework of a two-state problem in which the initial and final states involved in the process are given by

$$H^- + O_2(v = 0) \longrightarrow H + O_2^-(v' = 3). \qquad (5.17)$$

The asymptotic energy difference (ΔE) between these two states is given approximately by the electron affinity of the hydrogen atom (0.75 eV). In a two-state approximation, the total cross section contains an oscillatory term which depends upon the collision velocity,[61]

$$\sigma(v) \approx M(v)\sin^2(\Delta Ez/2v) \qquad (5.18)$$

In Eq.(5.18), z/v represents the average time spent in the region where transitions can take place and M(v) represents the coupling of the initial state ($H^- + O_2$) to the final state ($H + O_2^-$).

It is interesting to note that, by inserting reasonable values of z and ΔE into Eq.(5.18), the two maxima and one minimum of Fig.20 are well reproduced, as is indicated in table 3.

TABLE 3

A comparison of the observed extrema of Fig.20 and those predicted by Eq.(5.18) with $z=7a_o$.

Velocities at which extrema are observed (10^6 cm/sec)	Velocities at which extrema are predicted from Eq.(5.18) (10^6 cm/sec)	$\frac{\Delta Ez}{v}$
3	4.5	$3\pi/2$
7	6.8	π
14	13.6	$\pi/2$

Moreover, the total cross section, which should be on the order of $\pi(z/2)^2$ is observed to be just this value. The isotope effect which is observed is compatible with this rather simple model.

At the lowest energies (i.e., E < 3 eV), the cross section for the production of O_2^- decreases with decreasing energy. This may be due to the onset of associative detachment channel (5.12), which will compete with various channels for slow-ion production.

Finally, it should be pointed out that the measured charge-transfer cross section is possibly underestimated by as much as 20%, since about 20% of the O_2^- product ions will be collected on element A, if the O_2^- ions have an isotropic angular distribution. Also, similar to N_2 and CO, a small number of negative ions from large-angle elastic or inelastic scattering of the primary ions will undoubtedly reach element B, causing $\sigma_I(E)$ to be overestimated by (in this case) 5-10%.

Fig.21 shows the cross section for electron detachment, $\sigma_e(E)$, for collisions of H^- and D^- with O_2 as a function of relative collision energy. $\sigma_e(E)$, as shown in the figure, is obtained by subtracting 25% of $\sigma_I(E)$ from the measured detachment cross section. This subtraction procedure is important for these systems since the charge-transfer cross section is relatively large by comparison.

Curves representative of the experimental measurements for $\sigma_e(E)$ by Bailey and Mahadevan[38] and Risley and Geballe[9] are also given in Fig.21. It can be seen that the results of Bailey and Mahadevan are in good agreement with the present results. At the highest energies, where the present results overlap with those of Risley and Geballe, the measurements of Risley and Geballe lie about 35% higher than the present results.

For $H^- + O_2$, there are several mechanisms in addition to direct detachment which can result in the production of free electrons. The charge exchange reaction (5.13) is endothermic by 0.31 eV for the formation of $O_2^-(v' = 0)$. However, O_2^- may be produced in a vibrationally stable (i.e., $v' \leq 3$) or unstable (i.e., $v' > 3$) state. For $v' > 3$, O_2^- will autodetach to give free electrons and the neutral O_2 molecule.

This has been found to be the case in the experiments of Itoh et al.[49] and Esaulov et al.[13] who have reported the results of measurements of the energy distribution of detached electrons resulting from the collisions of H^- with O_2. Itoh et al. performed the experiment at a laboratory collision energy of 150 eV and found that charge transfer to the autodetaching O_2^- states was dominant over direct detachment at that collision energy. Structure in the kinetic energy spectrum of the detached electrons was found to correspond to the process

$$H^- + O_2(v=0) \dashrightarrow H + O_2^-(v') \longrightarrow H + O_2(v'') + e \qquad (5.19)$$

where $v' = 4, 5, 6, 7,$ and 8 and $v'' = 0$. The state with $v' = 4$ had the dominant excitation.

The experimental findings of Esaulov et al.[13] are similar to those of Itoh et al.[49] and extend from 4.5 eV to 4 keV. These experiments also reveal that charge transfer to the vibrationally excited state of $O_2^-(v' > 3)$ is the dominant channel (compared to direct detachment) for electron production over the entire energy range investigated. At the highest collision energy some evidence for electronic excitation of O_2^- was also observed.

For E > 4 eV, the results for $\sigma_e(E)$ as presented in Fig.21 will then have a contribution from both direct detachment and detachment via the autodetaching states of $O_2^-(v' > 3)$. In the present experiments it is impossible to separate direct detachment from detachment via charge transfer. However, based upon the above discussion, it seems reasonable to assume that direct detachment is minor compared to detachment via charge transfer to the vibrationally excited states of $O_2^-(v' > 3)$ over the energy range presented in this study.

Previous experimental studies have demonstrated that, for selected reactants, associative detachment may compete with direct collisional detachment and charge transfer at very low collision energies.[36,62] Thus, associative detachment [Eq.(5.12)] may be an important source of detached electrons. The apparent increase in the measured detachment cross section $\sigma_e(E)$ as the energy is decreased below 2.4 eV is probably due to the onset of associative detachment. In this energy region, $\sigma_I(E)$ decreases while $\sigma_e(E)$ increases as the energy is decreased. Finally, the decrease in $\sigma_e(E)$ as E is increased above 150 eV is in accordance with the observations of Risley and Geballe[9] and Bailey and Mahadevan.[38]

5.3.4 $\underline{H^-(D^-)} + \underline{CO_2}$

The various possible channels of interest for these systems are

$$H^- + CO_2 \longrightarrow H + CO_2 + e \qquad (0.75\ eV), \tag{5.20}$$

$$\longrightarrow O^- + HCO \qquad (\sim 3.6\ eV), \tag{5.21}$$

$$\longrightarrow OH^- + CO \qquad (-0.026\ eV), \tag{5.22}$$

$$\longrightarrow (CO_2^-)^* + H \longrightarrow O^- + CO + H \qquad (4.74\ eV) \tag{5.23}$$

The energy defects for the ground-state reactants and products are listed for each channel. Fig.22 shows the experimental results for $\sigma_I(E)$ for collisions of H^- and D^- with CO_2 as a function of relative collision energy. These cross sections show distinct peaks at 13 eV with the most pronounced peak being observed for the H^- projectile. In order to identify the product ions that contribute to $\sigma_I(E)$, experiments were performed for the $D^- + CO_2$ system with the same differential apparatus as was used for O_2^- identification . A thorough search was made for O^-, OD^-, O_2^-, and C^- and it was found that at 13 and 17 eV, essentially all of the low-energy product ions were O^-, implying that the peak observed at 13 eV is due to the production of O^- ions. For E = 7.4 eV, around 85% of the signal was found to be O^- and 15% of the observed ions were OD^-.

Several of the resonance states of CO_2^- (at 4.4, 8.2, and 13.0 eV) are known[63-64] to be instrumental in the production of O^- ions in collisions of electrons with CO_2,

$$e + CO_2 \longrightarrow (CO_2^-)^* \longrightarrow O^- + CO \qquad (5.24)$$

It may well be that these same resonances are involved in the production of O^-(Eq. 5.23) which is observed in these experiments. However, the present total cross section measurements cannot establish which, if any, of these resonance states might be involved. It is of interest to point out that doubly differential cross section measurements for the $H^- + CO_2$ system performed in this laboratory indicate that these resonances are involved in the inelastic (but nondetaching) scattering of H^- by CO_2. This observation is similar to that reported earlier for the system $Cl^- + CO_2$.[65]

At the lowest collision energies, $E \lesssim 10$ eV, the partial cross section for large-angle elastic and inelastic scattering for H^- becomes large, rendering an unambiguous interpretation of the low-energy data for $\sigma_I(E)$ impossible.

The results of electron detachment cross sections $\sigma_e(E)$ for collisions of H^- and D^- with CO_2 are presented in Fig.23 as a function of relative collision energy. The detachment cross sections for both isotopes scale very well with relative collision energy in the low-energy (i.e., $E < 7$ eV) region. For $7 < E < 30$ eV, a strong isotope effect (25 - 30%) is observed where the D^- projectile gives the larger detachment cross section. This isotope effect changes character as the collision energy is increased above 30 eV, where the H^- projectile gives the larger detachment cross section. An interesting feature of $\sigma_e(E)$ is that it decreases in a region where $\sigma_I(E)$ increases. The maxima in $\sigma_I(E,H^-)$ observed at $E \simeq 13$ eV may be correlated to the minima in $\sigma_e(E,H^-)$ at the same energy due to a competition among the channels responsible for O^- production and electron detachment.

Another interesting feature of $\sigma_e(E)$ is seen in Fig.24 where the cross sections are plotted as a function of relative collision velocity. Here the basic features of $\sigma_e(E)$ are seen to scale rather well with velocity, except for the lowest collision velocities where the results scale with energy, as mentioned earlier.

Tuan and Esaulov[66] and Tuan et al.[67] have reported the results of measurements of differential TOF energy loss spectra of neutral H atoms which are the products of H^- + CO_2 collisions. These studies reveal that the $^2\Pi_u$ resonance state of CO_2^- is definitely involved in the neutralisation of H^- by CO_2 for $150 \leq E \leq 1000$ eV. Studies of the kinetic energy spectra of the detached electrons in H^- + CO_2 collisions give further evidence that the $^2\Pi_u$ resonance state participates in the dynamics of detachment for collision energies above 100 eV[13].

The neutral H atom spectra at E = 500 eV indicate that the $^2\Pi_u$ resonance channel becomes relatively more important (compared to direct detachment) as the scattering angle is increased.[66] Furthermore, a significant amount of detachment with concomitant target (projectile) excitation is also observed at this energy. The energy loss ($\Delta E \approx -11$ eV) associated with the target (projectile) excitation is commensurate with the several core-excited resonance states of CO_2^- [68]. By integrating over all possible scattering angles, Tuan and Esaulov estimate that at E = 500 eV about 40% of total detachment cross section arises from detachment with simultaneous excitation.

Thus, in the collisional detachment of H^- by CO_2, direct detachment may not be the principal mechanism of producing free electrons at high collision energies ($E \geq 50$ eV). For $E \geq 50$ eV, $\sigma_e(E)$ as

shown in Fig.23 may have a significant contribution from detachment via charge transfer to the $^2\Pi_u$ shape resonance and detachment with simultaneous target (projectile) excitation. Detachment at low collision energies may be solely due to direct detachment.

5.3.5 $\underline{H^-(D^-)} + \underline{CH_4}$

Total electron detachment cross sections $\sigma_e(E)$ for H^- and D^- incident on CH_4 are given in Fig.25 as a function of relative collision velocity. The cross sections display behavior similar to that which has been observed for other molecular targets: at low collision energies, $\sigma_e(E)$ scales well with relative energy, and at high collision energies the cross sections scale remarkably well with relative collision velocity. One distinctive feature for these reactants is that $\sigma_e(E)$ decreases with increasing collision energy for $E \geq 50$ eV.

Fig.26 shows the cross sections for $\sigma_B(E)$, for collisions of H^- and D^- with CH_4 as a function of relative collision energy. A significant isotope effect is observed for $E \geq 40$ eV, with $\sigma_B(H_2)/\sigma_B(D_2) \sim 2$ for $E = 200$ eV. The general shapes of $\sigma_B(E)$ for both isotopes are observed to be similar over the entire energy range.

It is not known which product ions contribute to $\sigma_B(E)$. The formation of CH_2^- or CH^- is endothermic by a few eV and they may be formed by some direct ion-molecule interaction or by charge transfer to a resonance state of CH_4^-.[69]

A comparison of Fig.26 with Fig.25 reveals that $\sigma_B(E)$ increases in a region where $\sigma_e(E)$ decreases. Furthermore, it can be seen that for a particular isotope, the decrease in $\sigma_e(E)$ is comparable with the increase in $\sigma_B(E)$. The process responsible for the structure observed in $\sigma_B(E)$ may then compete with the detachment channel thereby depleting $\sigma_e(E)$ at higher collision energies.

5.4 SUMMARY

Measurements of total cross sections for the production of electrons and slow negative ions which result from collisions of H^- and D^- with the molecules N_2, CO, O_2, CO_2, and CH_4 illustrate that several processes are important in the dynamics of detachment. At low collision energies, the detachment cross sections scale with relative collision energy, whereas at high collision energies the cross sections scale with relative collision velocity with respect to isotopic substitution. $\sigma_e(E)$ for O_2 show behavior which is different from that of other molecular targets. The different scaling behavior of $\sigma_e(E)$ at different regions of energy suggests that for all the molecular targets except O_2 direct detachment may be the unique detachment mechanism at low collision energies. At high collision energies, both direct detachment and detachment via charge transfer become important in electron production.

The systems $H^-(D^-) + O_2$ show a unique behavior. At low collision energies, i.e., $E < 4$ eV, $\sigma_e(E)$ displays structure and is attributed to a competition between associative detachment and charge transfer. Above 4 eV, the autodetaching states of $O_2^-(v' > 3)$ is suggested to be the principal source of electrons. This suggestion is consistent with the experimental findings of Esaulov et al.[13] and Itoh et al.[49]

For the CO_2 target a strong isotope effect and structure is observed in the detachment cross section. The structure observed in $\sigma_e(E)$ is attributed to possible competition between direct detachment and charge transfer to the negative-ion resonance states of CO_2^-.

The cross sections for the production of slow negative ions, $\sigma_I(E)$, which is zero for N_2, is found to be negligible for CO. For

O_2, the cross section for O_2^- formation is observed to exceed that found for electron detachment. The striking feature of these charge-transfer cross sections is that large oscillations in these cross sections are observed to scale remarkably well with relative collision velocity. A simple two-state model is used to describe the observed charge transfer. The electron detachment channel is neglected in this description of charge transfer. Neglect of the detachment channel is consistent with the observation that detachment for these systems occur predominantly via the autodetaching states of O_2^-. For CO_2 and CH_4, the ion production cross section quite small and displays some structure. In the case of CO_2, the product ions are identified as O^- and it is suggested that the negative-ion states of $(CO_2^-)^*$ may be instrumental in the production of these O^- ions.

Chapter VI

REACTIVE SCATTERING AND ELECTRON DETACHMENT OF HALIDE IONS BY ISOTOPIC HYDROGEN MOLECULES

6.1 INTRODUCTION

For many systems, electron detachment by molecular targets cannot be treated in isolation. This is due to the fact that some type of rearrangement or reactive collision channel often accompanies (and sometimes dominates) electron detachment, especially at low collision energies. The manner in which electron detachment "competes" with conventional reactive scattering in collisions of negative ions with molecules is not well understood.

In this chapter we consider collisions of systems which illustrate the competition between electron detachment and rearrangement processes (such as reactive and ion-exchange collisions). The results of the measurements of absolute total cross sections for electron detachment and reactive scattering which arises from collisions of F^- and Cl^- ions with the isotopic hydrogen molecules are presented. The reactions which have been studied are

$$A^- + BC \longrightarrow C^- + AB \qquad (6.1)$$

and

$$A^- + BC \longrightarrow e + \text{products} \qquad (6.2)$$

where A^- = F^-, Cl^- and BC = H_2, D_2, and HD. The collision energy for the experiments extends from below the energetic thresholds for both reactions (6.1) and (6.2) up to a laboratory collision energy of about 300 eV.

A theoretical description of reactions (6.1) and (6.2) for reactions of O^- with D_2 has been presented in a "trajectory surface leaking" model[70] by Herbst et al.[71] In this calculation, detachment is described in terms of a complex potential with a local width.[72] Other than this, it appears that there are no detailed theoretical studies of reactive collisions of negative ions with molecules.

Although reactive scattering involving the negative ions F^- and Cl^- has received only minimal attention, the same is not true for the neutral parents of these negative ions. Over the past few years, a considerable amount of work has been devoted to studies of the reaction dynamics of hydrogen-halogen systems, particularly for F and Cl on H_2, D_2, and HD.[73-80] An extensive review on the application of classical trajectory techniques to reactive scattering has been given by Muckerman[73] and this review has revealed considerable insight into the dynamics of the F + H_2, D_2 and HD systems. Although most of this work is relevant to collision energies which are lower than those of the present study, there has been one theoretical study[76] at higher collision energies for the F + HD system. These "hot-atom-chemistry" results bear some resemblence to our present results for F^- + $H_2(D_2)$. This will be discussed later.

In what follows we will give a description of experimental method, and the results for F^- and Cl^- projectiles.

6.2 EXPERIMENTAL METHOD

For these systems, some product ions with kinetic energies in excess of a few electron volts were detected. The product negative ion current collected on element A increased slightly with increasing trapping voltage applied between grids I and II. This is because the energetic product ions are scattered in the forward direction in the laboratory frame and are specularly reflected to A by the electric field between grids I and II.

In order to determine the cross sections for the processes

$$F^- + H_2 \longrightarrow e + \text{products} \qquad (6.3)$$

$$F^- + H_2 \longrightarrow H^- + \text{products} \qquad (6.4)$$

separately, it was necessary to perform the experiments with two values of the trapping voltage which can be designated V_{LO} and V_{HI}. In the first experiment, the ion signal to A was minimized by using a low trapping voltage $1 \lesssim V_{LO} \lesssim 5$ V, which was nonetheless sufficient to trap all the detached electrons. Still, there will be some small $H^-(D^-)$ current arriving at plate A. In order to ascertain the fraction of $H^-(D^-)$ yield which is collected on A, experiments were performed at relative collision energies below the threshold for electron production (~2 eV) but above the threshold for forming H^- or D^- products (~1.28 eV). This assures that all of the current detected at plate A is due to product negative ions. A branching ratio can be defined as

$$R(E) = \frac{I_A(E)}{I_B(E)}, \qquad E \lesssim 2 \text{ eV} \qquad (6.5)$$

where $I_A(E)$ and $I_B(E)$ are the product ion currents detected to plate A and cup B. R(E) thus defined represents the ratio of $H^-(D^-)$ yield which reaches A compared to that which reaches B. R(E) was found to be approximately independent of energy and for F^- was 2% - 5% depending upon the target molecule. The cross section for electron production $\sigma_e(E)$ is obained by assuming that R(E) will remain constant for E > 2 eV:

$$\sigma_e(E) = \sigma_A(E) - R\,\sigma_B(E) \tag{6.6}$$

where $\sigma_A(E)$ and $\sigma_B(E)$ are cross sections computed in the usual manner from the signals observed on A and B.

To deduce the cross section for $H^-(D^-)$ production it is necessary to increase the trapping voltage to assure that all of the fast, forward scattered $H^-(D^-)$ is reflected. The trapping voltage was increased until the sum $\sigma_A(E) + \sigma_B(E)$ reached saturation. The cross section for $H^-(D^-)$ production was then determined by

$$\sigma_I(E) = \sigma_A(E) + \sigma_B(E) - \sigma_e(E) \tag{6.7}$$

where $\sigma_e(E)$ is determined by the procedure described above. To assure saturation, it was found that the trapping voltage V_{HI} should be approximately one-third of the laboratory kinetic energy of the primary negative ion beam. This indicates that some of the forward scattered $H^-(D^-)$ ions have fairly high laboratory kinetic energies.

It should be mentioned that these measurements should not be contaminated by F^- or Cl^- scattering to cup B because of the small maximum scattering angle for these reactants (e.g., 6^o for $F^- + H_2$).

The mass of Cl^- was taken to be 35.5 for the conversion to relative energies since the wien filter has insufficient resolution to separate the two isotopes of Cl^-. The cross sections reported here should have an accuracy of $\pm$15%, the uncertainty being primarily due to the subtraction technique employed in Eq.(6.6).

6.3 RESULTS AND DISCUSSION

6.3.1 $F^- + H_2$, D_2 , HD

For these reactants, there are several distinct product channels which may be important in the present studies. For the hydrogen target, they are

$$F^- + H_2 \longrightarrow H^- + HF \qquad (1.28\ eV)\ , \qquad (6.8)$$

$$\longrightarrow H^- + H + F \qquad (7.12\ eV)\ , \qquad (6.9)$$

$$\longrightarrow H + HF + e \qquad (2.03\ eV)\ , \qquad (6.10)$$

$$\longrightarrow F + H_2 + e \qquad (3.40\ eV)\ , \qquad (6.11)$$

$$\longrightarrow F + H + H + e \qquad (7.87\ eV)\ . \qquad (6.12)$$

The endothermicities for ground state reactants and products are listed along with each product channel. The endothermicities for the analogous reactions with D_2 and HD targets are slightly different [except for Eq.(6.11)] due to differences in the zero-point energies of the various deuterated molecules. The experimental results for $\sigma_e(E)$, the cross section for free electron production and $\sigma_I(E)$ the cross section for H^- or D^- production, are displayed in Fig.27 for the D_2 target, where they are plotted as a function of the relative collision energy. $\sigma_I(E)$ is the sum of cross sections for Eqs.(6.8) and (6.9) and $\sigma_e(E)$ is the sum of the cross sections for Eqs.(6.10) - (6.12). The endothermicities for the product channels (6.8)-(6.12) are also indicated in the figure.

At low energies, $\sigma_I(E)$ is found to be an order of magnitude larger than the electron detachment cross section and exhibits an onset compatible with channel (6.8). For E < 7 eV, energetic considerations dictate that the sole mechanism for D^- production is due to process (6.8). It is of interest to note that the general shape and magnitude of $\sigma_I(E)$ for E < 10 eV strongly resembles the results of trajectory calculation by Muckerman[76] for the reactive scattering of fast F atoms,

$$F + HD \longrightarrow HF(DF) + D(H) \qquad (6.13)$$

The detachment cross section $\sigma_e(E)$ is seen to be surprisingly small over the entire energy range of the experiment. For low energies, electron detachment may accompany reactive scattering according to the following scheme:

$$\begin{aligned} F^- + H_2 \longrightarrow (F\text{-}H\text{-}H)^- &\longrightarrow H^- + HF \\ &\longrightarrow HF + H + e \end{aligned} \qquad (6.14)$$

This suggestion is supported by the bell-shaped form of $\sigma_e(E)$, which is similar in shape to that of $\sigma_I(E)$ and essentially all endothermic ion-molecule reactions. For $E \geq 10$ eV, the dominant contribution to $\sigma_e(E)$ is probably from direct detachment as in Eq.(6.11).

For $E \geq 10$ eV, the $H^-(D^-)$ production may arise from either Eq.(6.8) or (6.9). The trajectory calculations of Muckerman for F + HD[76] show a substantial tailing of the cross section for the reactive scattering for relative collision energies up to about 30 eV. Moreover, these same calculations also indicate a rather large (~2.2 A^2) and flat cross section for collision-induced dissociation (CID) F + HD

---> F + H + D which is predicted to be the dominant channel at high energies. It is plausible that in our case the rather flat behavior of $\sigma_I(E)$ for $E \geq 10$ eV is also indicative of the CID channel (6.9). However, since we do not observe such a large cross section for $E \geq 10$ eV, any connection between our observations for negative ion-molecule reactions and the calculations for the comparable neutral reactants must be made with caution.

Let us next examine the effects of isotopic substitution upon $\sigma_I(E)$. These results are shown in Fig.28, where these cross sections for H_2, HD, and D_2 targets are presented. For the HD target the cross section measurement does not distinguish between H^- and D^- products.

A substantial isotope effect is observed in the region of the maximum of $\sigma_I(E)$. At low energies ($E < 10$ eV), the magnitude of the cross secton increases in the order D_2 : HD :H_2. This ordering is not preserved, however, for $E \geq 10$ eV, where the cross section for the HD target behaves somewhat differently than that of the H_2 and D_2 targets. The behavior of the isotope effect with energy can be seen more clearly if one examines the ratios of the cross sections for the various isotopic targets. Let us define these ratios as

$$R_{24} = \frac{\sigma_I(H_2)}{\sigma_I(D_2)}, \text{ etc.} \qquad (6.15)$$

where the subscripts on R refer to the masses of H_2 and D_2 respectively. The ratios $R_{24}(E)$ and $R_{23}(E)$ are given in Fig.29. The interesting feature for $R_{24}(E)$ is that this ratio decreases slowly as the energy is increased from threshold, and then displays a local maximum at an energy

of about 7 eV. In contrast to $R_{24}(E)$, the plot of $R_{23}(E)$ shows a minimum at this energy. These features at about 7 eV are observed in a region which is near the onset of the CID channel and where the cross section for electron detachment maximizes. As may be seen in Fig.29, a plot of the ratio of the summed cross sections

$$\mathcal{R}_{24} \equiv \left[\frac{\sigma_I(H_2) + \sigma_e(H_2)}{\sigma_I(D_2) + \sigma_e(D_2)} \right] \qquad (6.16)$$

also displays a similar feature in the same region. This suggests that the origin of this structure lies mainly in the reactive scattering dynamics.

Fig.30 shows the cross sections for electron detachment $\sigma_e(E)$ for all three targets. The scale for the cross section is enlarged by a factor of about 8 when compared to Figs.27 and 28. The measurements clearly demonstrate that electron detachment occurs by two distinct mechanisms. For $E \gtrsim 10$ eV, it is found that $\sigma_e(E)$ increases in the order D_2 : HD : H_2. Thus for a given E, the reactants with the higher collision velocity exhibit the larger detachment cross section for $E \gtrsim 10$ eV. Moreover, in this energy range, the three detachment cross sections are found to be approximately the same when compared at identical collision velocities (or laboratory energies). This behavior, along with a small detachment cross section, is indicative of electron detachment via dynamic coupling rather than a curve crossing of the negative ion state into the continuum of states representative of product channels which include free electrons. Thus, it appears that the potential surface for (F^--H_2) generally lies below that for (F-H_2) and

that detachment occurs via Eq.(6.11) for $E \geq 10$ eV. The mechanism which "promotes" the electron from the negative ion surface up to the detachment continuum depends upon the velocity of the colliding nuclei. Such a mechanism has been observed for several negative ion-atom systems[31,81] and has been discussed in some detail by Gauyacq.[5,6]

For $E < 10$ eV, detachment by the different isotopes is not a universal function of the collision velocity, but rather is a universal function of the relative collision energy. The mechanism for detachment in this low energy regime must be due to some type of surface crossing which is not available for the direct electron detachment channel given by Eq.(6.11). This is compatible with the earlier suggestion that low energy electron detachment occurs by Eq.(6.10) as a companion to reactive scattering given by Eq.(6.8).

To illustrate the above idea with a model, let us assume that there exists a region in configuration space associated with reactive scattering where the ($FH-H^-$) surface lies above that for (FH-H). Such a region will be unstable with respect to detachment, and one can attempt to describe detachment in terms of the decay of a quasistationary state of width Γ as was done in the trajectory leaking model.[70,71] If one assumes that the total reactive cross section is given by Eq.(6.14), i.e., $\sigma_R(E) = \sigma_e(E) + \sigma_I(E)$, then (within the framework of our model) the low energy electron detachment cross section may be written as

$$\sigma_e(E) = \sigma_R(E)\, P_d(E) \qquad (6.17)$$

where $P_d(E)$ is the average detachment probability for a given E. As $P_d(E)$ is small, one can write

$$P_d(E) \simeq 1 - \exp(-\bar{\Gamma}\,\Delta t/h) \simeq \bar{\Gamma}\,\Delta t/h \tag{6.18}$$

where Δt is the time the product H^- or (D^-) spends in the aforementioned unstable region and $\bar{\Gamma}$ is the suitably averaged value for the autodetachment width. Thus,

$$\frac{\sigma_e(E,H_2)}{\sigma_e(E,D_2)} \approx \mathcal{R}_{24}(E)\frac{\bar{\Gamma}(H_2)\Delta t(H_2)}{\bar{\Gamma}(D_2)\Delta t(D_2)} \tag{6.19}$$

For $E \simeq 6$ eV, the above ratio of the detachment cross sections is observed to be about 1.1. If we approximate $\Delta t(H_2)/\Delta t(D_2)$ by the square root of the ratio of the reduced masses of the products (H^- + HF and D^- + DF) and take $\mathcal{R}_{24}(6\text{ eV})$ from Fig.29, then

$$\bar{\Gamma}(H_2) \,/\, \bar{\Gamma}(D_2) \approx 1.25 \tag{6.20}$$

Such a result is not unreasonable, since the impact parameters which lead to reactive scattering in Eq.(6.14) for the H_2 target are undoubtedly different from those which lead to reactive scattering for the D_2 target [this is presumably the reason that $\mathcal{R}_{24}E) > 1$]. Consequently, one cannot expect the ratio $\bar{\Gamma}(H_2)/\bar{\Gamma}(D_2)$, which is an average over all reactive impact parameters and molecular orientations, to be unity. Although this analysis and description of the low energy electron detachment is plausible, it is probably an oversimplified description of the reaction dynamics.

To conclude our discussion on F^-, let us examine the near-threshold region for $\sigma_I(E)$ in some detail. As indicated in Eq.(6.8), the endothermicity for reactive scattering is 1.28 eV. It is of inter-

est to know if there is a potential barrier to reactive scattering for the $F^- + H_2(D_2)$ reactants. In order to explore this question it is necessary to correct the results of Fig.28 for the effects of broadening which, in this experiment, are due primarily to the thermal motion of the target gas (which is at 300K). The near-threshold results for $\sigma_I(E)$ for both D_2 and H_2 targets are shown in Fig.31. Also shown in this figure are the results of a convolution which assumes a step function cross section, a target gas temperature of 300K, and a threshold of 1.28 eV. These convolutions [from Eq.(29) of Ref.56] are seen to be in excellent agreement with the experimental observations. It is clear that, if a barrier to reactive scattering exists, it is no larger than about one-tenth of an eV.

6.3.2 $\underline{Cl^-} + \underline{H_2}$, $\underline{D_2}$, $\underline{HD}$

The several channels which have been studied for these systems, along with their ground state endothermicities are listed below for the H_2 target.

$$Cl^- + H_2 \longrightarrow H^- + HCl \qquad (2.91\ eV)\ , \qquad (6.21)$$

$$\longrightarrow H^- + H + Cl \qquad (7.34\ eV)\ , \qquad (6.22)$$

$$\longrightarrow HCl + H + e \qquad (3.66\ eV)\ , \qquad (6.23)$$

$$\longrightarrow Cl + H_2 + e \qquad (3.60\ eV)\ , \qquad (6.24)$$

$$\longrightarrow Cl + H + H + e \qquad (8.09\ eV)\ . \qquad (6.25)$$

The endothermicities for the D_2 and HD targets are slightly different from those given in Eqs.(6.21)-(6.25) for H_2.

Fig.32 shows $\sigma_I(E)$ and $\sigma_e(E)$ for $Cl^- + D_2$. As in the case of F^- projectile, $\sigma_I(E)$ displays a local maximum at about twice the threshold energy for Eq.(6.21), i.e., at about 6 eV. However, in the present case, the magnitude of $\sigma_I(E)$ at low energies is about an order of magnitude smaller than the detachment cross section. At higher energies ($E > 8$ eV), a broad plateau is observed for $\sigma_I(E)$, which could be related to the CID channel (6.22). In this region the magnitude of the cross section is of the same order as for F^-, viz. 0.42 A^2. In contrast to the $F^- + D_2$ case, $\sigma_e(E)$ is found to be large and is the dominant process for energies above 8 eV.

Fig.33 illustrates $\sigma_I(E)$ for all three isotopic targets. It is interesting to note that the ordering of the maxima in Fig.33, HD :

H_2 : D_2, is the same as that for Eq.(6.21) with isotopic substitutions, viz.,

$$Cl^- + HD \longrightarrow H^- + DCl \qquad (2.89\ eV)\ , \qquad (6.26)$$

$$\longrightarrow D^- + HCl \qquad (2.94\ eV)\ , \qquad (6.27)$$

$$Cl^- + H_2 \longrightarrow H^- + HCl \qquad (2.91\ eV)\ , \qquad (6.28)$$

$$Cl^- + D_2 \longrightarrow D^- + DCl \qquad (2.93\ eV)\ . \qquad (6.29)$$

Hence, the lowest threshold gives the largest cross section.

The results for $\sigma_e(E)$ are shown in Fig.34 for all three targets. The endothermicities for Eqs.(6.23) and (6.24) are essentially identical, thus prohibiting an unambiguous identification of the electron channel. However, based upon the slight bump in $\sigma_e(E)$ (at $E \simeq 6$ eV) for HD target, it appears that low energy electron detachment may occur with accompanying reactive scattering [Eq.(6.23)] for HD, but perhaps not for H_2 and D_2 targets. For $E \gtrsim 7$ eV, the three detachment cross sections exhibit similar behavior, but the results for the HD target again appear to be somewhat unique with $\sigma_e(E)$ having the smallest magnitude. The isotope effects observed in $\sigma_e(E)$ are not consistent with a simple model for detachment based upon either a quasistationary state or dynamic coupling type description, since according to these descriptions, the detachment cross sections for HD target should lie between those of H_2 and D_2 targets. This is contrary to present observation. This behavior indicates that detachment must be affected by some other inelastic channel which in this case may be reactive scattering as in Eq.(6.23). Thus, contrary to the F^- case, detachment in Cl^- colli-

sions appears to occur as a companion of reactive scattering even at relatively high energies.

There is additional experimental evidence in support of this conclusion. Cheung and Datz[16] studied the electron detachment of Cl^- in collisions with H_2 and D_2 in the energy range commensurate with the present study. Using TOF techniques to determine the energy loss spectra of chlorine atoms produced by detachment, they were able to resolve four distinct detachment channels characterized by different energy losses. The energy loss spectra indicate that three different detachment mechanisms are operative throughout the whole energy range investigated. These mechanisms correspond to i) direct detachment, ii) dissociation of the target molecule which probably leads to $H^-(D^-)$ production or detachment and iii) detachment via charge transfer to the $^2\Sigma_g^+$ state of H_2^- (which involve Franck-Condon transitions from ground state H_2). Since the $^2\Sigma_g^+$ state crosses the $(^3\Sigma_u^+)$ H_2 molecular potential curve, the H_2^- can decay into either a pair of H atoms plus a free electron or into an H atom and an H^- ion.

Relative cross section measurements of the above three processes indicate that the direct detachment channel becomes dominant at the higher energies, but that all channels are important in this energy range. It should be pointed out that the energy dependence of the sum of these individual cross sections is in general agreement with the detachment cross section measurements presented in Fig.34. Based upon the observations of Cheung and Datz, it is now clear why no single mechanism is capable of explaining the isotope effects as observed in the total detachment cross sections in the present study.

6.4 SUMMARY

Absolute total cross sections for inelastic collisions of F^- and Cl^- with H_2, D_2, and HD have been measured over the relative energy range $1 \leq E \leq 30$ eV. The product channels investigated in this study include both electron detachment and the production of hydrogen (or deuterium) negative ions.

F^- PROJECTILE

The electron detachment cross sections $\sigma_e(E)$ are considerably smaller than the cross sections for ion production $\sigma_I(E)$. For the $F^- + H_2$, D_2, and HD reactants, the mechanisms for electron detachment and $H^-(D^-)$ production appear to be different at low ($E < 10$ eV) and high ($E \geq 10$ eV) collision energies:

Low energy

The production of H^- is accompanied by the formation of HF, and $\sigma_I(E)$ is about an order of magnitude larger than $\sigma_e(E)$. It is suggested that electron detachment occurs at low collision energies in conjunction with reactive scattering. A model for electron detachment is proposed in which detachment occurs due to the "electron" leaking from H^- into the continuum as H^- exits from HF. For all three targets, the near-threshold behavior of $\sigma_I(E)$ is consistent with a reactive cross section which is assumed to have the form of a step-function with a threshold of 1.28 eV. The magnitude of $\sigma_I(E)$ are dependent upon target with an isotope effect of about 20% [$\sigma_I(E)$ is the largest for the H_2 target.]

High energy

Significant isotope effects are observed for $\sigma_e(E)$, which indicate that the electron detachment cross sections scale with the collision velocity rather than the relative collision energy, as in the low energy region. Thus, detachment occurs via dynamic coupling of the negative ion state to that of the continuum representative of electron detachment. For the F^- projectile $\sigma_e(E)$ does not exceed 0.6 A^2 for the energy range studied. This contrasts with $\sigma_e(E)$ for F^- and other molecules.[29] $\sigma_I(E)$ also remains small (~0.8 A^2) for this high energy region and is attributed to collision-induced-dissociation.

Cl^- PROJECTILE

The results for Cl^- projectile are strikingly different from those for F^-. Here electron detachment is the dominant feature rather than the production of $H^-(D^-)$. The cross sections for $\sigma_e(E)$ are similar to those observed for other Cl^- - molecule systems.[45] For the HD target, a small bump in $\sigma_e(E)$ at low collision energies suggests that electron detachment may occur in conjunction with reactive scattering, as was observed for the F^- projectile. This is not observed for the H_2 and D_2 targets. The cross sections for $\sigma_I(E)$ exhibit maxima at $E \simeq$ 6 eV, irrespective of target. The magnitudes of the maxima are strongly target dependent, however. The isotope effects found in $\sigma_e(E)$ suggest that detachment cannot be described by any single mechanism for these reactants.

Calculations of potential surfaces for these systems are not currently available. The many and varied features observed for the various cross sections in this study should provide adequate tests for trajectory calculations and models for collisional detachment.

Chapter VII

ABSOLUTE CROSS SECTIONS FOR CHARGE TRANSFER AND ELECTRON DETACHMENT OF HALIDE IONS ON CHLORINE

7.1 INTRODUCTION

This chapter presents the results of cross section measurements for collisions between the halide ions Cl^-, Br^-, and I^- and the chlorine molecule, Cl_2. The absolute total cross sections for electron detachment and for reactive scattering leading to the production of slow ions have been determined for relative collision energies from a few eV to about 120 eV. We also report doubly-differential measurements of the inelastic scattering cross section of I^- on Cl_2 for relative energies of about 17-40 eV. The following processes need to be considered:

$$X^- + Cl_2 \longrightarrow e + \text{products}, \tag{7.1}$$

$$\longrightarrow Cl^- + Cl + X, \tag{7.2}$$

$$\longrightarrow Cl_2^- + X, \tag{7.3}$$

$$\longrightarrow Cl^- + Cl^+ + X^-, \tag{7.4}$$

$$\longrightarrow XCl^- + Cl, \tag{7.5}$$

$$\longrightarrow Cl^- + XCl. \tag{7.6}$$

where $X^- \equiv Cl^-$, Br^-, and I^-. The slow ion production cross section represents a sum of the processes (7.2) - (7.6).

Interest in the chlorine molecule stems from its usage in the rare gas-chlorine laser media[82-85] and its practical value in ionized media for material processing.[86] There is at present considerable interest in the environmental effects of molecular negative ions containing chlorine in the D-region of the ionosphere.[87]

There has been one early study by Hasted and Smith[27] which reported cross sections for electron detachment in collisions of Cl^- with Cl_2 in the energy range 10-2500 eV. These results are compared with ours later, but it appears that at the lowest energies these earlier studies did not manage to fully resolve ions from electrons. Dimov and Roslyakov[88] have measured the cross sections for Cl^- and Cl_2^- formation in collisions of Cl^-, Br^-, and I^- with Cl_2 molecules. The energy range of their study extended from 300 eV to 3000 eV. Hughes et al.[89] have studied other halide-halogen systems at energies below those in the present study. They observed thresholds and branching ratios but did not obtain the absolute cross sections. The study of dissociative electron attachment to Cl_2 has yielded useful information[90,91] about various intermolecular potentials. Peyerimhoff and Buenker[92] have calculated potential curves for the ground and excited states of Cl_2 and ground state of Cl_2^-. The molecular anion has also been the subject of photodissociation studies by Sullivan et al.[93] The existence of bound linear trihalide ions is well established,[89,94-96] but little is known yet of their potential structure. Charge transfer and dissociative charge transfer measurements can provide information on the crossings of the various potential surfaces.[97,98]

To the best of our knowledge there appear to be no published simultaneous measurements of absolute cross sections for electron detachment and slow ion production in collisions of halogen negative ions with Cl_2 molecules over the energy range extending from a few eV to about 120 eV in the c.m. frame. In this region the cross section for the production of slow ions is greatest, and a relatively simple classical analysis can be used to explain some features of the potential structure.

7.2 EXPERIMENTAL METHOD

For these reactants, the cross sections calculated from the signal observed on element B, $\sigma_B(E)$ was found to be much larger than those calculated from the signal observed on element A, $\sigma_A(E)$ (viz., for $I^- + Cl_2$, $\sigma_B(E) \approx 41A^2$ and $\sigma_A(E) \approx 1\ A^2$ at a relative energy of about 13 eV). Consequently, the measurements of electron detachment cross sections, $\sigma_e(E)$, which are based on the signal observed on element A overestimate the true detachment cross section by $f\sigma_B(E)$, where f represents the fraction of the slow ions that reach plate A. The detachment and ion production cross section should therefore be corrected, and they are determined in the following manner: Let $\sigma_T(E)$ represent the sum of the cross sections $\sigma_e(E)$ and $\sigma_I(E)$. We can write

$$\sigma_T(E) = \sigma_A(E) + \sigma_B(E) = \sigma_e(E) + \sigma_I(E) \tag{7.7}$$

and

$$\sigma_A(E) = \sigma_e(E) + f\sigma_I(E) \tag{7.8}$$

Therefore

$$\sigma_I(E) = \sigma_B(E)/(1-f) \qquad (7.9)$$

and

$$\sigma_e(E) = \sigma_A(E) - f\sigma_B(E)/(1-f) \qquad (7.10)$$

The initial angular distribution of the ions produced in the reaction strongly influences the value of f, which is not known except for the special case of isotropic scattering, when it is approximately 0.2, as was discussed in chapter V. Scattering can be expected to be isotropic in the case of complex formation and, perhaps, when the products result from dissociative charge transfer, as in (7.2.)

For collision energies below the threshold for electron detachment the entire signal on A must be due to ions. The value of $\sigma_A(E)$ at this point is approximately $0.02\sigma_B(E)$, so f is taken to be 0.02 here.(The exact values were slightly different for the different reactants). The behavior of f(E) as E increases above a few eV has to be estimated. There are two extremes: f can rise linearly with E to a maximum of 0.2 (due, say, to an increasing importance of Eq.(7.2), or alternately f can remain constant and small at a few percent. For the purpose of presenting the experimental data we will choose the former extreme, in which f rises linearly with rising collision energy, reaching its maximum (corresponding to isotropically scattered products) at about 100 eV. Error bars on the data will be used to illustrate how the data would vary if the alternate choice for f(E) were used. It is em-

phasiized that the general conclusions and observations about the measurements reported herein are not appreciably altered by either prescription for f(E).

For all of the experiments reported here the magnitude of the trapping voltage used was 8% of the laboratory kinetic energy of the primary ion beam, with a maximum of 5V for $E_{lab} \geq 50$ eV. Thus, product ions having forward lab energy greater than 5 eV will only be detected with low efficiency, and the term "slow" ions is used in this discussion to mean those product ions which are fully trapped. Accurate measurements of detachment and ion production cross sections in collisions of negative ions with reactive gases such as chlorine is difficult. The chlorine took an exceptionally long time to reach a stable pressure on being admitted to the target chamber. This may have been because a chemical equilibrium was being established between the gas and the walls of the apparatus. In order to minimize such effects, the whole collision chamber (made out of brass) was passivated with chlorine for several hours before measurements were made. Cross section measurements made under such conditions were reproducible to within 10-15%. Later, the collision chamber was gold plated, and many of the measurements were repeated. There was no systematic change in the data, but a marginal improvement in the equilibrium time was observed. There was no improvemnt in the scatter in the data.

The differential apparatus was used for two purposes: measuring relative differential cross sections and identifying product ions. In connection with this second use, it has to be borne in mind that the radiofrequency mass filter (RFMF) is looking at an energy-analyzed sam-

ple, and is covering a small solid angle of the product ions. When the fluxes of two different products are compared, a systematic error will be present if the laboratory spatial distributions differ. Quantitative integration of the differential cross section has not yet been accomplished. This problem is present in apparatuses used elsewhere.[99] As the product energy approaches zero, the sensitivity of the secondary ion analysis system decreases rapidly. As a result, product ions with more than 10 eV energy are easily detected, but for those below a few eV detection becomes difficult, and estimates of total fluxes of very slow ions cannot be reliably compared to count rates observed at higher product energies.

7.3 RESULTS AND DISCCCUSSION

In Figs.35, 36, and 37, measurements of the total cross sections for electron detachment, $\sigma_e(E)$, and for "slow" ion production, $\sigma_I(E)$, are presented for Cl^-, Br^-, and I^- respectively on Cl_2. The striking feature of these measurements is the large magnitude of the cross sections for "slow" ion production. The peak in the $I^- + Cl_2$ cross section is the largest observed in this laboratory for any system. Equally surprising is the very small size of the electron detachment cross section shown in Fig.37 for the $I^- + Cl_2$ system: within the experimental limits discussed above, $\sigma_e(E)$ could well be zero for collision energies below 40 eV. The only other systems[35,81] known to have such a low detachment cross section for energies well above threshold is $I^- + Ne$, although other detachment cross sections for I^- are significantly smaller than those of the other halides. This observation has not been explained in terms of any property of I^-.

The following discussion will mainly concern the systems $I^- + Cl_2$, although analogous conclusions may be drawn for the other systems measured. The channels available to the system are listed below:

$$I^- + Cl_2 \longrightarrow e + I + Cl_2 \qquad (3.06\ eV) \qquad (7.11)$$

$$\longrightarrow Cl_2^- + I \qquad (0.61\ eV) \qquad (7.12)$$

$$\longrightarrow Cl^- + Cl + I \qquad (1.92\ eV) \qquad (7.13)$$

$$\longrightarrow Cl^- + ICl \qquad (-0.23\ eV) \qquad (7.14)$$

$$\longrightarrow \quad ICl^- + Cl \qquad (0.2\ eV) \qquad (7.15)$$

$$\longrightarrow \quad Cl^- + Cl^+ + I^- \qquad (11.8\ eV) \qquad (7.16)$$

The endothermicities for ground state reactants and products are given beside each channel.

Hughes et al.[89] have made studies on systems that are analogous to those studied here. By studying the reactions

$$\begin{aligned} Cl^- + I_2 &\longrightarrow I_2^- \\ &\longrightarrow ClI^- + \text{products}, \\ &\longrightarrow I^- \end{aligned} \qquad (7.17)$$

and isotope exchanges in

$$\begin{aligned} Br^- + Br_2 &\longrightarrow Br_2^- \\ &\qquad\qquad + \text{products} \\ &\longrightarrow Br^- \end{aligned} \qquad (7.18)$$

they conclude that a linear trihalide complex is involved in reactions for energies below about 3 eV. Above this threshold, non-reactive charge transfer dominates. This picture presumably holds for $I^- + Cl_2$, in that ICl and ICl^- may be formed preferentially below about 3 eV according to the scheme

$$\begin{aligned} I^- + Cl_2 &\longrightarrow (Cl\text{-}I\text{-}Cl)^- \longrightarrow ICl^- + Cl \\ &\qquad\qquad\qquad\quad \longrightarrow Cl^- + ICl \end{aligned} \qquad (7.19)$$

However, at low energies, large angle elastic scattering in our total cross section apparatus (which has 4π sensitivity and no mass discrimi-

nation) rises steeply as the primary ion energy is reduced thus rendering cross section measurements below 3 eV ambiguous.

Based upon the observations of Hughes et al., we will assume that for $E \geq 5$ eV, the principal contributions to the cross sections presented in Figs. 35 - 37 are due to charge transfer and dissociative charge transfer, (7.12) and (7.16).

The measurements of σ_I cannot distinguish between channels (7.12)-(7.16), so the apparatus for differential cross section measurements was used to identify products. The branching ratios so obtained should be taken as qualitative. Only a small solid angle at 0^o in the forward direction was sampled, and no search was made for ICl^-. Both Cl^- and Cl_2^- were observed as products with most probable kinetic energies of about zero eV. No attempt has been made to allow for the different spatial distributions of the two products in estimating the following branching ratios at a given relative collision energy. It was observed that for E_{rel} = 6 eV to 18 eV (which spans the peak in σ_I) 75% of the observed slow ion flux was due to Cl^-, but that this fraction fell to 40% at E_{rel} = 35 eV. Small signals corresponding to product Cl^- and Cl_2^- ions with lab energies higher than 7 eV were also observed in the differential apparatus. Their contributions to the total σ_I are insignificant.

Considerable information about the potentials of Cl_2 and Cl_2^- is available. For example, the potentials of Cl_2^- have been investigated[90,91] by observing the attachment of free electrons to Cl_2. Electron attachment to the $^1\Sigma_g^+$ ground state of neutral chlorine can lead to the formation of bonding $^2\Sigma_u^+$ ground state or the unbound states of

the negative molecular ion Cl_2^-. The potential curves of all of these states of Cl_2^- are found to cross the ($^1\Sigma_g^+$) Cl_2 state at various distances and correspond to the dissociation limit $Cl(^2P_{3/2}) + Cl^-(^1S_0)$ of Cl_2^-. The energy of the $^2\Sigma_u^+$ state and the various excited states of Cl_2^- at the crossing points is greater than the dissociation energy of Cl_2^-. Therefore if a Cl_2^- ion is formed by electron attachment to the $^1\Sigma_g^+$ state of Cl_2, then the resulting Cl_2^- must dissociate into Cl^- and Cl fragments with kinetic energies of a few tenths of an eV.

Peyerimhoff and Buenker[92] have calculated potentials for the ground state and many excited states of Cl_2 along with the ground state of Cl_2^-. Fig.38 depicts the ground state potentials for Cl_2 and Cl_2^- with I^- or I serving as a benign spectator. Also indicated in Fig.38 is one antibonding potential for Cl_2^- representative of the $^2\Pi_{g1/2}$ and $^2\Pi_{g3/2}$ states.[90] These potentials are obviously schematic in nature and are an oversimplification of the true three dimensional potential surfaces. Nevertheless, some qualitative inferences may be drawn from the potentials of Fig.38.

First, it can be noted that ground state Cl_2^- cannot be formed in a Franck-Condon transition since the equilibrium separation for Cl_2^- differs considerably from that of Cl_2. The role of "bond-stretching" in charge transfer of similar systems (e.g., $K + O_2$) has been discussed by Kleyn and co-workers.[97,98] In such bond stretching the target molecule relaxes as the electron donor approaches, reaching the equilibrium separation of the molecular negative ion for relatively large impact parameters. At this point charge transfer becomes highly probable and the charge transfer cross section may be quite large. For such a

picture to be valid, the collisional and vibrational times must be comparable. Using the measured cross section it can be inferred that the collision time for $I^- + Cl_2$ is about 1.3×10^{-13} seconds at 13 eV which is about twice the vibrational period of Cl_2. Clearly, such a mechanism may be important for charge transfer in the present systems.

For collisions which involve C_{2v} symmetry and small impact parameters, charge transfer may also occur through the ground state of ICl_2^-, which is bound when the I is between the two Cl atoms.[95] For other arrangements there is probably still an attractive potential seen by the incoming I^-. It is known that as the I^- approaches the Cl_2 molecule the equilibrium separation of the Cl atoms tends to increase,[96] at least in solution. This may also be regarded as a bond stretching mechanism.

In any case, as I^- approaches Cl_2, the Cl-Cl separation increases, and the potential surfaces cross, allowing transitions to the $I + Cl_2^-$ product states. Depending upon the degree of bond stretching, the final products may be vibrationally excited or even dissociate.

The production of Cl^- can occur by many mechanisms, including a Franck-Condon transition to the ground state of Cl_2^-. Any transition to an unbound state of Cl_2^- (one of the Π_g states is depicted in Fig.38) results in Cl^- products some of which may have kinetic energies of a few eV. It was observed that the most probable kinetic energy of the product Cl^- ions was close to zero eV. This suggests that dissociative charge transfer occurs primarily by a nearly vertical transition to the ground state of Cl_2^-. In the case of electron detachment, it appears that for $I^- + Cl_2$ the potential surface of the lowest free electron state does not have an accessible crossing with the incoming $I^- +$

Cl_2 channel. This is plausible since I + Cl_2 + e is repulsive, and there is a bound state of Cl_2^-. Some detachment is seen at higher energies, but the cross section is very small. If the conditions of a collision are such that a transition to I + Cl_2^- occurs, and also that the Cl-Cl separation falls below 2A (as might happen in a head-on collision in which the three atoms are approximately collinear), then the Cl_2^- can cross into the continuum of free electron states, and detachment is possible.

The observation of a clear threshold for electron detachment for the reactions of Br^- and Cl^- with Cl_2 suggests that a direct crossing into the continuum does occur for these systems. Presumably the $BrCl_2$ and Cl_3 potentials are either weakly attractive or at least less repulsive than that of ICl_2.

Measurements of the energy loss spectra for inelastic scattering of I^- on Cl_2 were made, and some results are shown in Figs.39 and 40. The ion counting statistics were poor, because the cross secction for I^- survival with inelastic scattering is low. Transitions of Cl_2 to electronically excited states are observed in the experiment. Theoretical calculations[92] for these excited potentials indicate the endothermicities of about 20 possible vertical transitions for $Q \geq -12$ eV, and a few more at slightly higher energies. Figs.39 and 40 show these endothermicities along with the measured energy loss spectra. It is not possible to identify individual transitions, but it is clear that many are occuring, and that the relative intensities of different structures in the spectra change rapidly for small changes in the primary ion energy and the angle of measurement. It appears that transitions

$$I^- + Cl_2 \longrightarrow I^- + (Cl_2^+)^* + e \qquad (7.20)$$

are occuring, and the presence of this source of electrons makes it impossible to say whether electron detachment from the I^- has been observed, or not. Additionally one cannot rule out the possibility that (7.16) contributes to $\sigma_I(E)$, since highly endothermic processes are observed in these differential spectra.

Chapter VIII

GRAND SUMMARY

At the beginning of this study, we set out to measure cross sections for electron detachment and ion production in collisions of atomic negative ions with various molecular targets. This was a natural sequel to a study of collisions of negative ions with atoms in which there is only one important inelastic product channel at low collision energies: electron detachment. It was expected that the number of product channels would increase considerably when the atomic target was replaced by a molecular target, including vibrorotational excitation, charge transfer, dissociative charge transfer and reactive scattering, in addition to electron detachment. The manner in which these heavy ion channels compete with electron detachment or with each other is not well understood. Thus, an experimental study was undertaken to investigate the importance of all of these processes in negative ion molecule collisions.

The specific systems studied include H^-, D^-, F^-, Cl^-, Br^-, and I^- ions as projectiles and H_2, D_2, HD, N_2, CO, O_2, CO_2, CH_4 and Cl_2 molecules as targets. The energy range of these experiments extended from a few eV to about 300 eV in the lab.

In chapter IV we have presented the results of measurements of total cross sections for collisions of H^- and D^- with H_2, D_2 and HD. The detachment cross sections showed a general behavior for all the mo-

lecular targets: at low collision energies the cross sections scale with relative collision energy and at high collision energies the cross sections scale with relative collision velocity with respect to isotopic substitution.

Threshold studies for these reactants have revealed some remarkable features: the detachment threshold for H^- is found to be higher than that of D^- by a quarter of an electron volt. Furthermore, the threshold for collisional detachment for both isotopes is found to lie much higher than the electron affinity of the hydrogen atom.

Rearrangement processes are found to be quite insignificant when compared with detachment cross sections for the hydrogenic reactants. Measurements of ion production cross sections above 9 eV are attributed to dissociative charge transfer.

Total cross sections for electron and ion production for collisions of H^- and D^- with N_2, CO, O_2, CO_2 and CH_4 are presented in chapter V. The scaling behavior that was observed for the isotopic hydrogen molecules also held true for these molecular targets. Although the detachment cross sections scaled with energy and velocity in different regions of energy, the observed features of detachment differed for various molecular targets. For example, for N_2 the detachment cross sections showed a "dual" isotope effect which was not observed for any other targets.

In the case of O_2 and CO_2, the detachment cross sections displayed some structure. For O_2, both associative detachment and the autodetaching states of $O_2^-(v'>3)$ are suggested to be the dominant source of electrons. A strong isotope effect is observed in the detachment

cross sections for CO_2. The structure observed in the detachment cross sections for CO_2 is ascribed to a competition between direct detachment and charge transfer to the negative ion resonance states of CO_2^-.

The charge transfer cross section for $H^- + O_2$ is found to be larger than the detachment cross section. The notable features of these cross sections are the large oscillations observed in the charge transfer cross sections which are found to scale remarkably well with relative collision velocity when H^- is replaced by D^-. A simple two-state model is used to describe the dynamics of charge transfer.

Collisions of F^- and Cl^- with H_2, D_2 and HD are presented in chapter VI. The differences of electron and ion production cross sections between these reactants and those which involve H^- and D^- ions as projectiles are noteworthy. For example, in the case of $H^-(D^-)$ projectiles, the detachment cross section is found to be the dominant inelastic product channel with no structure in it. On the other hand, for F^- projectile, the detachment cross section is found to be surprisingly small and exhibited a structure in the low energy region ($E < 10$ eV). In contrast to $H^-(D^-)$ cases, detachment in the halogen-hydrogen systems occurs as a minor companion to reactive scattering at low collision energies.

The cross sections for both electron and ion production show a remarkable variation when F^- is replaced by a different halide ion, namely Cl^-. The magnitude of the detachment cross sections for Cl^- is found to be much larger than that observed for the F^- ion. Furthermore, detachment in Cl^- is found to dominate the ion channel with no structure in it. Isotopic substitution revealed that for F^- detachment is a uni-

versal function of relative collision energy at low collision energies and of relative collision velocity at high collision energies. This observation is in sharp contradistinction to that observed for the Cl^- projectile.

Finally, in chapter VII we have presented the results of total cross sections for electron detachment and charge transfer and dissociative charge transfer in collisions of the halide ions I^-, Br^- and Cl^- with Cl_2 target. Some energy loss spectra of I^- ions are also presented in this chapter. It is observed that the charge transfer and the dissociative charge transfer are the dominant product channels in these collisions. Additionally, the detachment cross section is found to be unusually low for the I^- projectile. Energy loss measurements indicate that significant target excitation is involved in the dynamics of negative ion-molecule collisions for these systems.

The results presented in this dissertation show many varied features of detachment and ion production and illustrate unambiguously the importance of electron detachment, reactive scattering, charge transfer and dissociative charge transfer in negative ion molecule collisions.

REFERENCES

1. V.M. Dukel'skii and E.Ia. Zandberg, JETP 21, 1270 (1951).

2. J.B. Hasted, Proc. R. Soc. Lond. A212, 235 (1952).

3. V.A. Esaulov, D. Dhuicq, and J.P. Gauyacq, J. Phys. B11, 1049 (1978).

4. S.K. Lam, J.B. Delos, R.L. Champion, and L.D. Doverspike, Phys. Rev. A9, 1828 (1974).

5. J.P. Gauyacq, J. Phys. B13, 4417 (1980).

6. J.P. Gauyacq, J. Phys. B13, L501 (1980).

7. R. Taylor and J.B. Delos, Proc. R. Soc. A379, 179 and 209 (1982).

8. T.S. Wang and J.B. Delos, J. Chem. Phys. 79, 4306 (1983).

9. J.S. Risley and R. Geballe, Phys. Rev. A9, 2485 (1974).

10. H.H. Michels and J.F. Paulson, Potential Energy Surfaces and Dynamics Calculations, edited by D.G. Truhlar (Plenum Press, New York, 1981), p.535.

11. J.S. Risley, Phys. Rev. A16, 2346 (1977).

12. J.L. Montmagnon, V.A. Esaulov, J.P. Grouard, R.I. Hall, M.Landau, F. Pichou, and C. Schermann, J. Phys. B16, L143 (1983).

13. V.A. Esaulov, J.P. Grouard, R.I. Hall, M. Landau, J.L. Montmagnon, F. Pichou, and C. Schermann, Submitted to Phys. Rev. A, (1983).

14. B.K. Annis, S. Datz, R.L. Champion, and L.D. Doverspike, Phys. Rev. Lett. 45, 1554 (1980).

15. V.N. Tuan and V.A. Esaulov, J. Phys. B15, L95 (1982).

16. J.T. Cheung and S. Datz, J. Chem. Phys. 73, 3159 (1980).

17. H. Hotop and W.C. Lineberger, J. Chem. Phys. Ref Data 4, 539 (1975).

18. B.M. Smirnov, Negative Ions, edited by H.S.W. Massey, McGraw-Hill (1982).

19. L.G. Christophorou, Atomic and Molecular Radiation Physics, Wiley-Interscience, New York.

20. B.K. Janousek and J.I. Braumen, Gas Phase Ion Chem. 2, edited by M.T. Bowers (1979).

21. J.L. Franklin and P.W. Harland, Ann. Rev. Phys. Chem. 25, 485 (1974).

22. J.R. Hiskes, Lawrence Livermore Laboratory Report No. UCRL-82889, (1979).

23. M. Bacal and G.W. Hamilton, Phys. Rev. Lett. 42, 1538 (1979).

24. M. Allan and S.F. Wong, Phys. Rev. Lett. 41, 1791 (1978).

25. J.M. Wadehra and J.N. Bardsley, Phys. Rev. Lett. 41, 1795 (1978).

26. E.E. Muschlitz, Jr., T.L. Bailey, and J.H. Simons, J. Chem. Phys. 24, 1202 (1956); J. Chem. Phys. 26, 711 (1957).

27. J.B. Hasted and R.A. Smith, Proc. R. Soc. A235, 349 (1956).

28. See, for example, Brookhaven National Laboratory Report No. BNL 50727, (Unpublished).

29. M.S. Huq, L.D. Doverspike, R.L. Champion, and V.A. Esaulov, J.Phys.

30. G.B. Lopantseva and O.B. Firsov, Sov. Phys.- JETP 23, 648 (1966).

31. R.L. Champion, L.D. Doverspike, and S.K. Lam, Phys. Rev. A13, 617 (1976).

32. R.L. Champion, Advances in Electronics and Electron Physics, 58, 143 (1982).

33. R.E. Olson and B. Liu, Phys. Rev. A22, 1389 (1980).

34. D.G. Hummer, R.F. Stebbings, and W.L. Fite, Phys. Rev. 119, 668 (1960).

35. Yu.F. Bydin and V.M. Dukel'skii, Sov. Phys.-JETP 4, 474 (1957).

36. A.E. Roche and C.C. Goodyear, J. Phys. B2, 191 (1969).

37. B.T. Smith, W.R. Edwards, L.D. Doverspike, and R.L. Champion, Phys. Rev. A18, 945 (1978).

38. T.L. Bailey and P. Mahadevan, J. Chem. Phys. 52, 179 (1970).

39. J.F. Paulson, J. Chem. Phys. 52, 959 (1970).

40. C. Lifshitz, R.L.C. Wu, T.O. Tiernan, and D.T. Terwillinger, J. Chem. Phys. 68, 247 (1978).

41. R.A. Bennet, J.T. Moseley, and J.R. Peterson, J. Chem. Phys. 62, 2223 (1975).

42. F.W. Meyer, J. Phys. B13, 3823 (1980).

43. C. deVreugd, R.W. Wijanaendts van Resandt, J. Los, B.T. Smith, and R.L. Champion, Chem. Phys. 42, 305 (1979).

44. J. Feyton, D. Dhuicq, and M. Barat, J. Phys. B11, 1267 (1978).

45. L.D. Doverspike, B.T. Smith, and R.L. Champion, Phys. Rev. A22, 393 (1980).

46. D. Vogt and K.H. Opiela, Phys. Rev. Lett. A54, 331 (1975).

47. T.O. Tiernan, B.M. Hughes, and C. Lifshitz, J. Chem. Phys. 55, 5692 (1971).

48. D. Vogt, J. Mischke, and W. Dreves, J. Phys. E9, 38 (1976).

49. Y. Itoh, U. Hege, and F. Linder, Electronic and Atomic Collisions (XIIIth ICPEAC), edited by Eichler et al., Published by the International Conference on the Physics of Electronic and Atomic Collisions e.V. (Berlin), p. 397, (1983).

50. B.K. Annis and S. Datz, Electronic and Atomic Collisions (XIIth ICPEAC), B15, 951 (1982). edited by S. Datz, North Holland Publishing Co., p. xxx., (1982).

51. W. Frebin, C. Shlier, K. Strein, and E. Telroy, J. Chem. phys. 67, 5505 (1977); B. von Zyl, G.E. Chamberlain, and G.H. Dunn, J. Vac. Sci. Tech. 13, 721 (1976).

52. W. Paul, H.P. Reinhard, and U. von Zahn, Z. Physik 152, 143 (1958).

53. J.B. Hasted, Physics of Atomic Collisions (Butterworth Inc., Washington, D.C., 1964).

54. H.S. Landes, "The Analysis of of Ion Beams Using an R.F. Mass Spectrometer," University of Virginia Report No. EP-2894-106-60U (1960).

55. C.S. Leffel, Rev. Sci. Inst. 35, 1615 (1964).

56. P.J. Chantry, J. Chem. Phys. 55, 2746 (1971).

57. H.H. Michels, (Private Communication).

58. J.S. Risley, Phys. Rev. A10, 731 (1974).

59. D.L. Albritton, I. Dotan, W. Lindinger, M. McFarland, J. Tellinguisen, and F. Feshenfeld, J. Chem. Phys. 66, 410 (1977).

60. V.N. Tuan, J.P. Gauyacq, and A. Herzenberg, Proceedings of the 11th International Symposium on the Physics of Ionized Gases, edited by G. Pichler, (Zagreb University Press), 1982.

61. T.Y. Wu and T. Ohmura, Quantum Theory of Scattering (Prentice-Hall, Englewood, Cliff, 1962), p.324.

62. J. Comer and G.J. Schultz, Phys. Rev. A10, 2100 (1974).

65. M. Vedder, L.D. Doverspike, and R.L. Champion, Phys. Rev. A24, 615 (1981).

63. C.R. Claydon, G.A. Segal, and H.S. Taylor, J. Chem. Phys. 52, 3387 (1970).

64. P.J. Chantry, J. Chem. Phys. 57, 3180 (1972).

66. V.N. Tuan and V.A. Esaulov, Proceedings of the 11th International Symposium on the Physics of Ionized Gases, edited by G. Pichler, (Zagreb University Press), 1982.

67. V.N. Tuan, V.A. Esaulov, and J.P. Gauyacq, Electronic and Atomic Collisions (XIIIth ICPEAC), edited by Eichler et al., Published by the International Conference on the Physics of Electronic and Atomic Collisions e.V. (Berlin). p. 411, (1983).

68. S.J. Chantrell, D. Field, and P.I. Williams, J. Phys. B15, 309 (1982). J.P. Gauyacq and A. Herzenberg, Electronic and Atomic Collisions (XIIIth ICPEAC), edited by Eichler et al., Published by the International Conference on the Physics of Electronic and Atomic Collisions e.V. (Berlin). p. 411, (1983).

69. P. Marmet and L. Binette, J. Phys. B11, 3707 (1978).

70. R.K. Preston and J.S. Cohen, J. Chem. Phys. 65, 1589 (1976).

71. E. Herbst, L.G. Payne, R.L. Champion, and L.D. Doverspike, Chem. Phys. 52, 413 (1979).

72. W.H. Miller, J. Chem. Phys. 52, 3563 (1970).

73. J.T. Muckerman, Theoret. Chem. Adv. Perspectives 6A, 1 (1981).

74. J.T. Muckerman, J. Chem. Phys. 54, 1155 (1971).

75. J.T. Muckerman, J. Chem. Phys. 56, 2997 (1972).

76. J.T. Muckerman, J. Chem. Phys. 70, 3910 (1972).

77. D. Feng, E.R. Grant, and J.W. Root, J. Chem. Phys. 64, 3450 (1976).

78. A. Persky, J. Chem. Phys. 66, 2932 (1977).

79. A. Persky, J. Chem. Phys. 68, 2411 (1978).

80. A. Persky, J. Chem. Phys. 70, 3910 (1979).

81. S.E. Haywood, D.J. Bowen, R.L. Champion, and L.D. Doverspike, J. Phys.B14, 261 (1981).

82. F.A. Stevie and M.J. Vasile, J. Chem. Phys. 74, 5106 (1981).

83. C.A. Brau and J.J. Ewing, Appl. Phys. Lett. 27, 350 (1975).

84. J.J. Ewing and C.A. Brau, Appl. Phys. Lett. 27, 435 (1975).

85. C.H. Chen and M.G. Payne, Appl. Phys. Lett. 28, 219 (1976).

86. J.R. Murray and H.T. Powell, Appl. Phys. Lett. 29, 252 (1976).

87. R.P. Turco, J. Geophys. Res. 82, 3585 (1977).

88. G.I. Dimov and G.V. Roslyakov, Sov. Phys. - Tech. Phys. 17, 90 (1972).

89. B.M. Hughes, C. Lifshitz, and T.O. Tiernan, J. Chem. Phys. 59, 3162 (1973).

90. M.V. Kurepa and S.D. Belic, Chem. Phys. Lett. 49, 508 (1977).

91. R. Azria, R. Abouaf and D. Teillet-Billy, J. Phys. B15, L569 (1982).

92. S.D. Peyerimhoff and R.J. Buenker, Chem. Phys. 57, 279 (1981).

93. S.A. Sullivan, B.S.Freiser, and J.L. Beauchamp, Chem. Phys. Lett. 48, 294 (1977).

94. L.M. Babcock and G.E. Streit, J. Chem. Phys. 76, 2407 (1982).

95. W.B. Person, G.R. Anderson, J.N. Fordemwalt, H. Stammerich, and R. Forneris, J. Chem. Phys. 35, 908 (1961).

96. G.C. Piementel, J. Chem. Phys. 19, 446 (1951).

97. A.W. Kleyn, V.N. Khromov, and J. Loss, Chem. Phys. 52, 65 (1980) and A.W. Kleyn, E.A. Gislason, and J. Loss, Chem. Phys. 52, 81 (1980).

98. A.W. Kleyn, Ph.D. Thesis (1980), Amsterdam, and A.W. Kleyn, V.N. Khromov, and J. Loss, J. Chem. Phys. 72, 5282 (1980).

99. J.H. Futrell and C.D. Miller, Rev. Sci. Inst. 37, 1521 (1966).

LIST OF TABLES

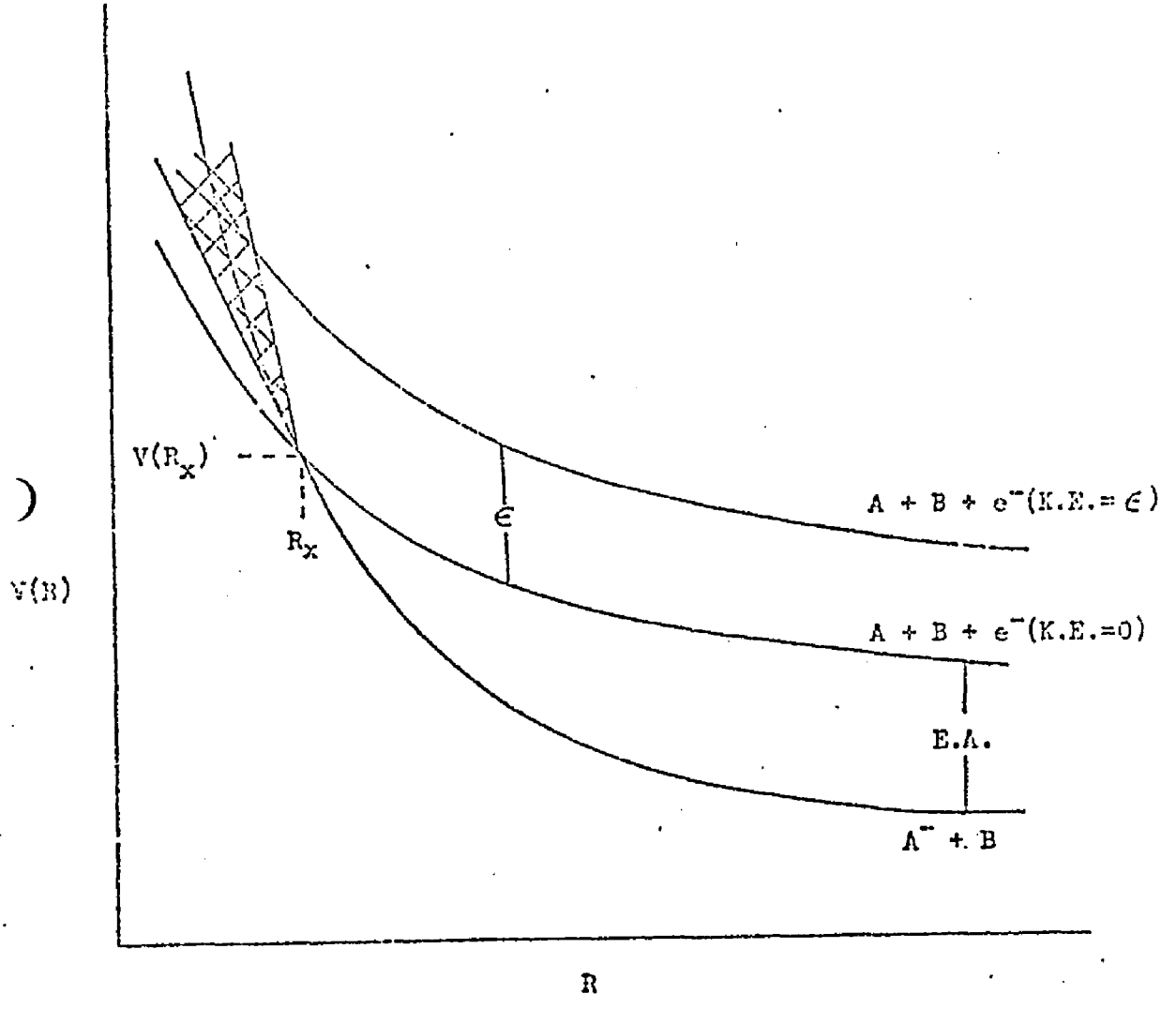

Figure 1: A schematic representation of the interaction potential for repulsive negative ion-atom states. The shaded region represents the decay width of the anion state as described in the text. Also shown is part of the continuum of free electron states.

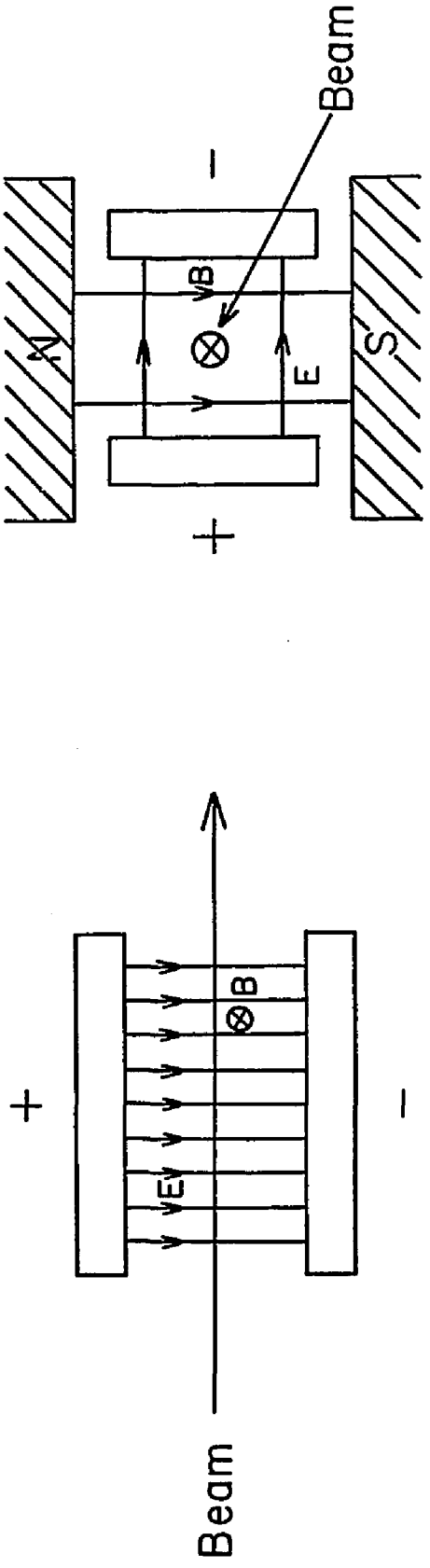

Figure 2: A schematic representation of Wien's velocity filter.

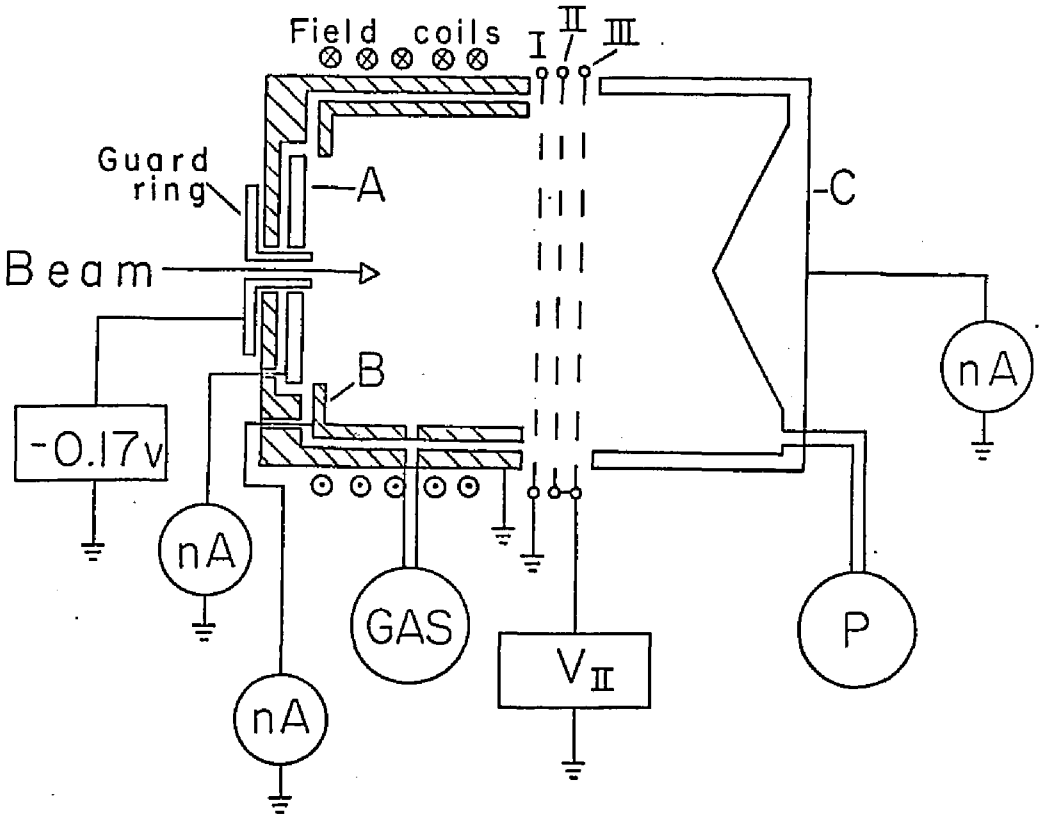

Figure 3: A schematic representation of the collision chamber used for total-cross-section measurements is given. An axial magnetic field along with an electrostatic field between grids I and II traps the detached electrons to plate A. Current at B, which is due primarily to low energy heavy particles (viz., O^-, O_2^-, etc.) can be monitored separately. The primary ion beam, which enters from left on the figure, can be monitored by the element C. The size of the guard ring is exaggerated. It comprises about 4% of the area of plate A.

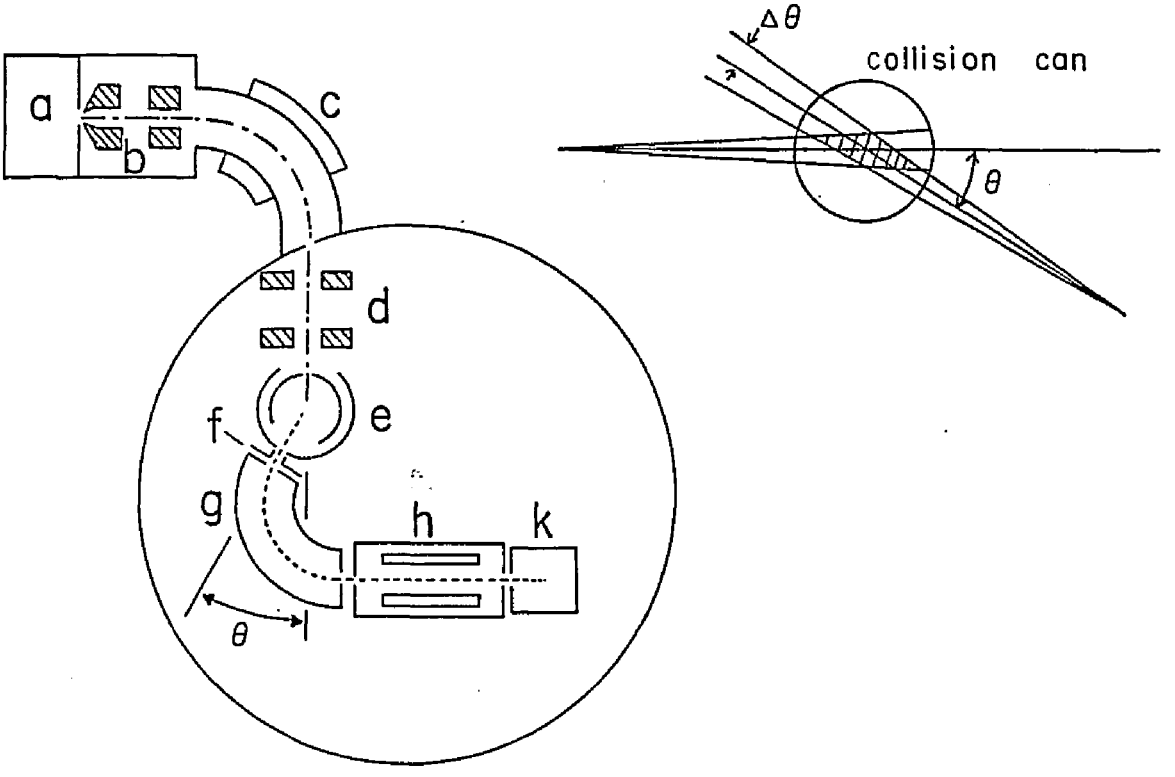

Figure 4: A schematic representation of the differential cross section apparatus. (a) Ion source. (b) and (d), Electrostatic ion optics. (c) 90^{o} magnet. (e) Collision can. (f) Retard/accel. gap. (g) 127^{o} electrostatic analyzer. (h) RF mass filter. (k) Channeltron. Inset: The active collision length depends upon the angle of the measurement.

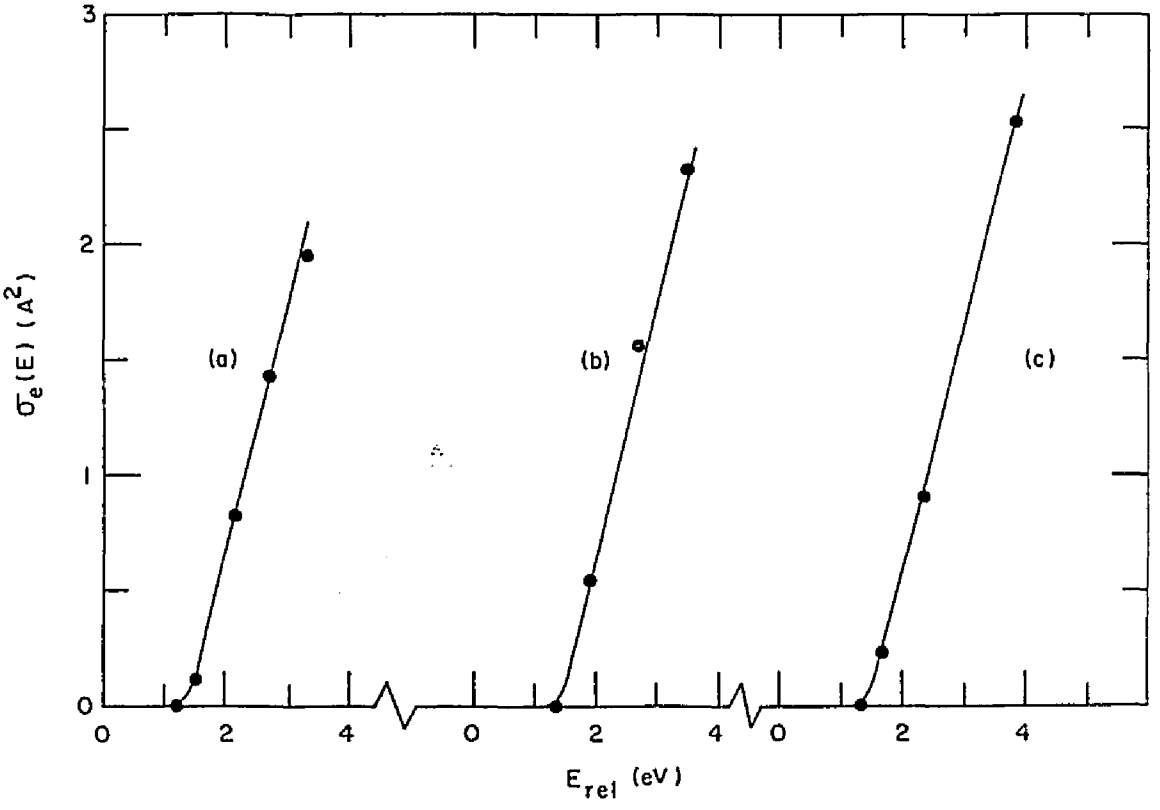

Figure 5: Total electron detachment cross sections in the threshold region for collisions of H^- with (a) H_2, (b) D_2, and (c) HD. Solid circles are the experimental results and solid lines are convolutions of a linear cross section given by Eq.(4.4).

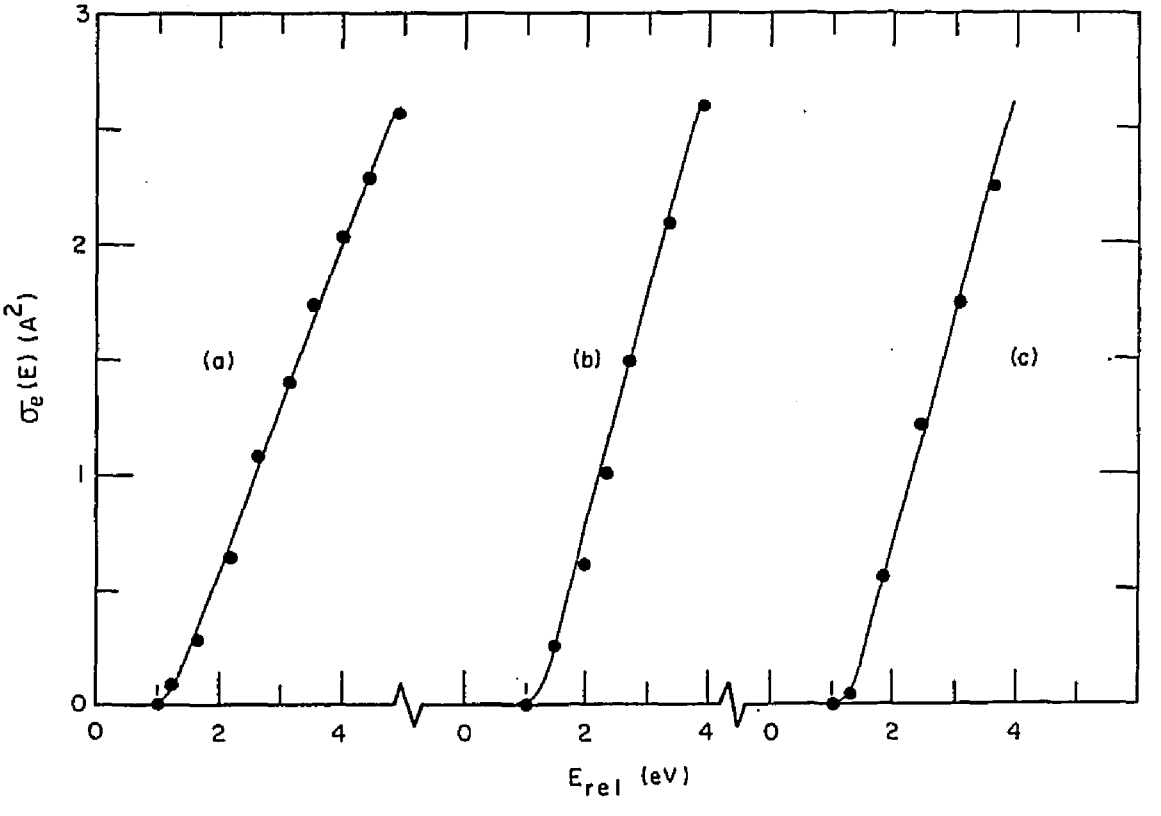

Figure 6: Total cross sections for electron detachment for collisions of D^- with (a) H_2, (b) D_2, and (c) HD in the threshold region. Solid circles are the experimental results and solid lines are convolutions of a linear cross section given by Eq.(4.4).

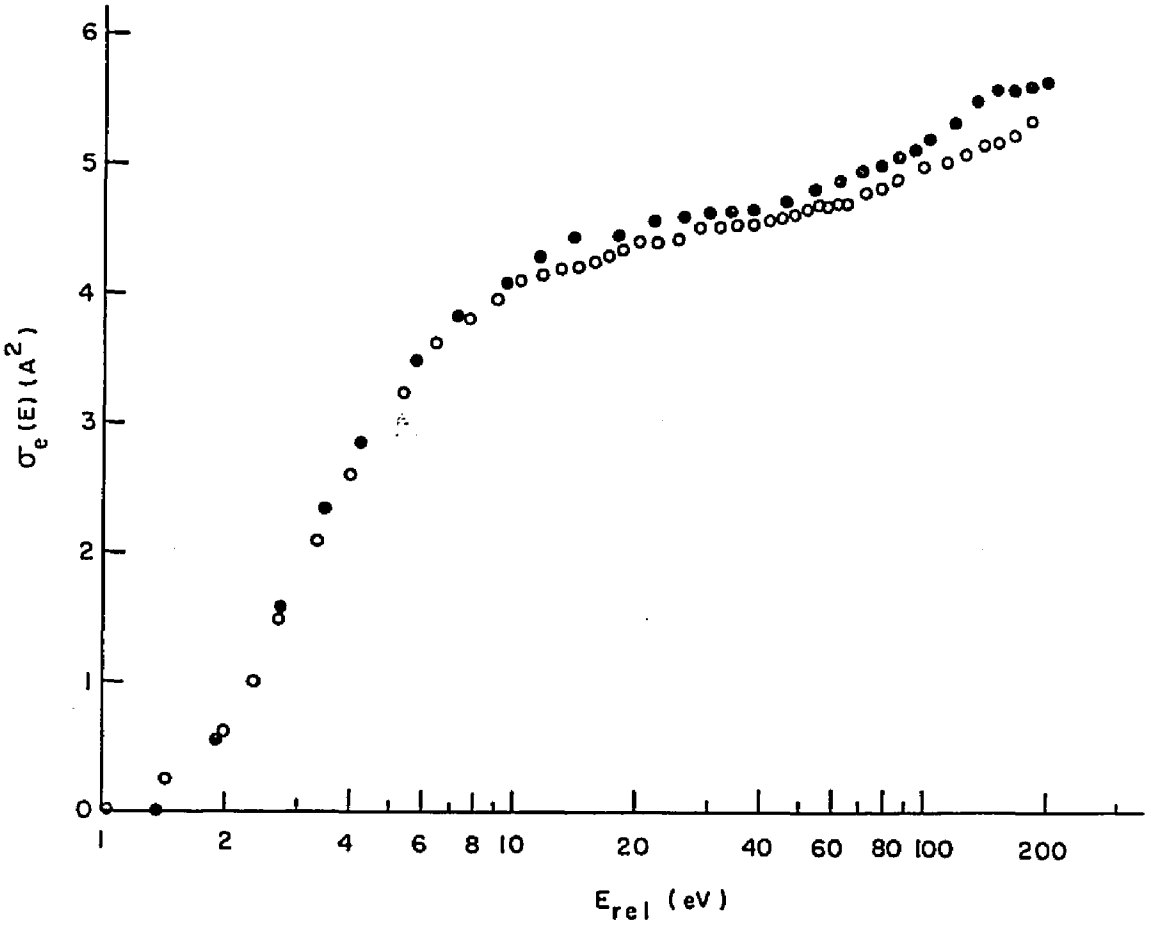

Figure 7: Total electron detachment cross sections for H^- and D^- on D_2 are given as a function of relative collision energy. Solid circles are the results for H^- and open circles are the results for D^-.

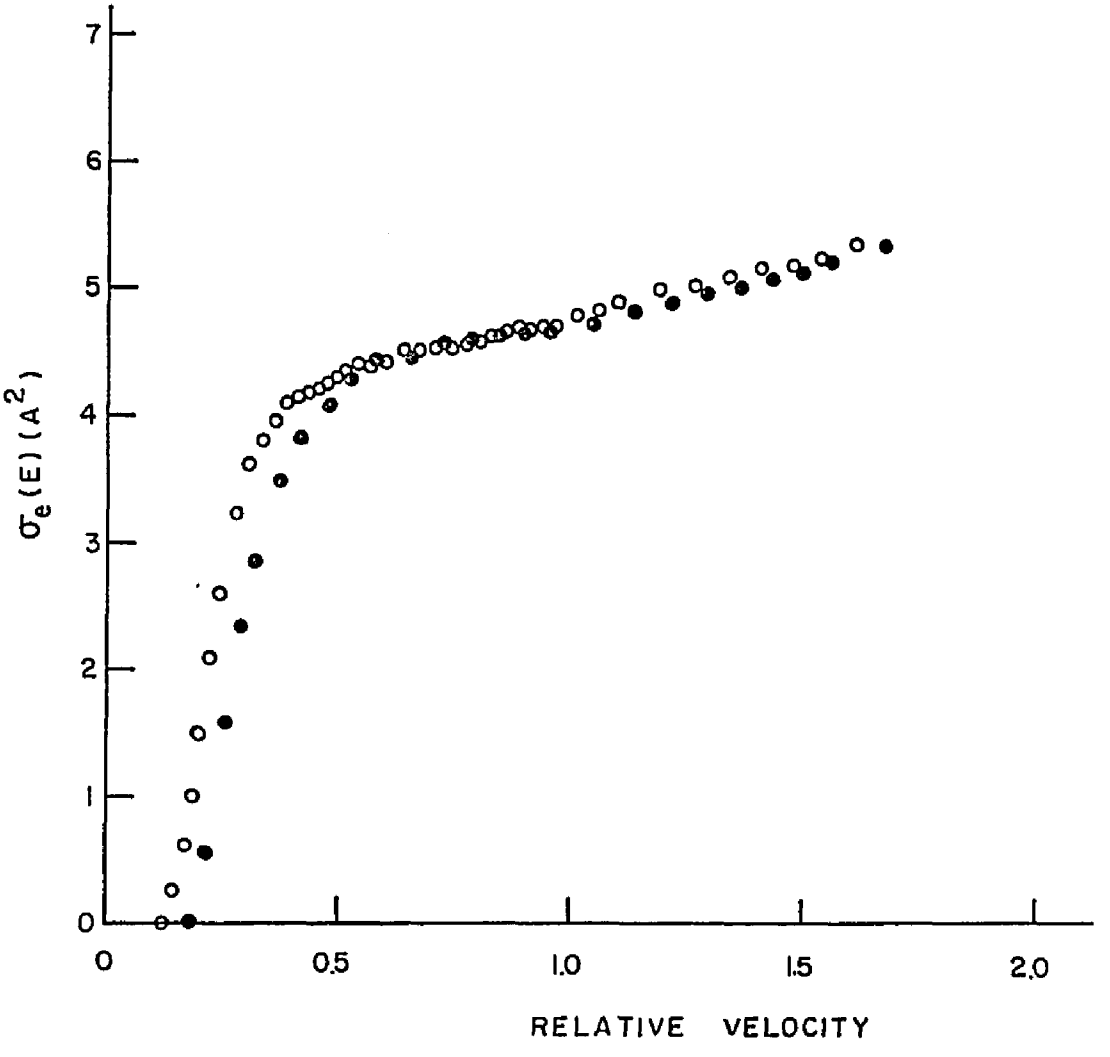

Figure 8: Total electron detachment cross sections for H^- and D^- on D_2 are given as functions of relative collision velocity which are expressed in units of 10^7 cm/sec. Solid circles refer to H^- and open circles are the results for D^- .

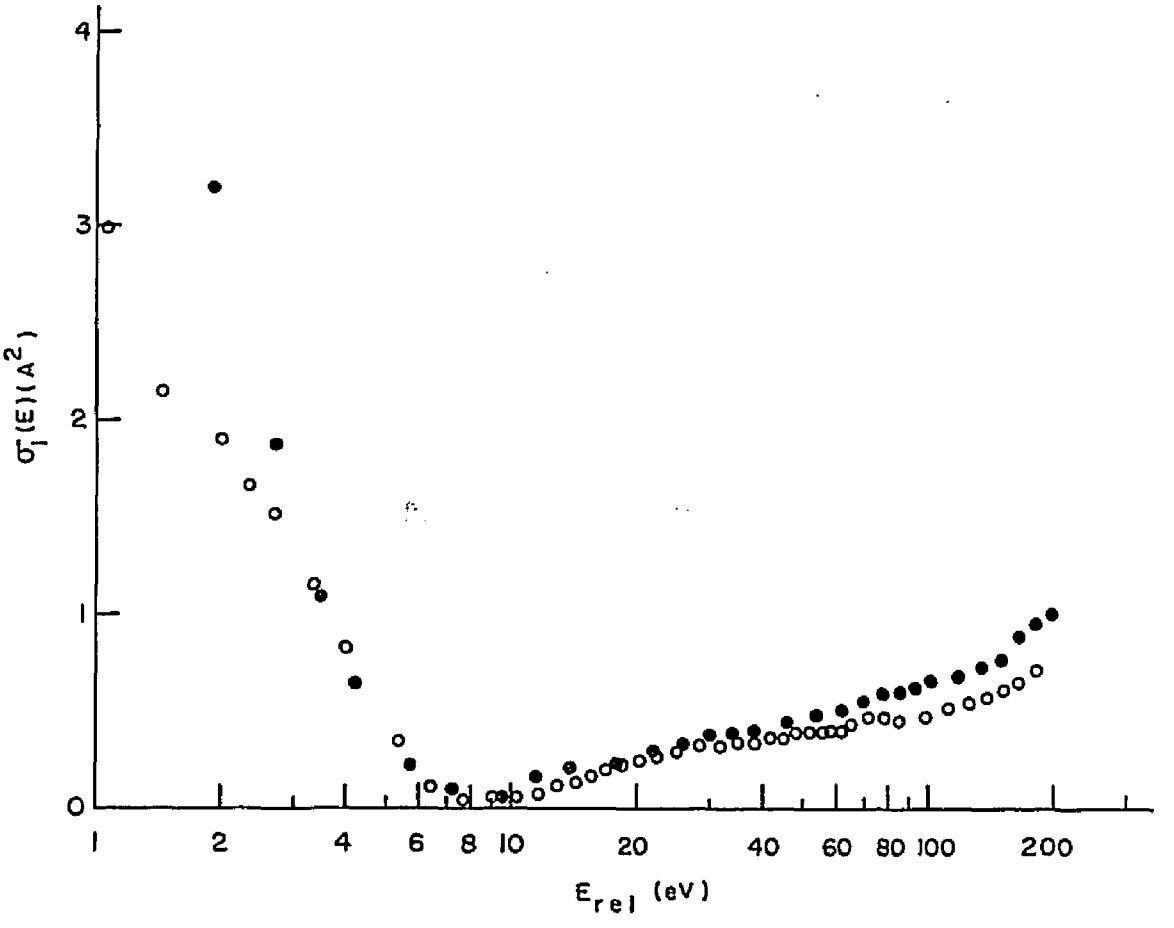

Figure 9: $\sigma_T(E)$, as discussed in the text, is given for collisions of H^- and $D^\pm$ with D_2 as a function of relative collision energy. Solid circles are the results for H^- and open circles refer to D^-.

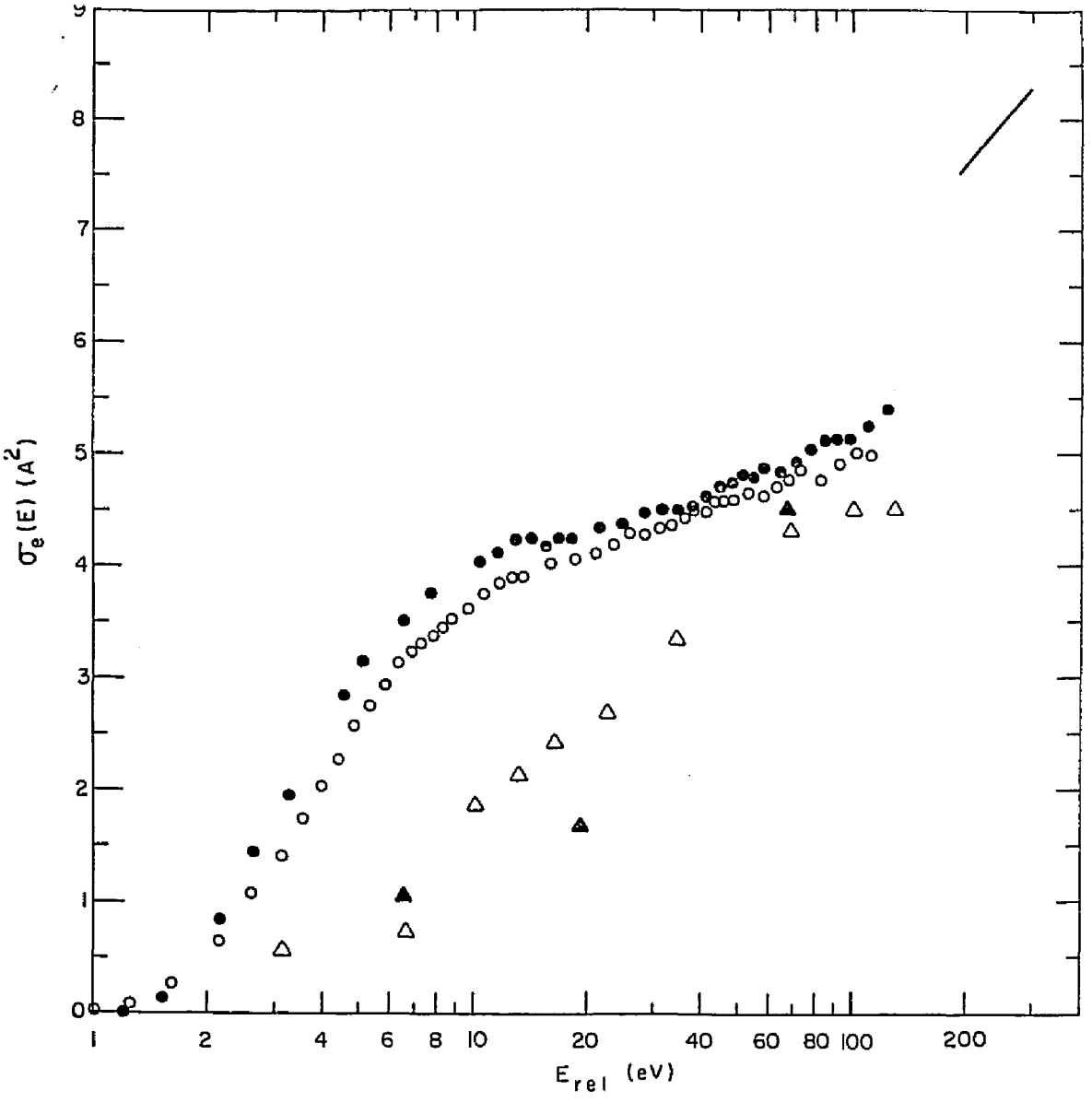

Figure 10: Total electron detachment cross sections for collisions of H^- and D^- with H_2 are given as functions of relative collision energy. Solid circles are the results for H^- and open circles are for D^-. Also given in the figure are the results of Hasted (Ref.27) (solid triangles), Muschlitz et al. (ref.26) (open triangles), and a solid line represents the results of Risley and Geballe (ref.9).

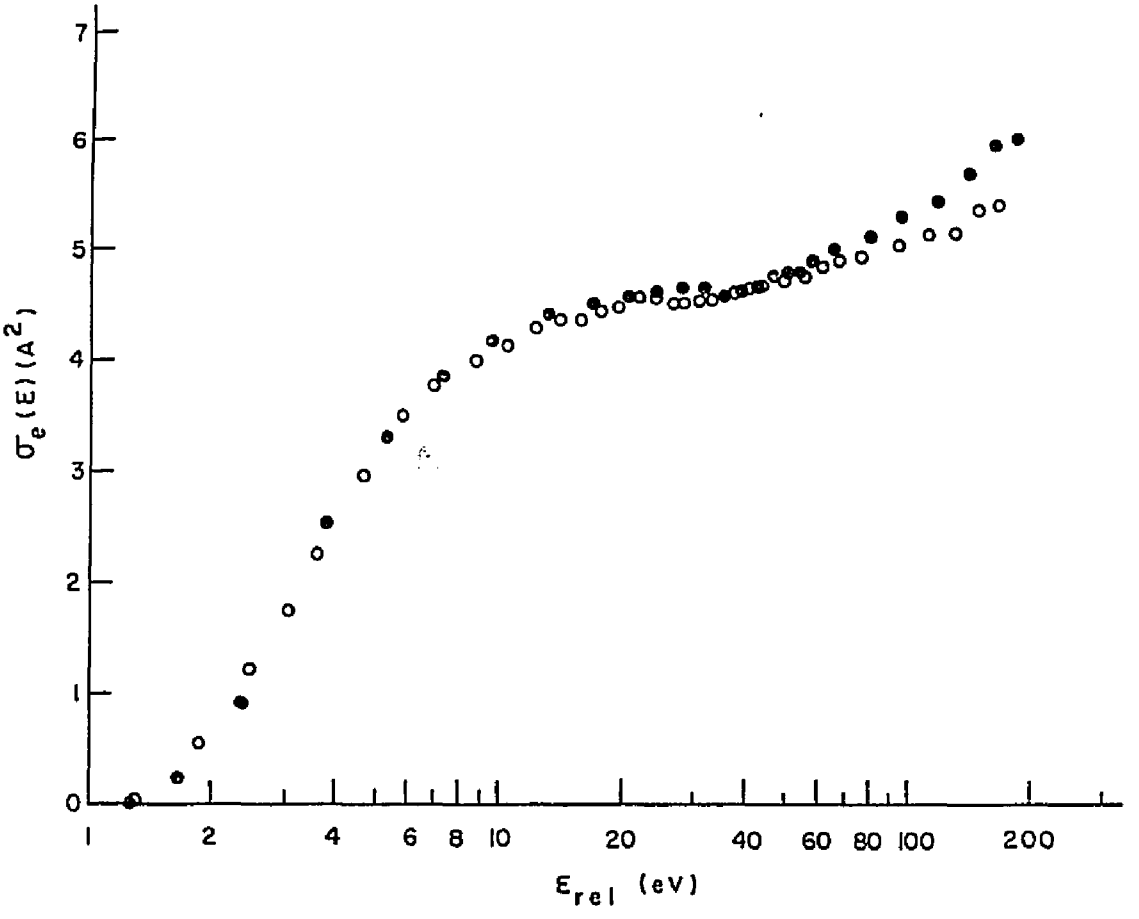

Figure 11: Total electron detachment cross sections for H^- and D^- on HD. Solid circles are the results for H^- and open circles are for D^-.

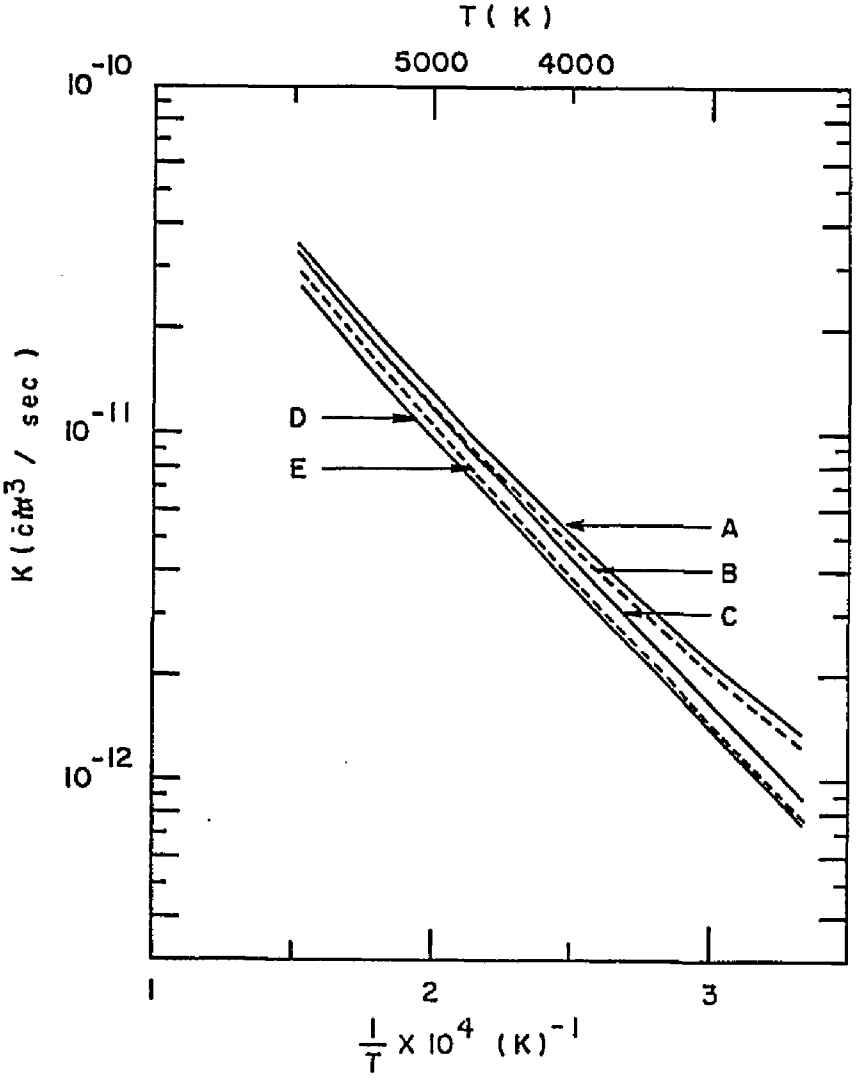

Figure 12: Upper and lower bounds of detachment rate constants for collisions of H^- with H_2, D_2, and HD, are given as functions of inverse temperature. Curves A and C are the upper and lower bounds of K(T) for the H_2 target, curve B is the upper bound of K(T) for both D_2 and HD targets, and D and E are the lower bounds of K(T) for HD and D_2 respectively.

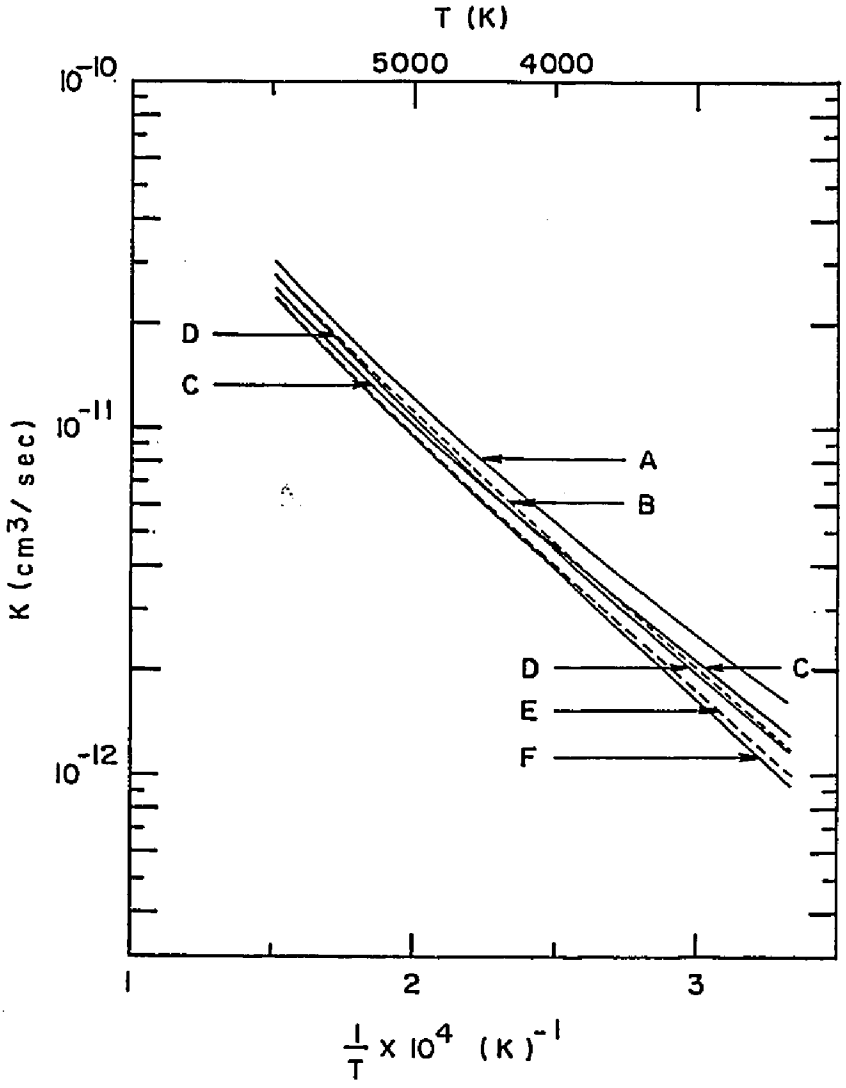

Figure 13: Upper and lower bounds of K(T) for D^- on H_2, D_2, and HD. A and B, upper and lower bounds of K(T) for D_2; C, upper bound for H_2; D, upper bound for HD; E, lower bound for H_2; and F, lower bound for HD.

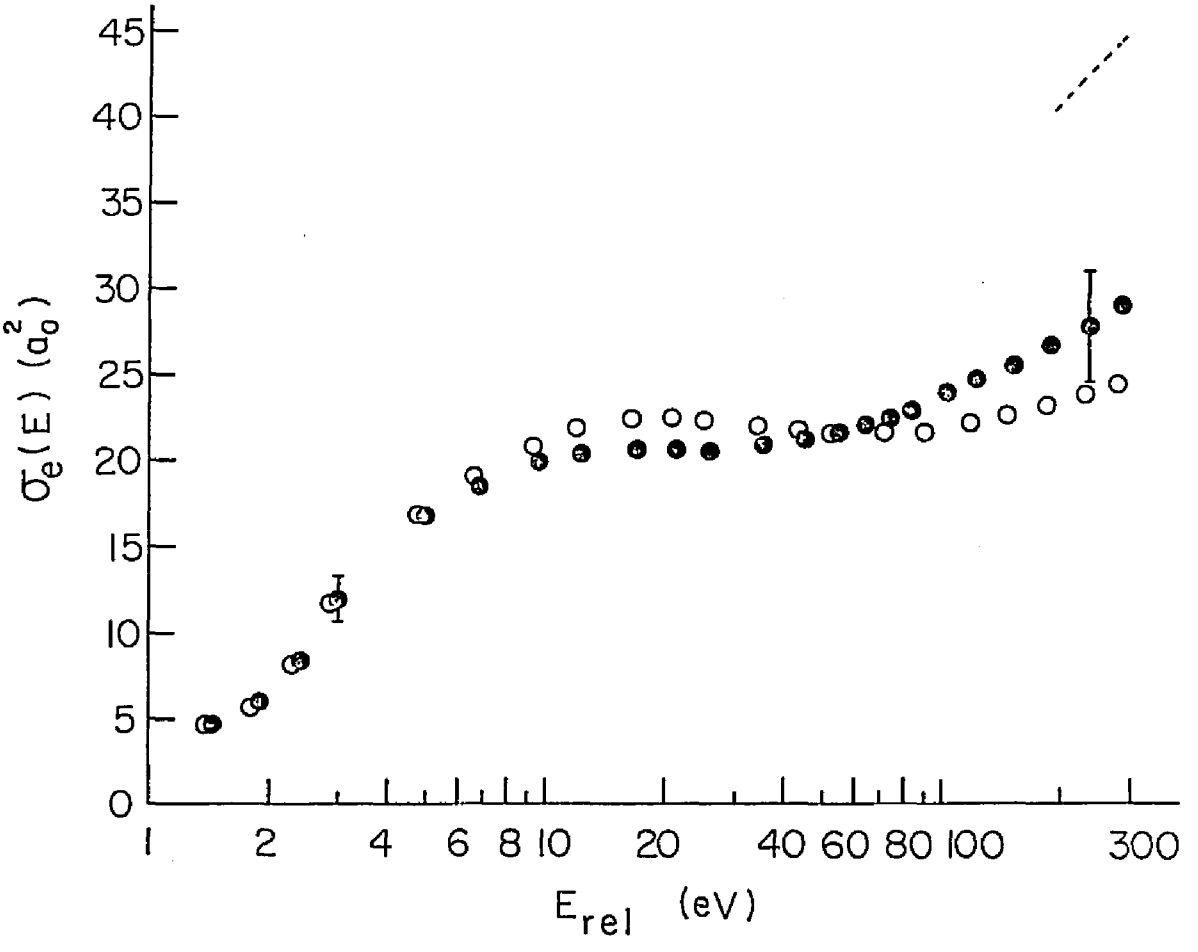

Figure 14: Total electron detachment cross sections σ_e for H^- and D^- on N_2 are given as a function of relative collision energy. The filled circles are the results for H^- projectiles and the open circles are the results for D^-. The dotted line is a representative of the results of Risley and Geballe (Ref. 9 and 61). Error bars on this and subsequent 10 figures represent our estimate of the systematic uncertainty in the measurements-any systematic error should be independent of which isotope is being studied.

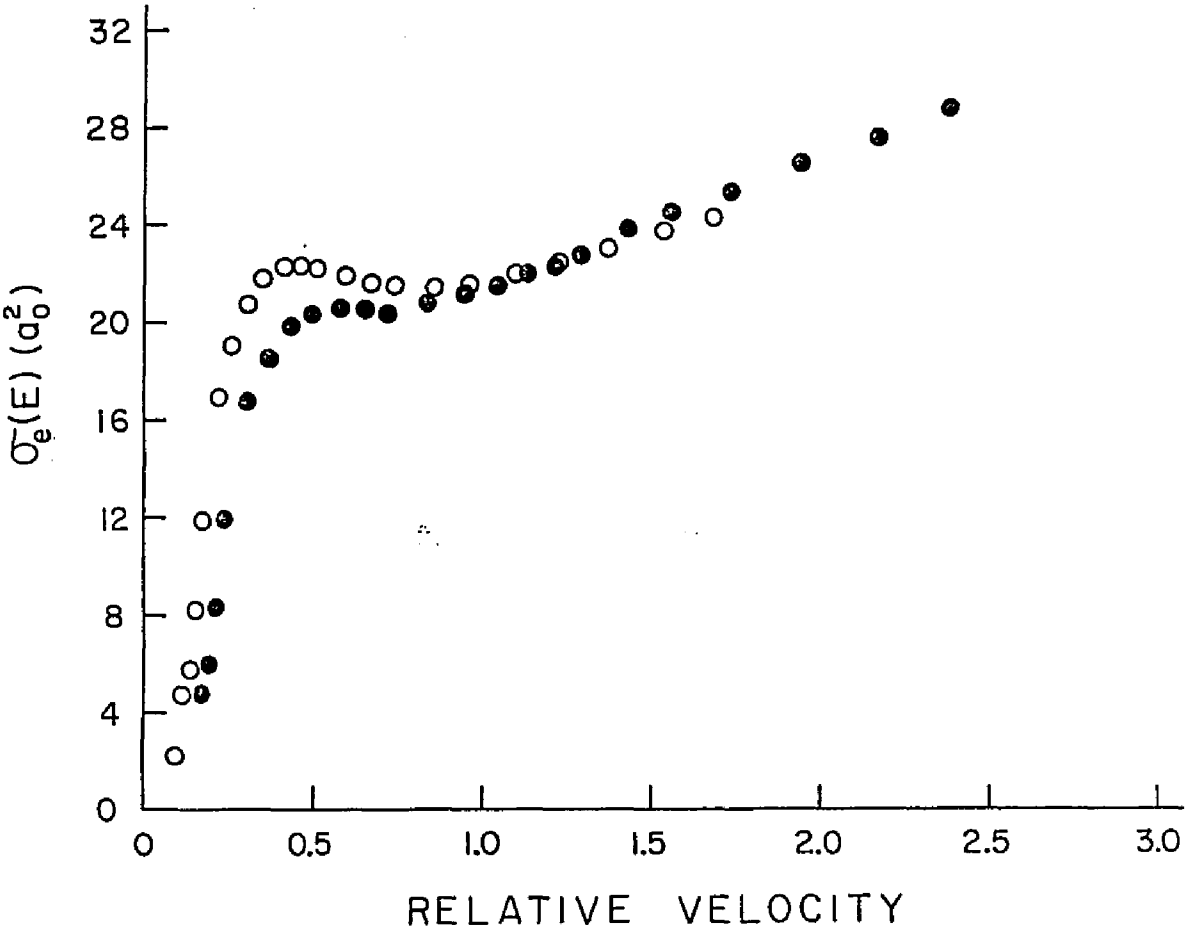

Figure 15: Total electron detachment cross sections σ_e for H^- and D^- on N_2 are given as a function of relative collision velocity, which is expressed in units of 10^7 cm/sec. The filled circles are the results for H^- projectile and the open circles are for D^-.

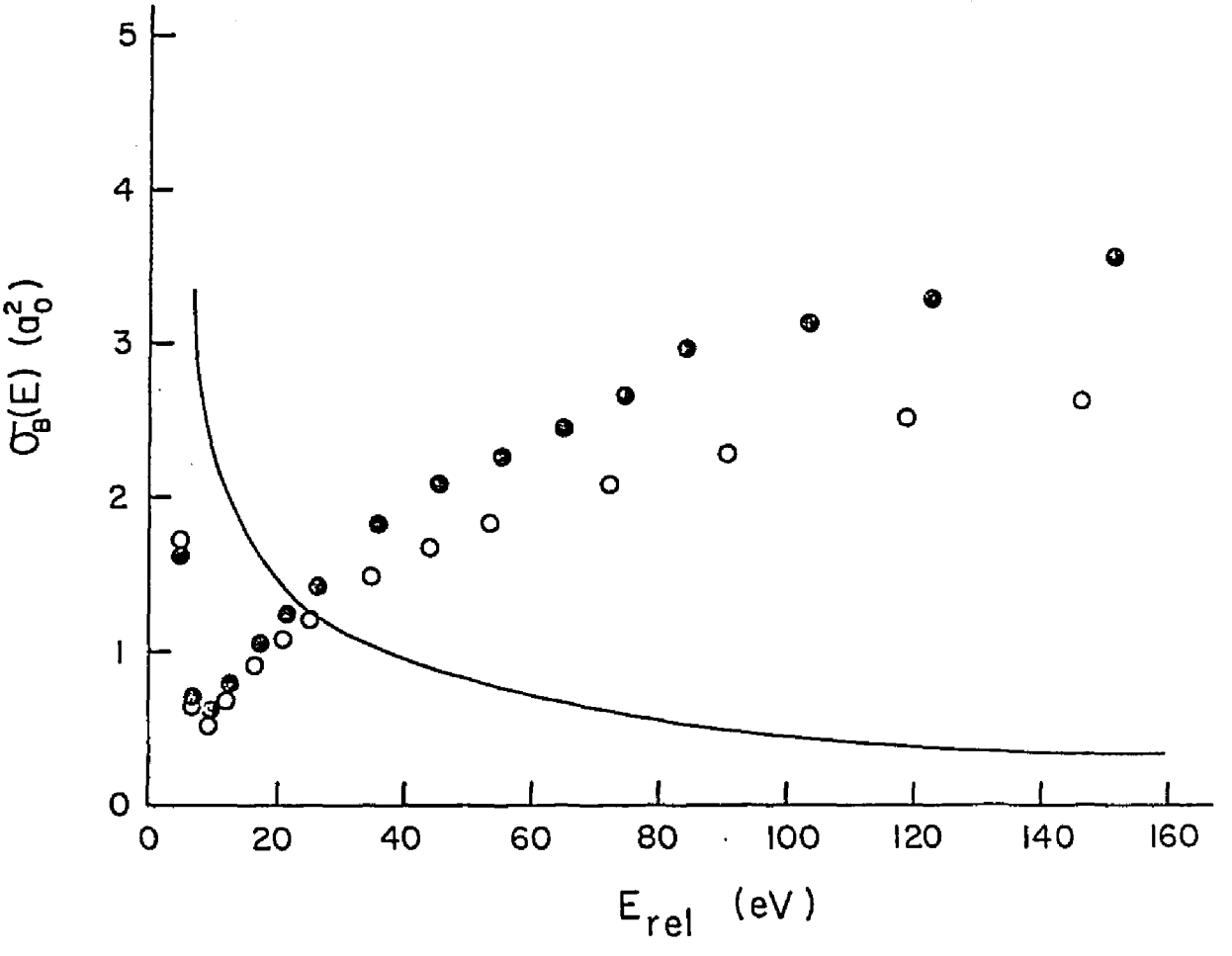

Figure 16: Total cross sections for partial elastic and inelastic scattering, σ_B, as described in the text are given for the $H^-(D^-)$ + N_2 systems as a function of relative collision energy. The full circles are the results for H^- and the open circles are for D^-. Also given in the figure is a curve representative of the partial cross section for large-angle elastic scattering of H^- and D^- by Ne.

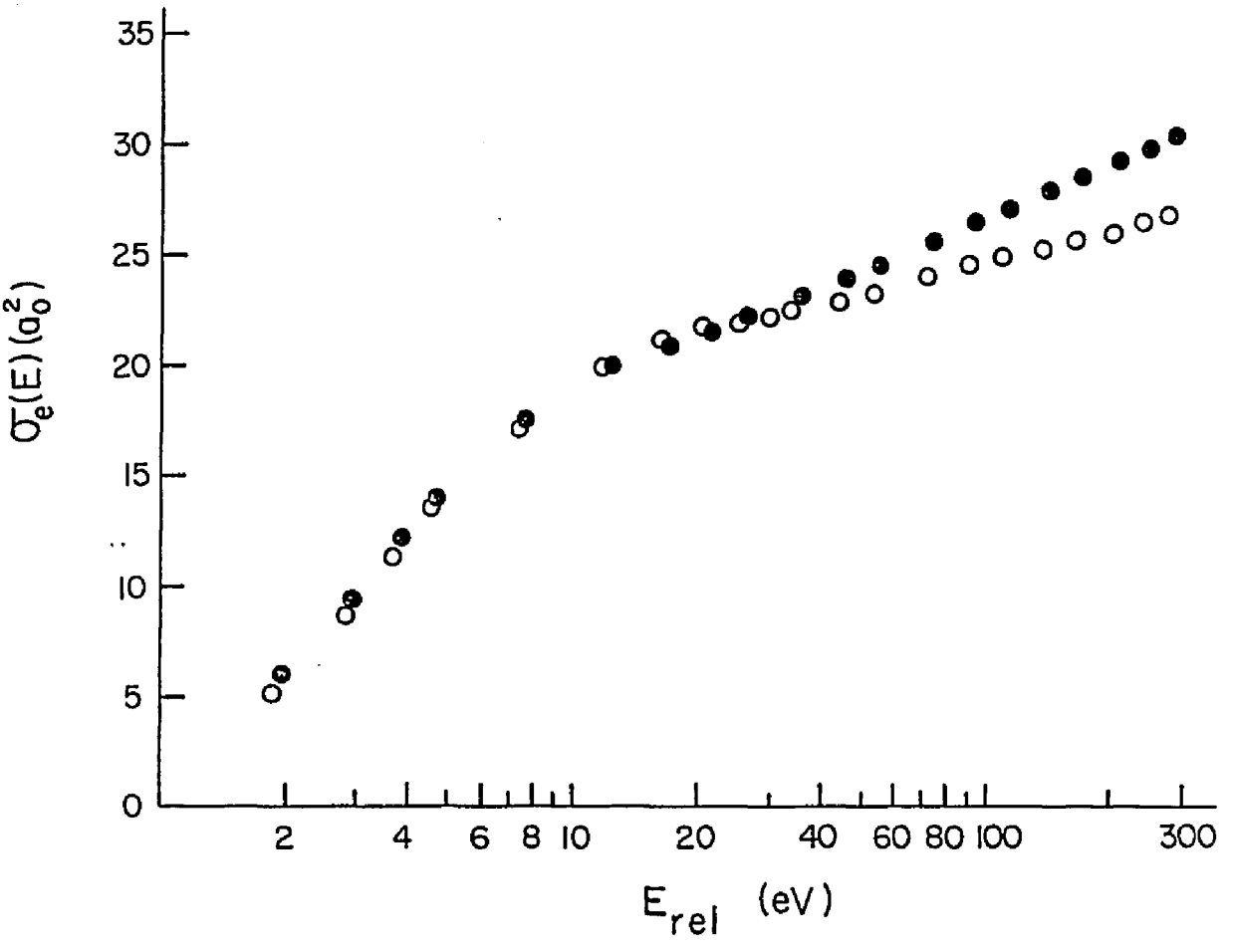

Figure 17: Absolute total cross sections for electron detachment, σ_e, for collisions of H^- and D^- with CO are given as a function of relative collision energy. The filled circles are the results for H^- and the open circles are for D^-.

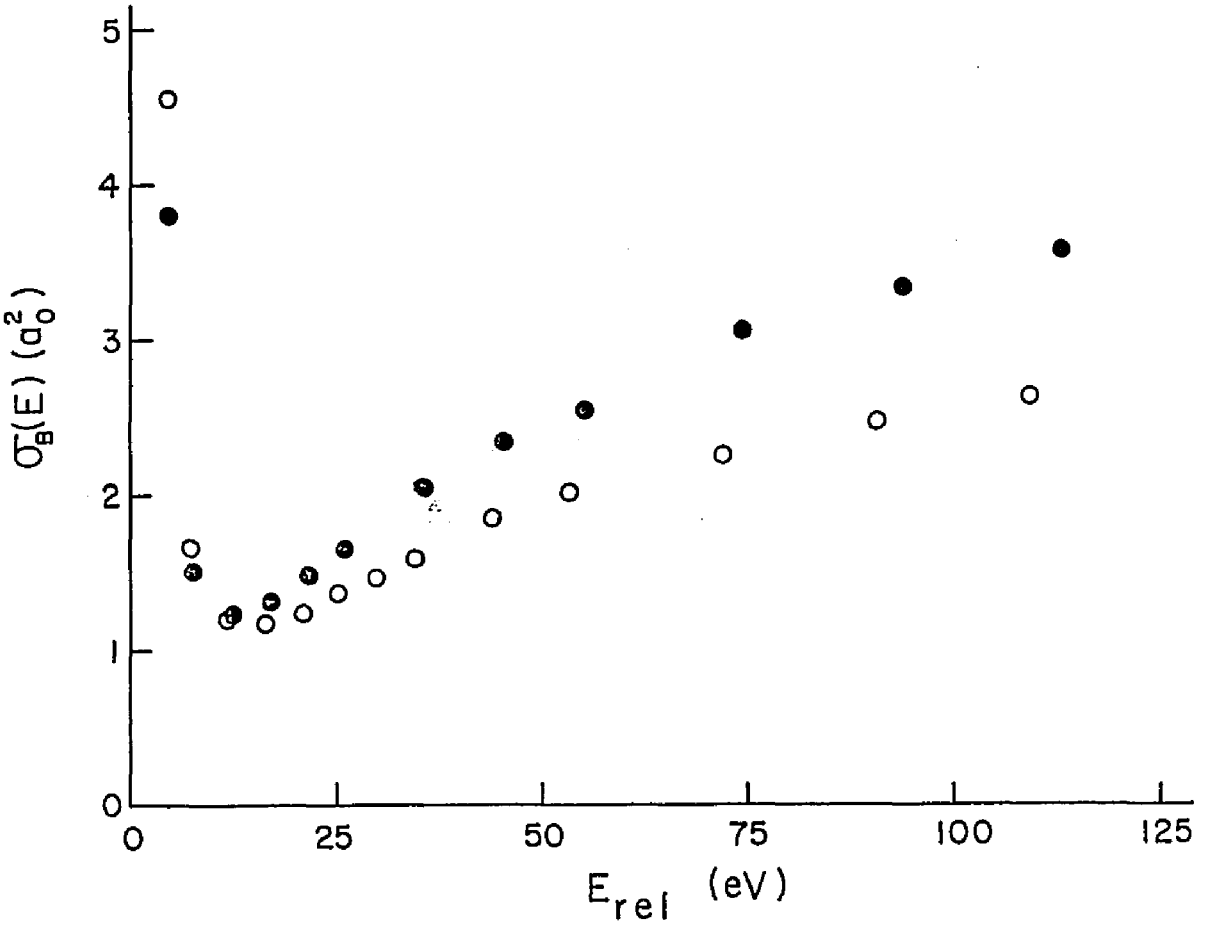

Figure 18: $\sigma_B(E)$, as discussed in the text, is given for collisions of H^- and D^- with CO as a function of relative collision energy. The filled circles are the results for H^- and the open circles are for D^-.

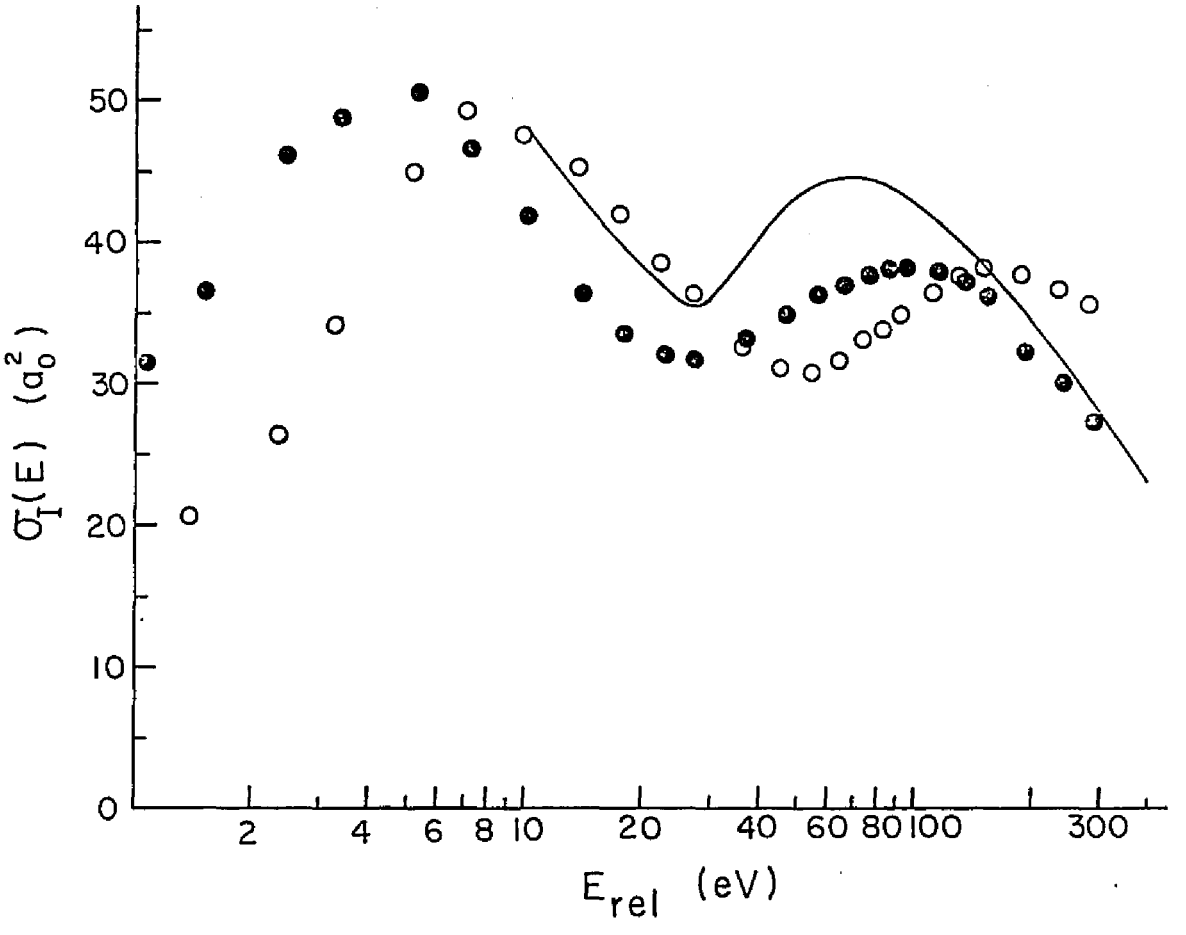

Figure 19: The total charge transfer cross sections for H^- and D^- on O_2 are given as a function of relative collision energy. The filled circles are the present results for H^- and the open circles are for D^-. The solid line is a curve representative of the results of Bailey and Mahadevan for slow ion production for collisions of H^- with O_2.

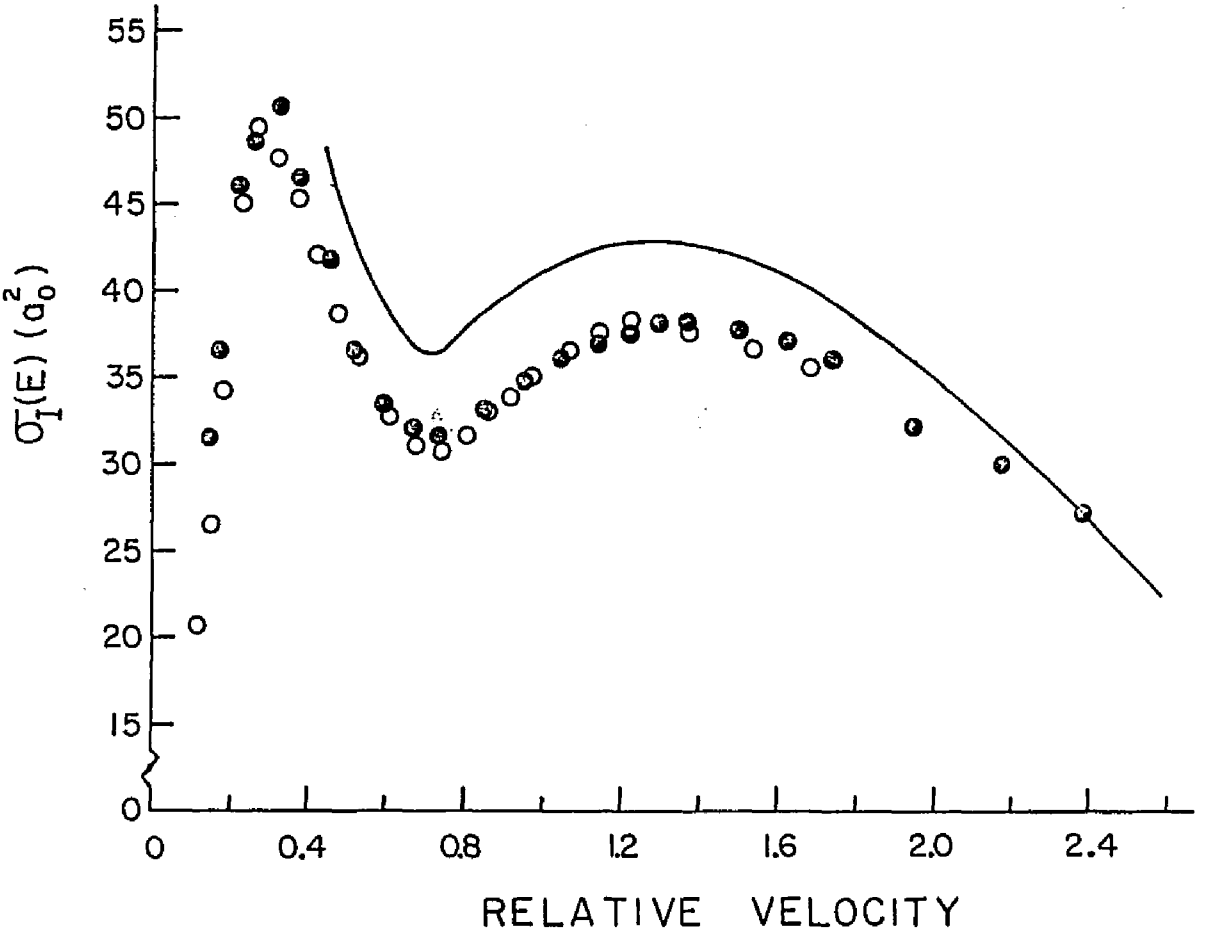

Figure 20: The total charge transfer cross sections for H^- and D^- on O_2 are given as a function of relative collision velocity, which is expressed in units of 10^7 cm/sec. The filled circles are for H^- and the open circles are for D^-.

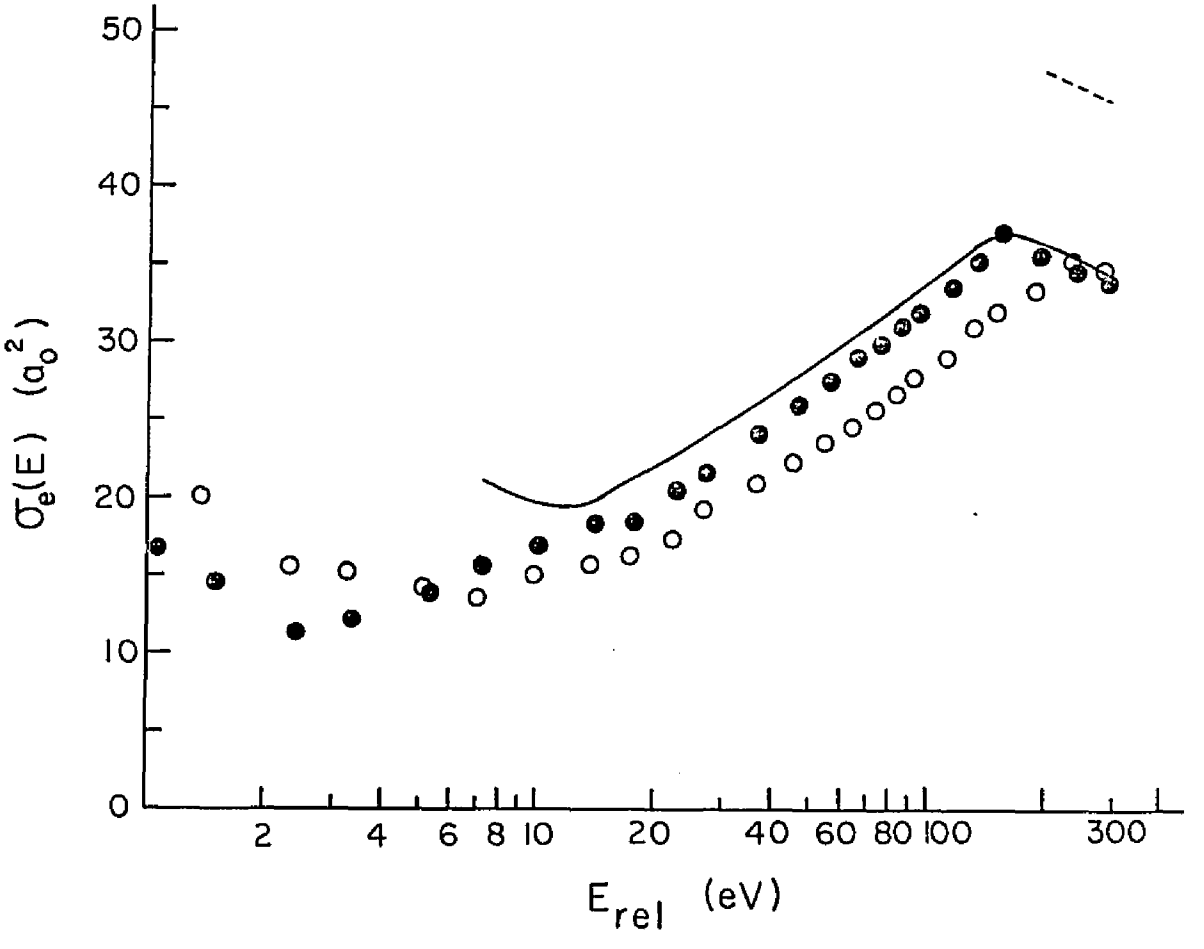

Figure 21: The total electron detachment cross sections, $\sigma_e(E)$, for H^- and D^- on O_2 are given as a function of relative collision energy. The filled circles correspond to the present results for H^- and the open circles are for D^-. The solid line is a curve representative of the results of Bailey and Mahadevan for electron detachment for collisions of H^- with O_2 and the dotted line is a representative of the results of Risley and Geballe.

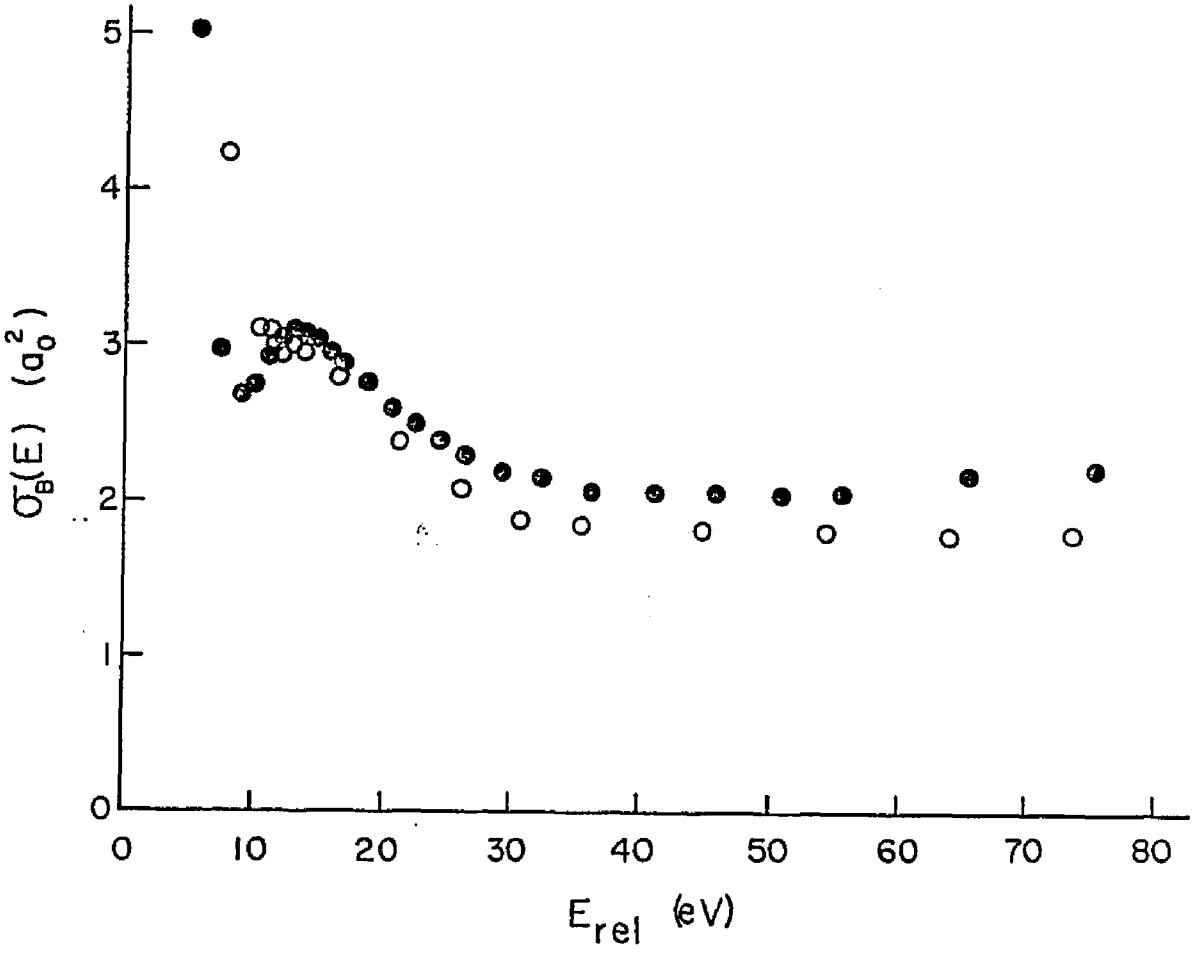

Figure 22: Total cross sections $\sigma_T(E)$ for collisions of H^- and D^- with CO_2 are given as a function of relative collision energy. The filled circles are the results for H^- and the open circles are for D^-.

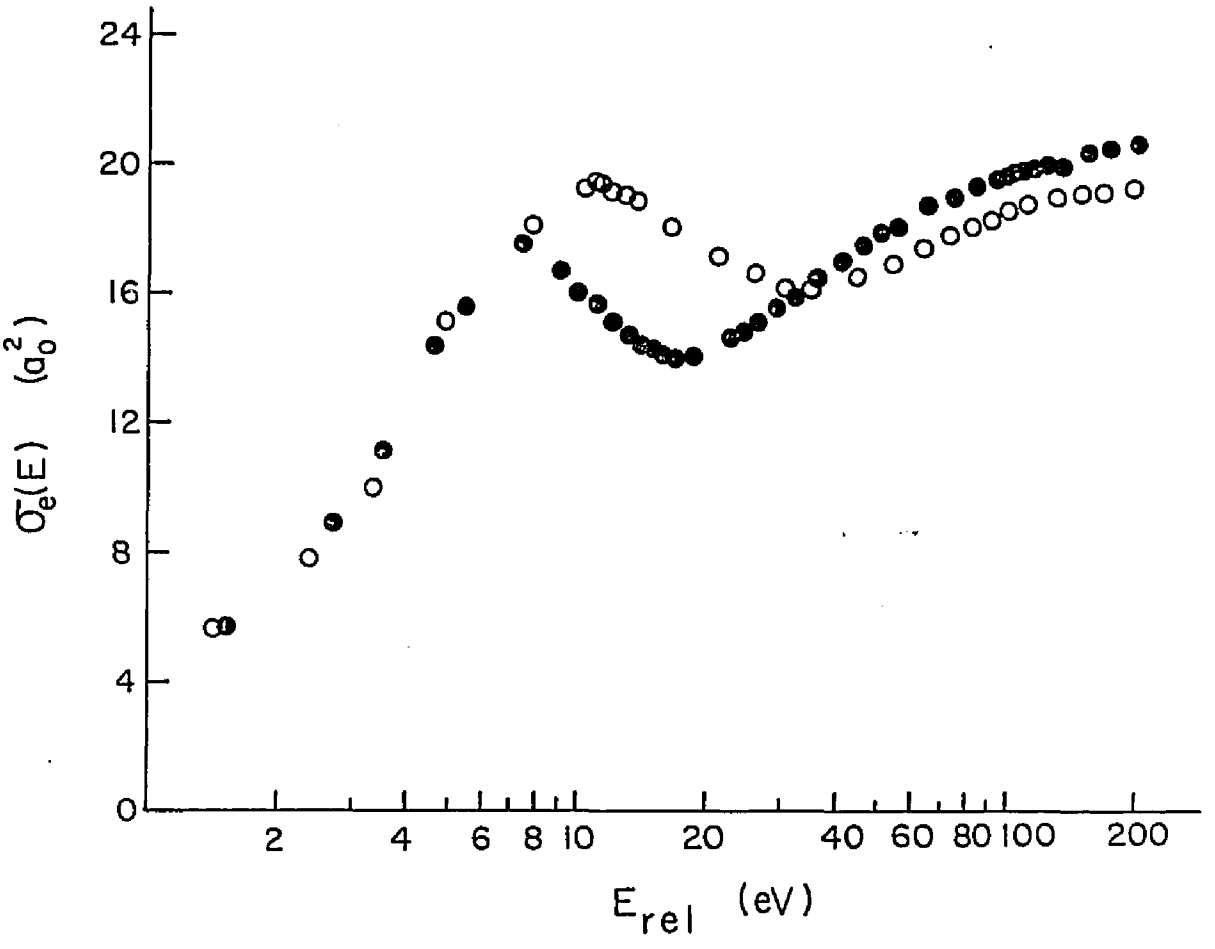

Figure 23: Absolute total electron detachment cross sections, $\sigma_e(E)$, for H^- and D^- incident on CO_2 are given as a function of relative collision energy. The filled circles are the results for H^- and the open circles are for D^-.

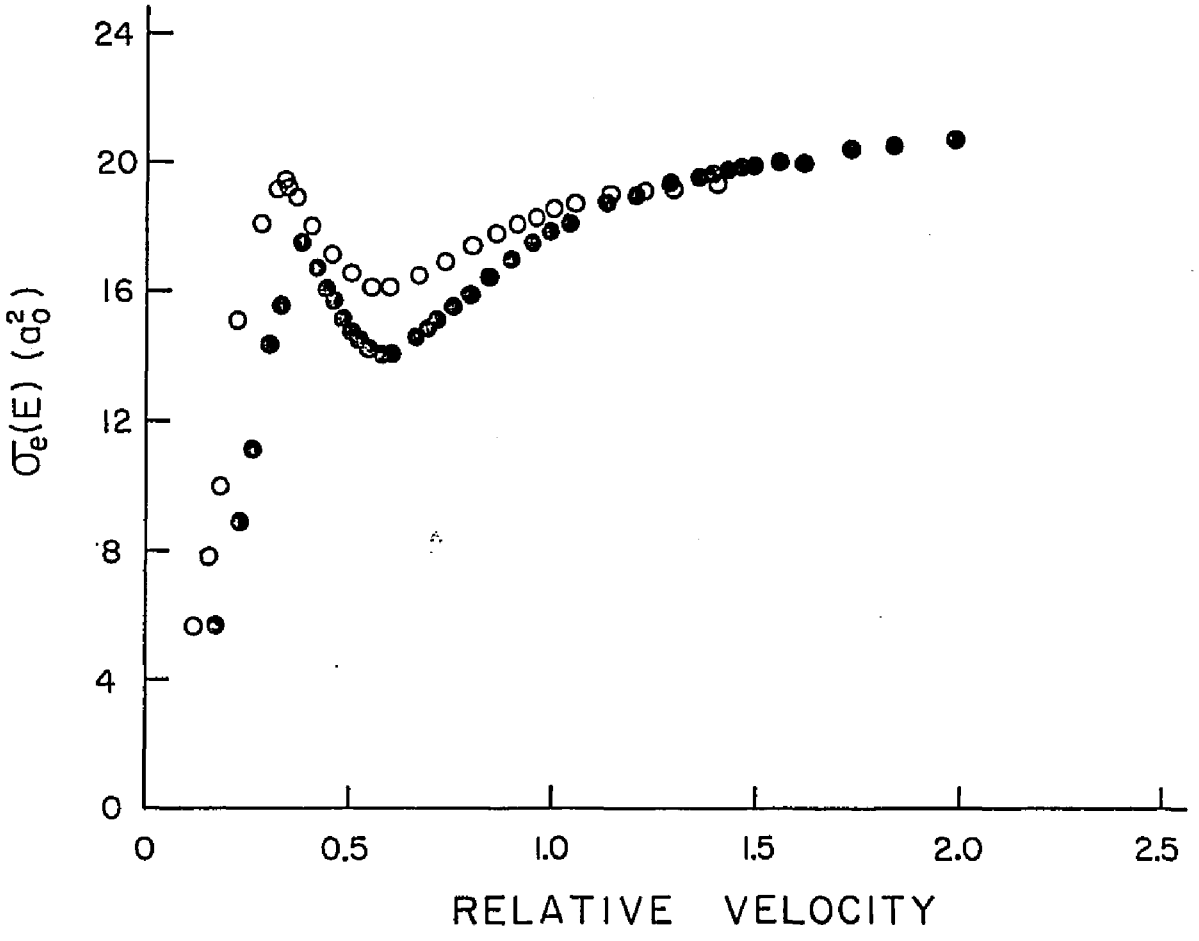

Figure 24: Absolute total electron detachment cross sections, σ_e, for H^- and D^- incident on CO_2 are given as a function of relative collision velocity, which is expressed in units of 10^7 cm/sec. The filled circles correspond to the results of H^- and the open circles are for D^-.

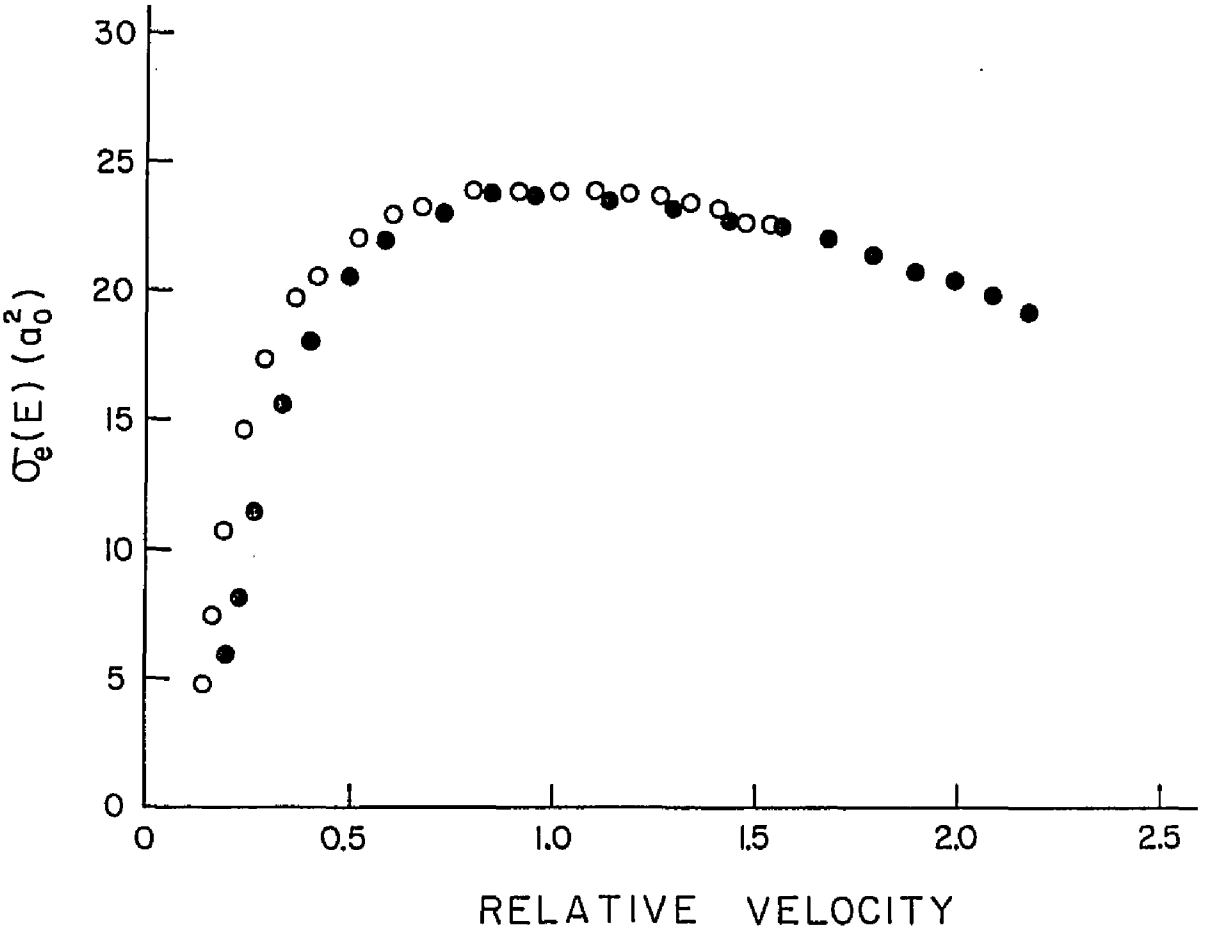

Figure 25: Absolute total cross sections for electron detachment, $\sigma_e(E)$, for H^- and D^- on CH_4 are given as a function of relative collision velocity, which is expressed in units of 10^7 cm/sec. The filled circles are the results for H^- and the open circles are for D^-.

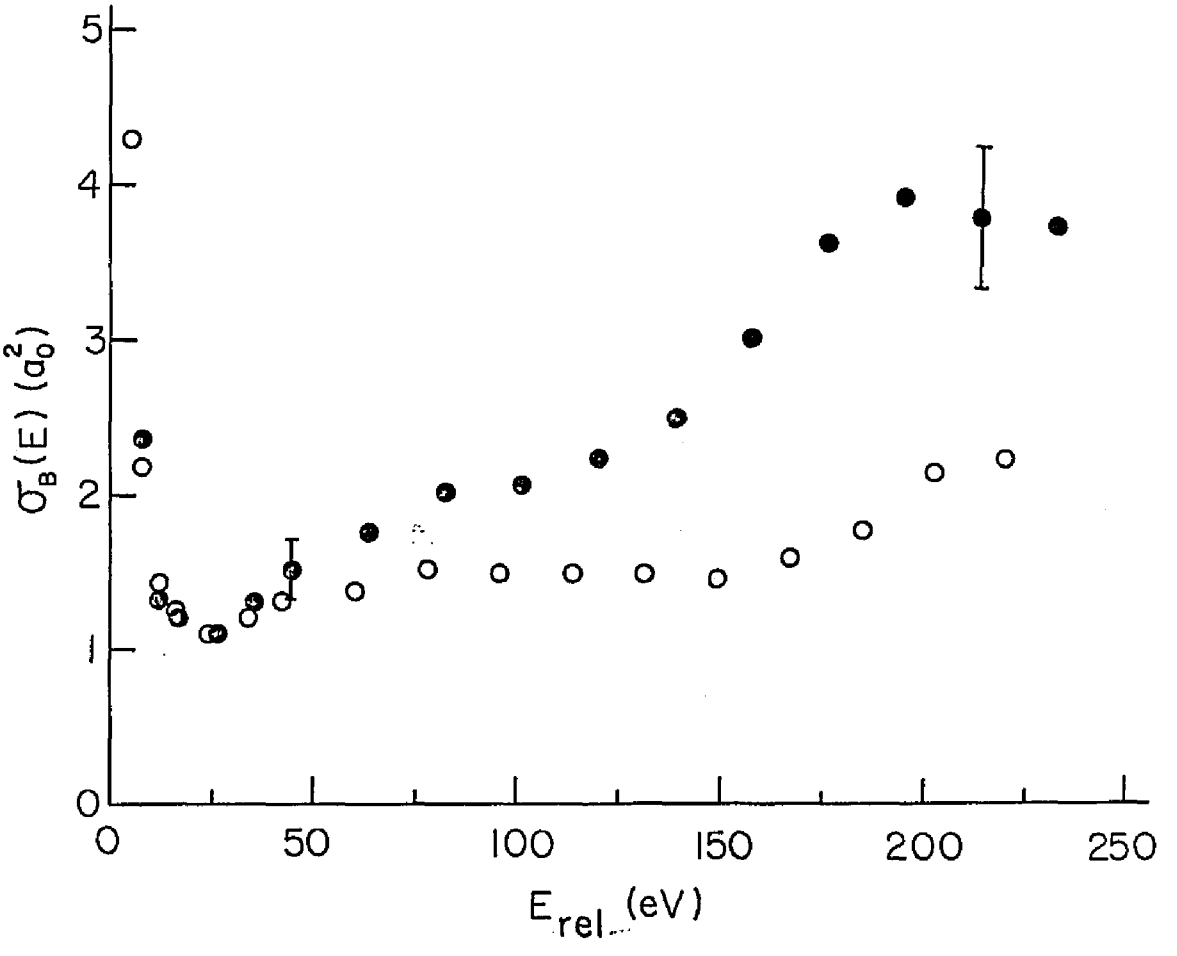

Figure 26: Total cross sections $\sigma_B(E)$ for collisions of H^- and D^- with CH_4 are given as a function of relative collision energy. The filled circles are the results for H^- and the open circles are for D^-.

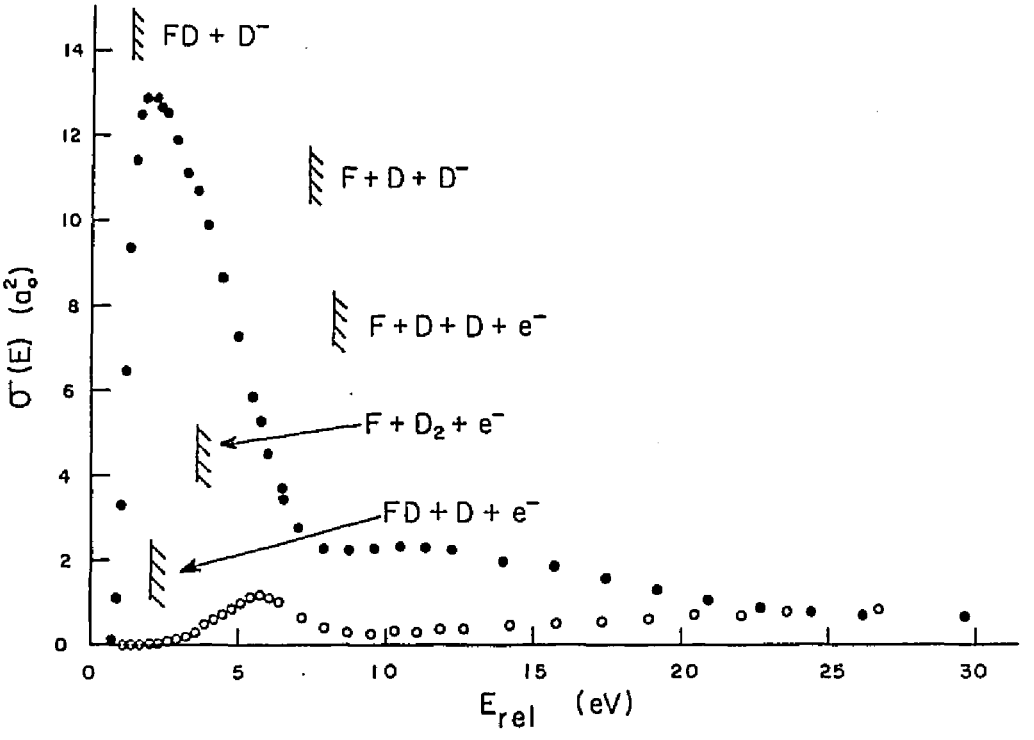

Figure 27: Absolute total cross sections for F^- on D_2 are given as a function of relative collision energy. The solid circles are the results for D^- production and the open circles refer to the production of free electrons. The energetic thresholds for various channels as described in the text are also given.

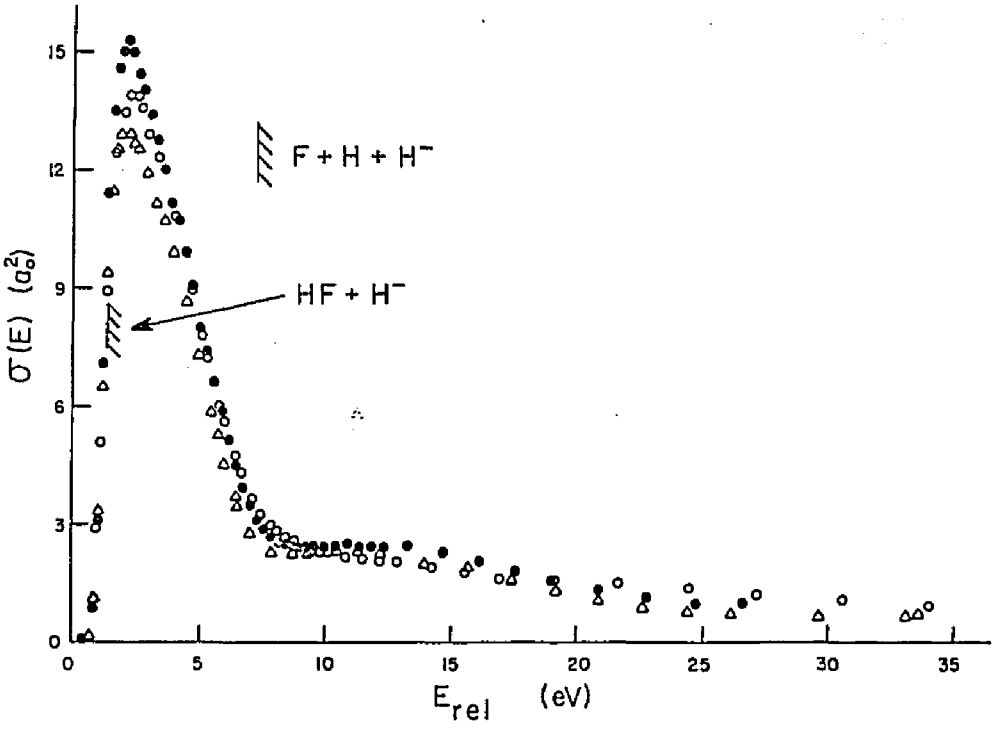

Figure 28: Absolute total cross sections for the production of $H^-(D^-)$ for collisions of F^- with H_2, D_2, and HD are given as a function of the relative collision energy. The solid circles are for H_2, open circles for HD, and the triangles are for D_2. The energetic thresholds for several $H^-(D^-)$ channels are also given.

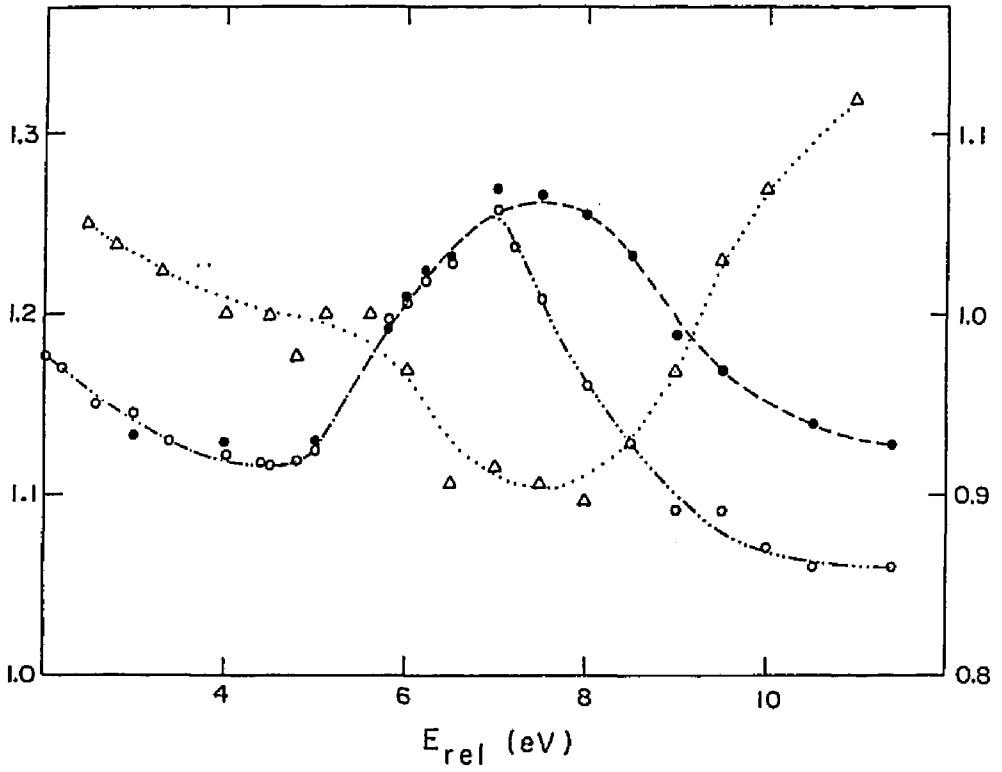

Figure 29: The ratios of the cross sections for $H^-(D^-)$ production, as described in the text, are given as a function of relative collision energy for the case of the F^- projectile. The solid circles are for R_{24}, open circles for $\mathcal{R}_{24}$ and the triangles are for R_{23}. The scales for R_{24} and $\mathcal{R}_{24}$ are indicated on the left of the figure, whereas that for R_{23} is indicated on the right. All the experimental points have been joined by a smooth curve.

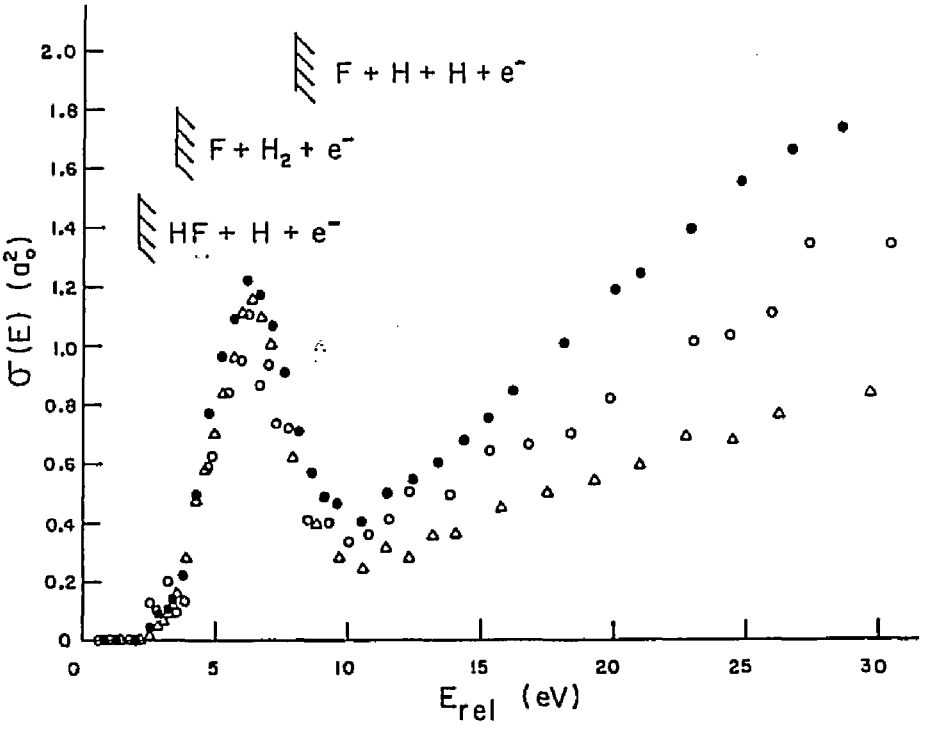

Figure 30: Absolute total electron detachment cross sections for F^- on H_2, D_2, and HD are given as a function of the relative collision energy. The solid circles are the results for H_2, the open circles for HD, and the triangles are for D_2. The energetic thresholds for various free electron channels are also given.

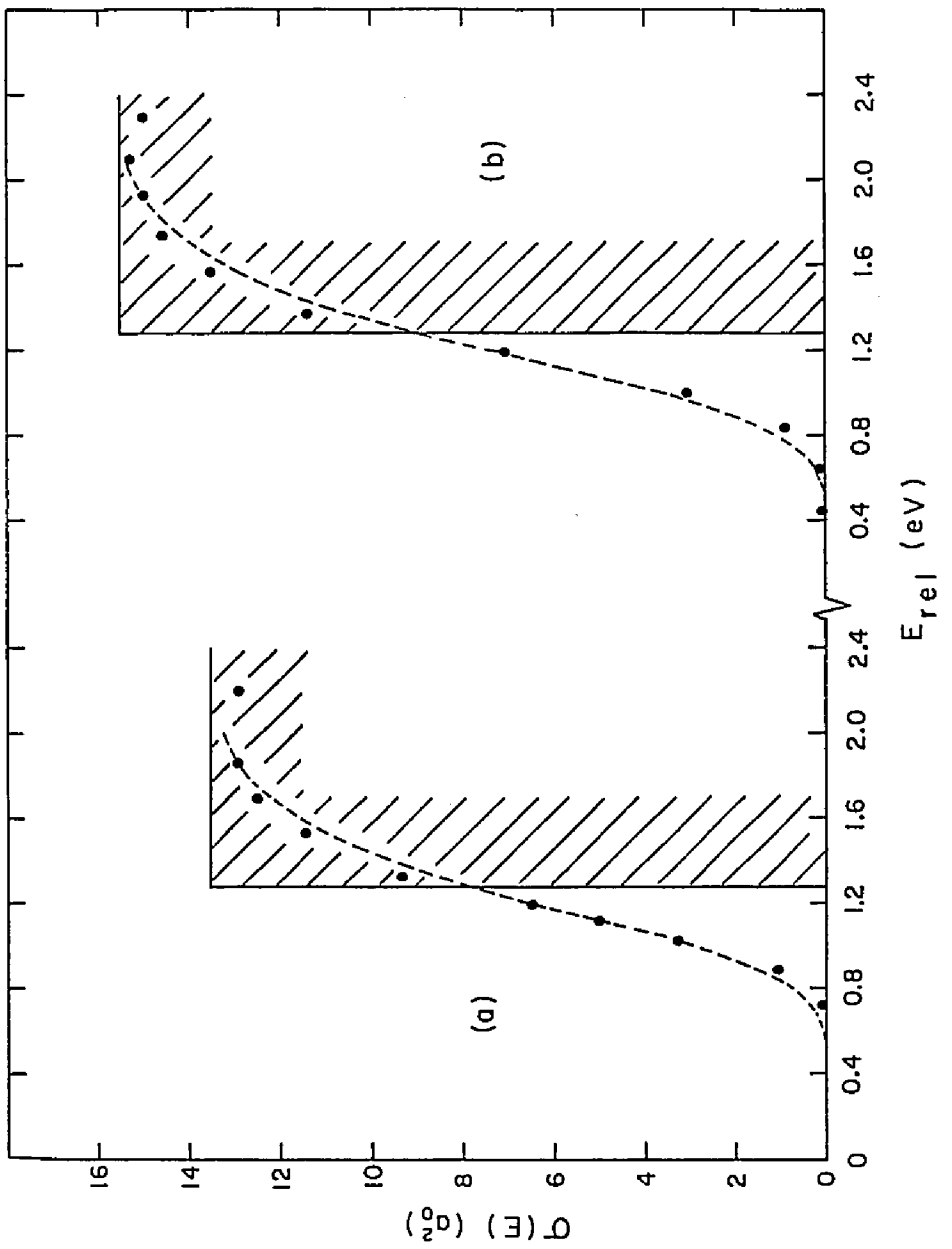

Figure 31: Absolute total cross sections for the production of $H^-(D^-)$ for F^- on H_2 and D_2 are presented for the near threshold region. (a) is for $F^- + D_2$ and (b) for $F^- + H_2$. The solid circles are the experimental results and the dashed line is the result of a convolution of the step function (of threshold energy 1.28 eV) which is also shown in the figure.

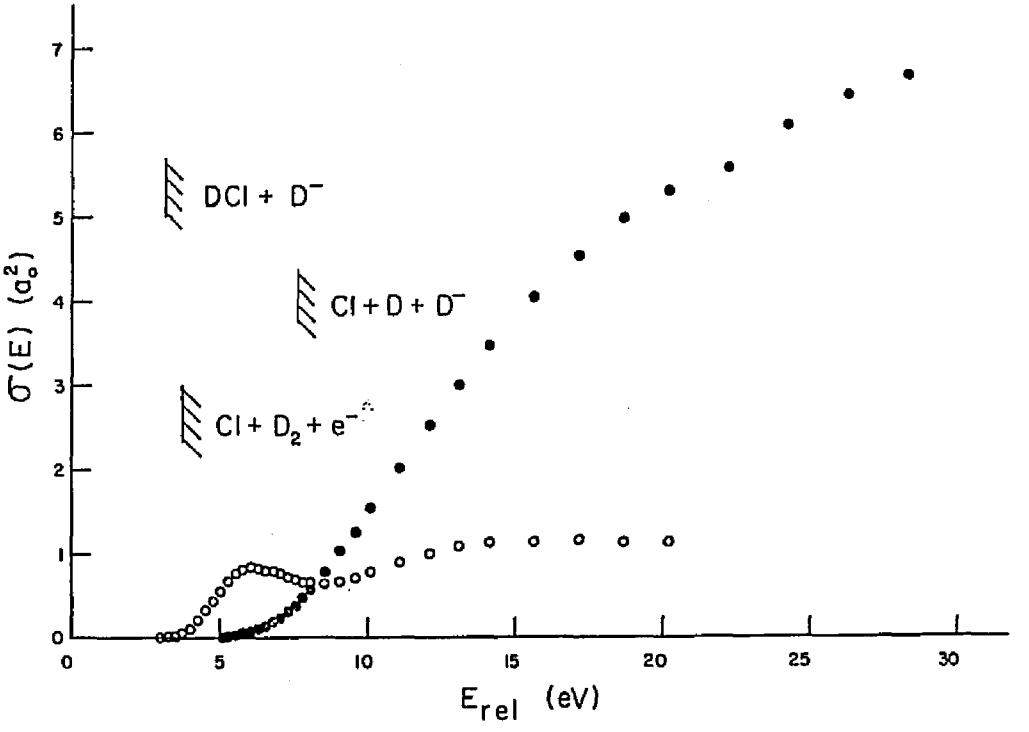

Figure 32: Absolute total cross sections for Cl^- on D_2 are given as a function of the relative collision energy. The solid circles are the results for free electron production and the open circles for D^- production. Energetic thresholds for various channels as described in the text are also indicated.

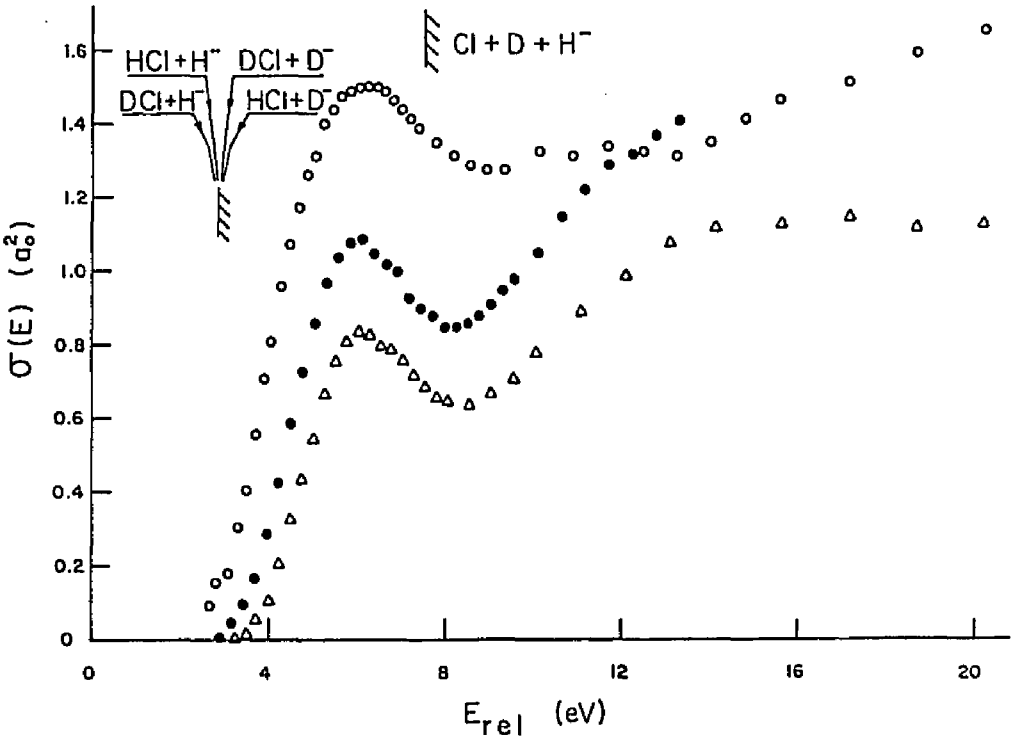

Figure 33: Absolute total cross sections for the production of slow negative ions (viz., H^- or D^-) for Cl^- on H_2, D_2, and HD are given as a function of the relative collision energy. The open circles are the results for the HD target, the solid circles for H_2 and the triangles are for D_2. The energetic thresholds for various $H^-(D^-)$ channels are also given.

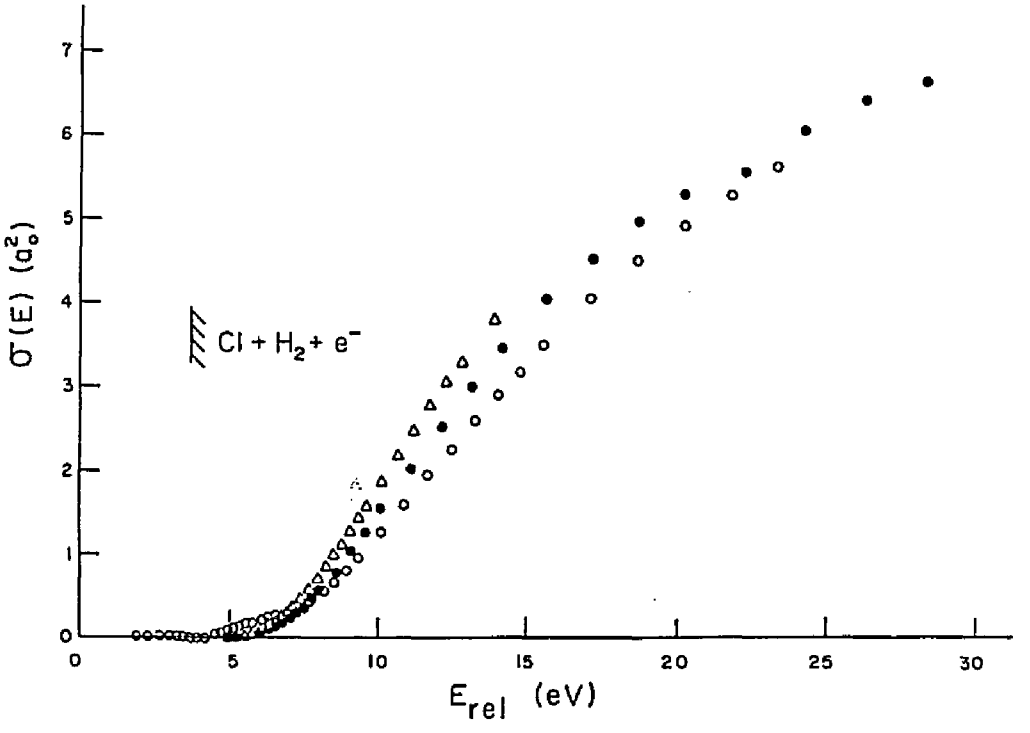

Figure 34: Absolute total cross sections for electron detachment for Cl^- on H_2, D_2, and HD are given as a function of the relative collision energy. The triangles are the results for H_2, the solid circles for D_2 and the open circles are for HD. The energetic threshold for simple electron detachment is given.

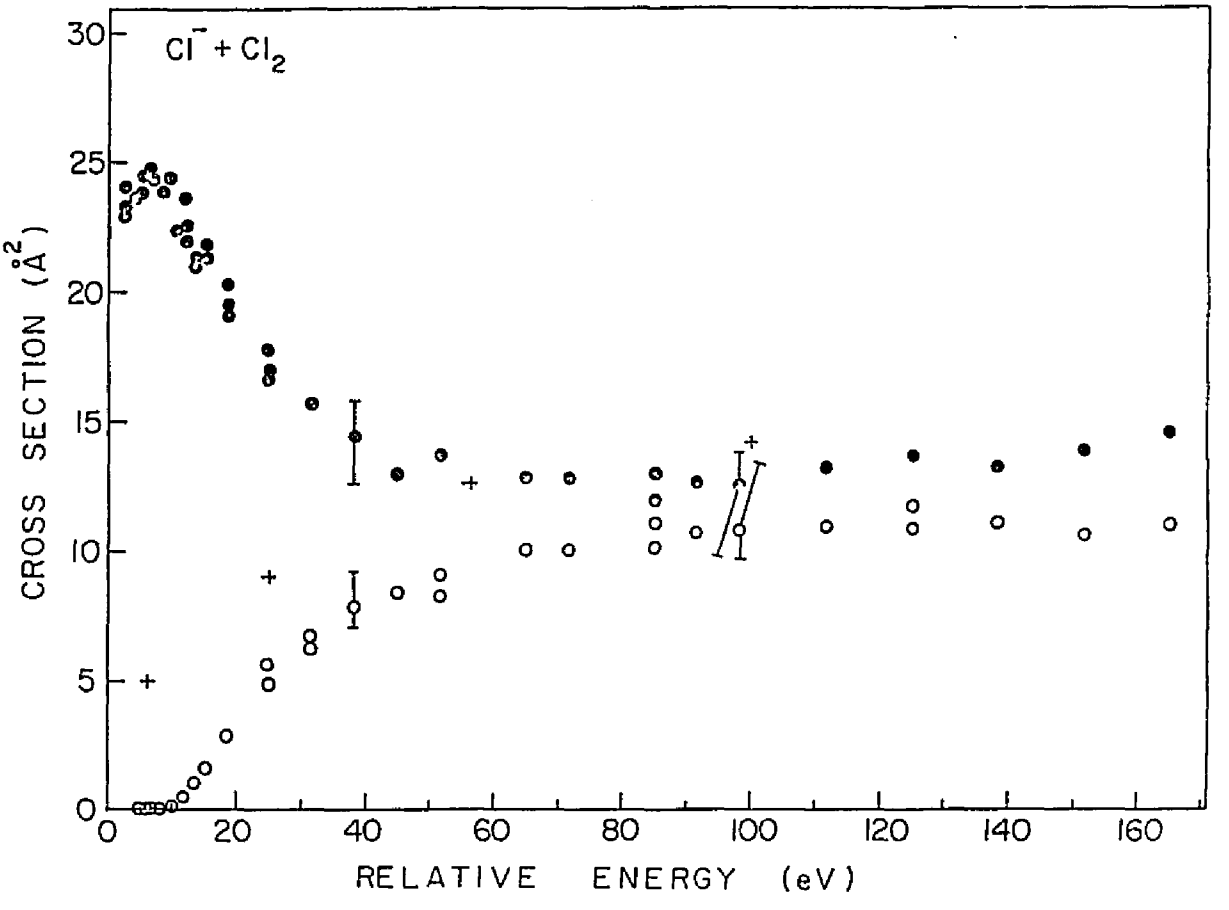

Figure 35: Measured total cross section for electron detachment (open circles) and slow ion production (solid circles) for $Cl^- + Cl_2$. The crosses show the earlier data of Hasted and Smith (Ref.27). The error bars result from a combination of statistical and systematic uncertainties. The choice of f(E), as discussed in the text, constitutes the largest systematic uncertainty.

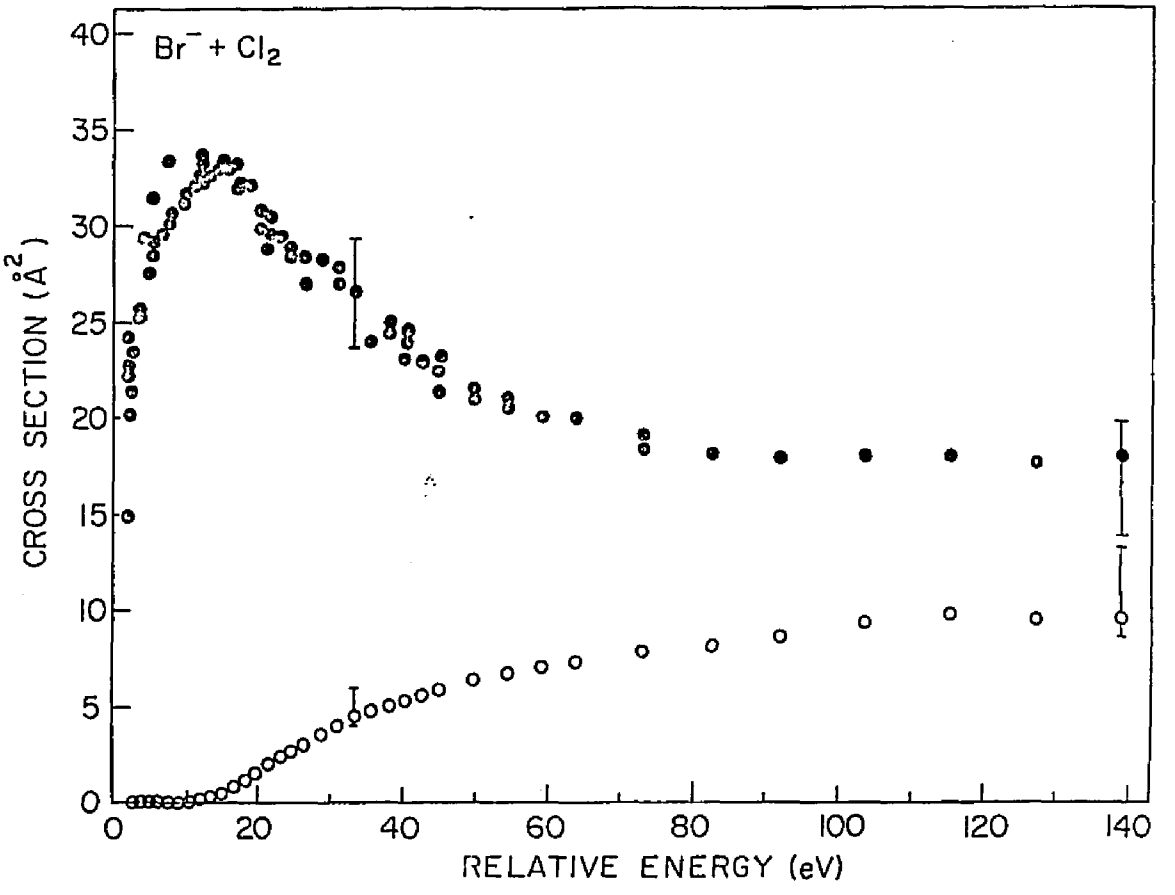

Figure 36: Measured total cross section for electron detachment (open circles) and slow ion production (solid circles) for $Br^- + Cl_2$.

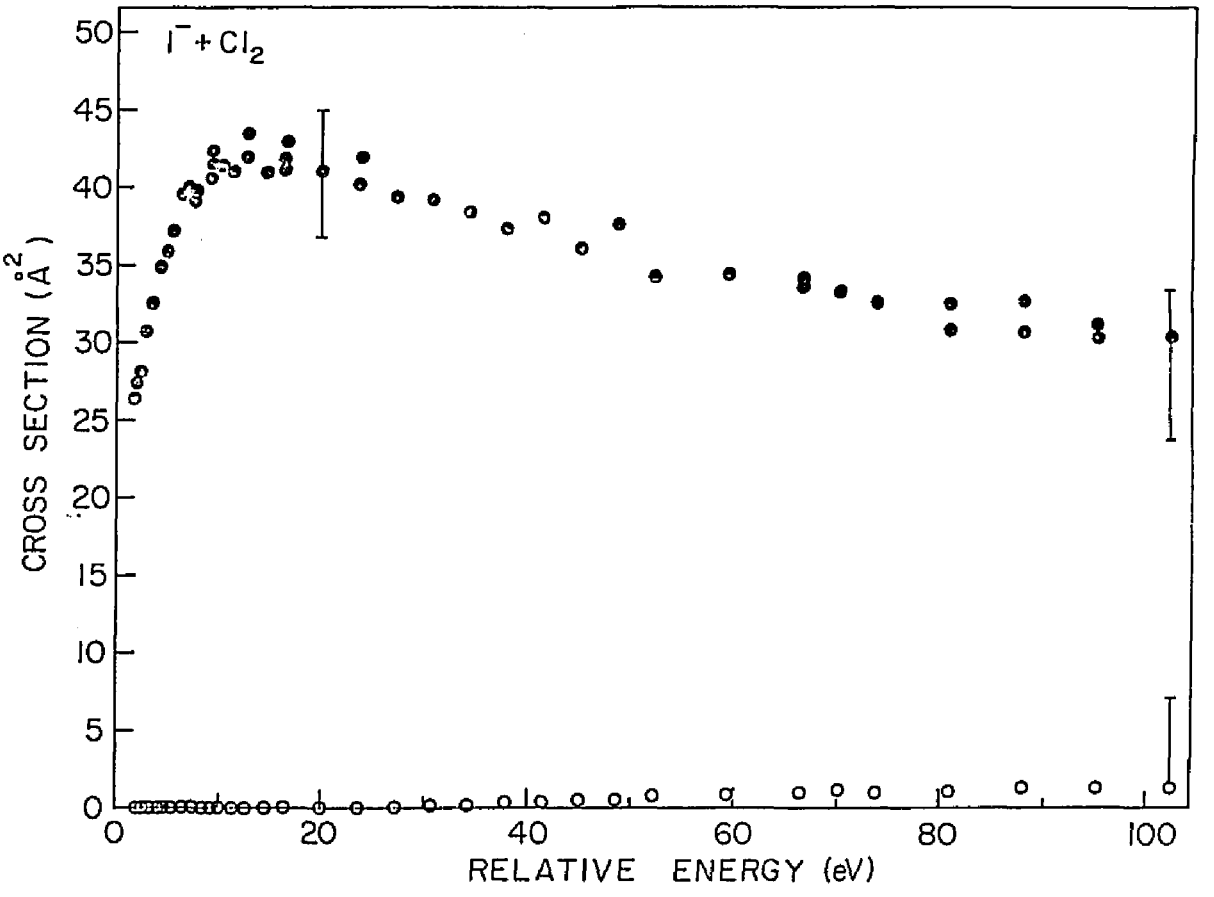

Figure 37: Measured total cross section for electron detachment (open circles) and slow ion production (solid circles) for $I^- + Cl_2$.

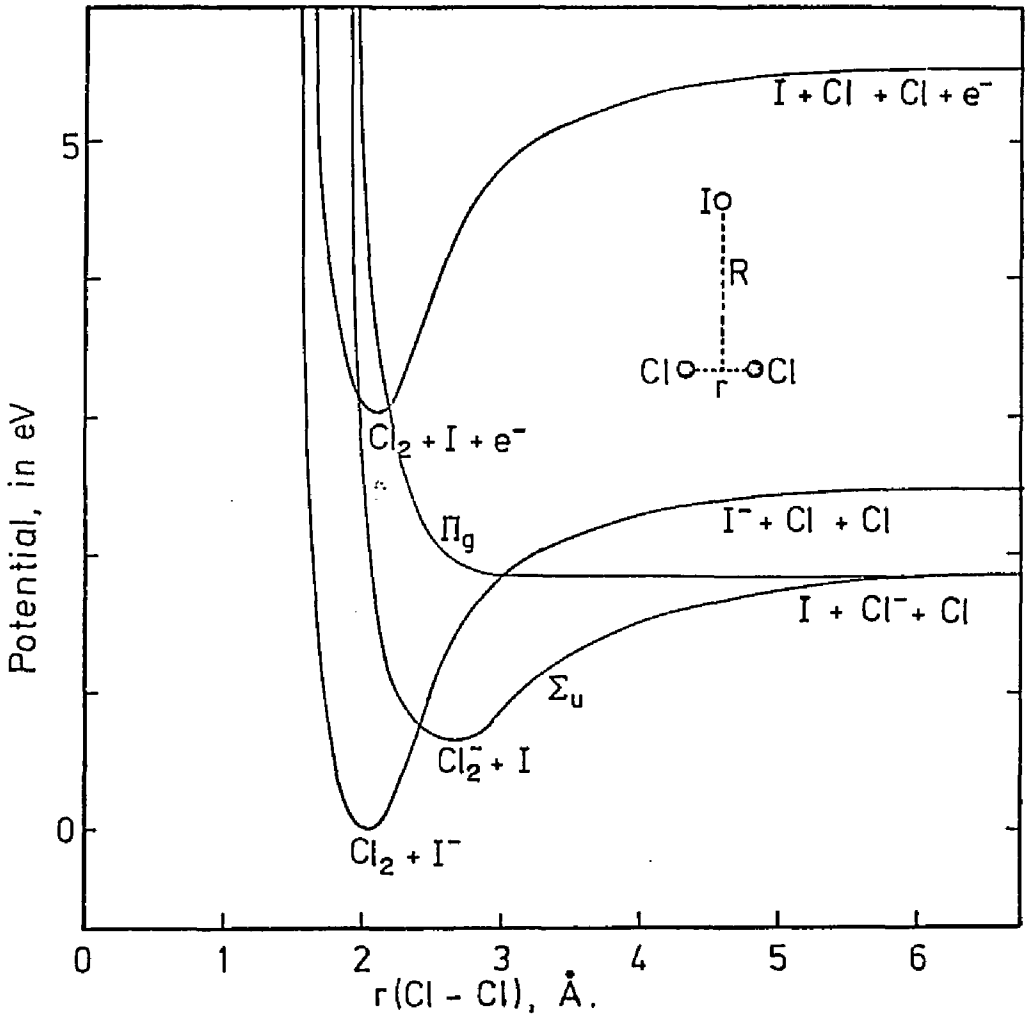

Figure 38: Potential curves for (I^- + Cl_2) and for (I + Cl_2^-) ground states, for R(I-Cl_2), as a function of chlorine separation, r(Cl-Cl). Also schematically shown is one antibonding potential for Cl_2^-, representative of the $^2\Pi_{g3/2}$ and $^2\Pi_{g1/2}$ states.

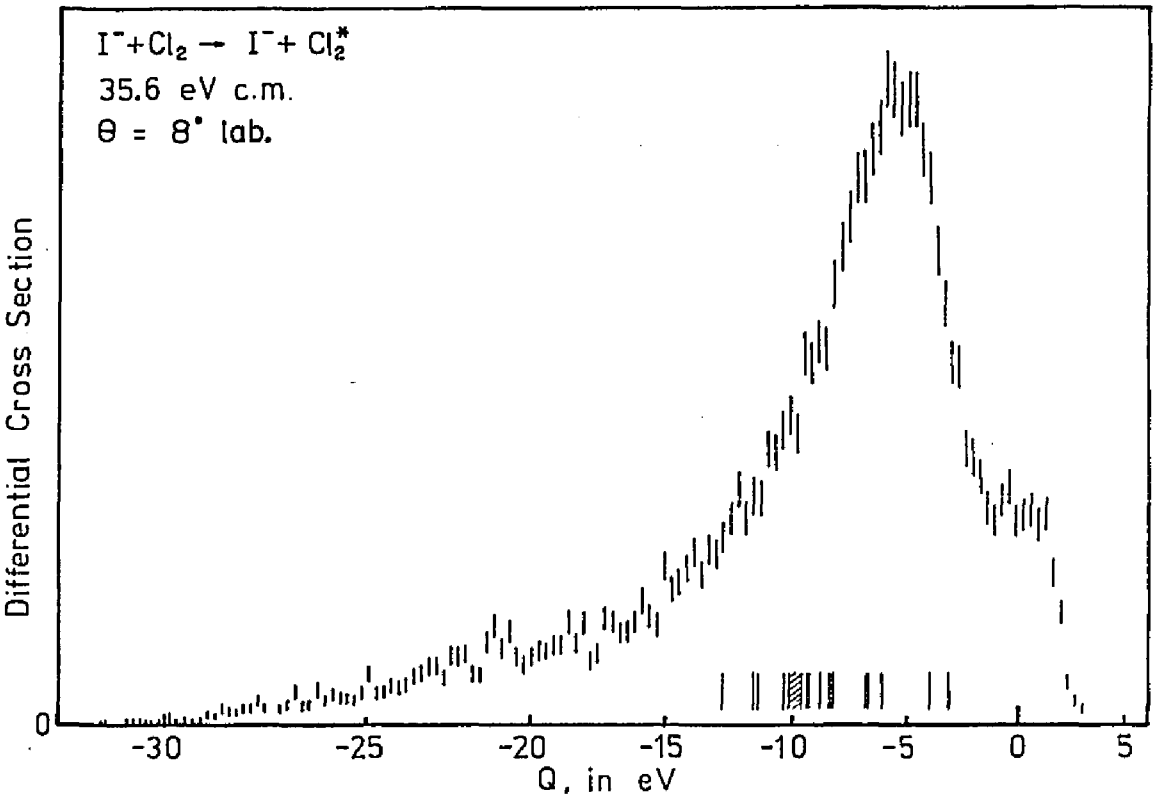

Figure 39: Energy loss spectra for I^- + Cl_2. The vertical marks along the abscissa represent energy losses associated with vertical transitions to various excited states of Cl_2, as calculated by Peyerimhoff and Buenker (Ref.95). The statistical uncertainty of the data is indicated by the error bars.

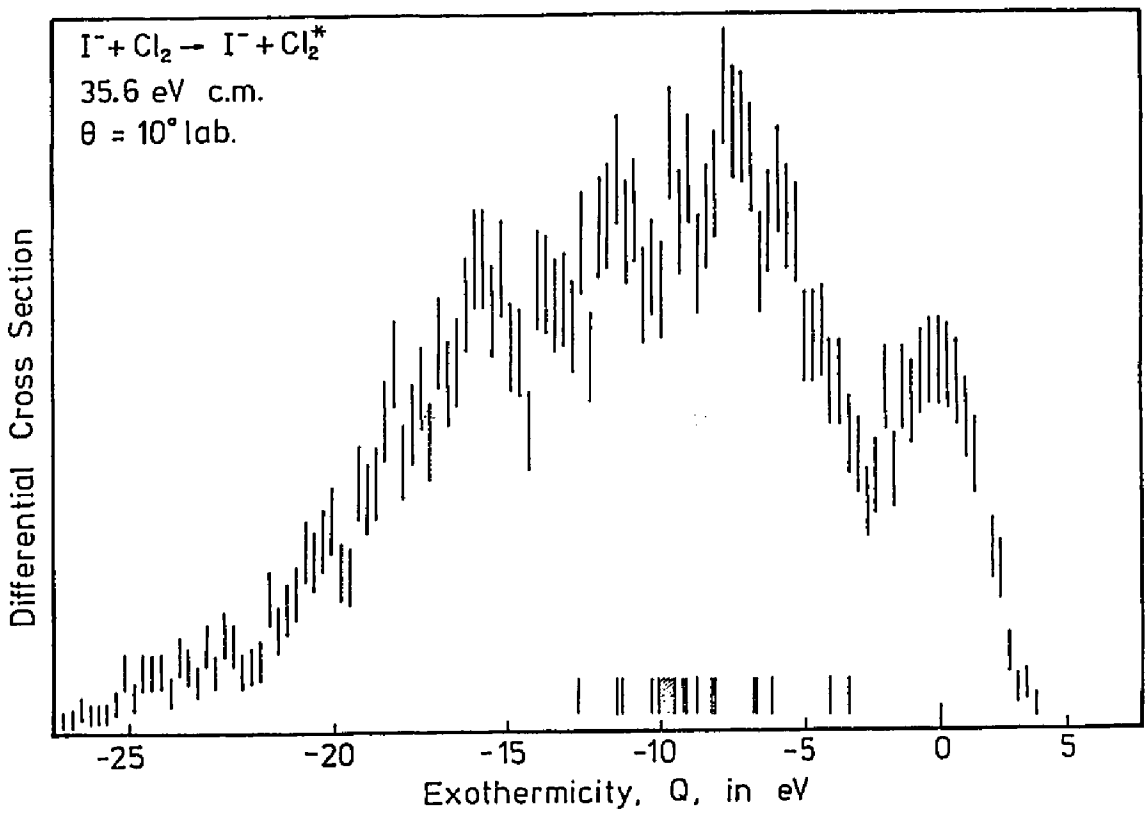

Figure 40 : Energy loss spectrum for I^- + Cl_2.

VITA

Mohammed Saiful Huq

Born in Noakhali, Bangladesh, on November 27, 1952. Passed the Secondary School Certificate Examination from Jamalpur Government High School in 1967 and Higher Secondary Certificate Examination from Dhaka College in 1969. Graduated from the University of Dhaka with B.Sc. (Honours) and M.Sc. degrees in Physics in 1974 and 1976 respectively.

Worked for Bangladesh Atomic Energy Commission as a Research Fellow from 1976 to 1977. In September 1977, the author entered the College of William and Mary as a graduate student in the Department of Physics.